POLITÉCNICA

ESCUELA TÉCNICA SUPERIOR DE INGENIEROS INDUSTRIALES
UNIVERSIDAD POLITÉCNICA DE MADRID

José Gutiérrez Abascal, 2. 28006 Madrid
Tel.: 91 336 3060
info.industriales@upm.es

www.industriales.upm.es

05 TRABAJO FIN DE MASTER

Alejandro Llop Máñez

INDUSTRIALES

TRABAJO FIN DE MASTER

OPTIMIZATION OF INDUCTIVE RESONANT COUPLING LINKS FOR LOW POWER AND MID-RANGE WIRELESS POWER TRANSFER

TRABAJO FIN DE MASTER
PARA LA OBTENCIÓN DEL
TÍTULO DE **MASTER EN ELECTRÓNICA INDUSTRIAL**

SEPTIEMBRE **2014**

Alejandro Llop Máñez

DIRECTOR DEL TRABAJO FIN DE MASTER:

Jesús Ángel Oliver Ramírez

INDUSTRIALES
ETSII | UPM

POLITÉCNICA

Abstract

Wireless Power Transfer (WPT) consists in transferring energy between circuits without cables connecting them. Such transference can be of several kinds: inductive, capacitive and radiated. Inductive is the most popular nowadays, and is being currently investigated and developed in companies, universities... although its interest appeared about two decades ago.

The transference of energy is carried out through the magnetic field between two coils inductively coupled. As the distance between the coils increases the lower is the coupling and so the energy transferred and the efficiency. To minimize this, working in resonance is used by means of capacitance compensation of the inductances; this way the efficiency and also the power transferred is increased, since the reactive elements of the circuits are compensated.

This work performs an extensive study of the magnetic link, its optimization and implementation, both through mathematical analysis, simulations and real assembly; namely for low power (100mW to 10W) and distances of transmission larger than diameters of the coils, which is commonly known as mid-range transmission. Its main purpose is the charge of mobiles devices such as tablets, mobile phones... while being used without the need of being very close to the charging device, as it occurs with Qi standard [1].

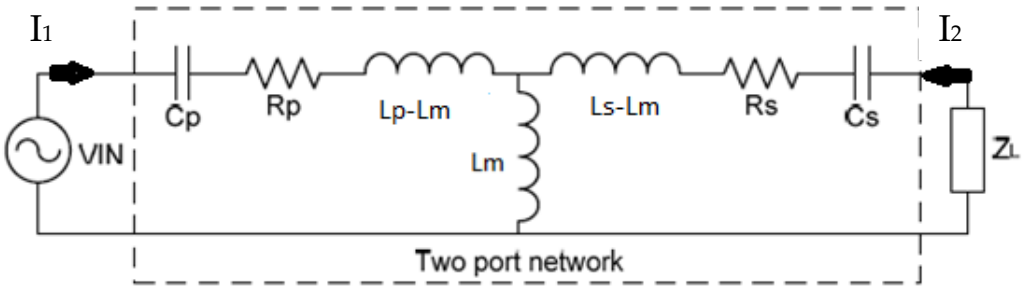

Figure 0.1. Example of resonant magnetic link

The first part of this work is an introduction to wireless power transfer and its state of the art, focused on low power and mid-range transmission. The second part focuses on the study of the resonant magnetic link, e.g. the geometry of the coils, the magnetic coupling and other factors whose understanding make possible the transmission of energy.

The third part develops the link optimization through analytical equations, and how it can be tackled depending on the circuit constraints; other works from our investigation group are quoted, but here will be focused on low power and higher distance between the coils, as mentioned above.

The fourth part includes the optimization of the coils (both primary and secondary) to achieve the best coupling and efficiency.

The fifth part shows the experimental results and how they validate the model proposed. The last part is composed of the conclusions and the future work.

In addition, several appendices are included, which contain the practical issues related to the implementation and software designed to do the simulations.

Acknowledgements

This master thesis is integrated in the *Centro de Electrónica Industrial*, inside the *Universidad Politécnica de Madrid*; I want to acknowledge them for having learnt a lot and for their labs, whose numerous instruments and devices have allowed me to perform this work.

I wish to express thanks to my supervisors Jesús Ángel Oliver and Pedro Alou for their support and guidance; also to the work group formed by them and José A. Cobos and Rafael Asensi, whose ideas and vast knowledge have make me possible continuous learning and having better points of view to tackle the problems.

I want to thank the company I work for, Zennio Avance y Tecnología, for making me possible attending to the master classes with a free schedule.

Finally, I want to express a big gratitude to Enrico di Lorenzo, from **FastFieldSolvers** [2], whose simulation software (FastHenry, Fastcap and Fastmodel) and his wide support made possible this project and fundamentally the simulations and its automation, saving me a lot of time.

Index

List of figures

List of tables

List of acronyms

WPT - Wireless Power Transfer.
IPT - Inductive Power Transfer.
LPT - Laser Power Transfer.
CPT - Capacitive Power Transfer.
ICPT - Inductive Coupling Power Transfer.
EMF - Electromagnetic fields.
RMS - Root Mean Square.
δ - Skin Depth.
Q - Quality factor.
RF - Radio frequency.
PCB - Printed Circuit Board.
SRF - Self Resonant Frequency.
GUI - Graphic User Interface.
CAD - Computer Aided Design.
FEM - Finite Element Method.
SS – Primary Series, Secondary Series compensation.
SP – Primary Series, Secondary Parallel compensation.
PS – Primary Parallel, Secondary Series compensation.
PP – Primary Parallel, Secondary Parallel compensation.
R – Resistance.
C – Capacitance.

L – Inductance.

R_L – Load Resistance.

M – Mutual Inductance, equivalent to X_m.

k – Coupling factor.

f – Frequency.

I_p – Primary Current.

I_s – Secondary Current.

η – Efficiency.

L_m – Mutual inductance.

1. INTRODUCTION AND STATE OF THE ART

1.1. INTRODUCTION

Wireless Power Transfer (WPT) consists in transferring energy between circuits without any cables connecting them; it can be radiative or non-radiative depending on the mechanism used to transfer energy. Radiative power can be emitted from an antenna and propagates through a medium (such as vacuum or air) over long distance (many times larger than the dimension of the antenna) in form of electromagnetic wave. However, due to the omni-directional nature of the radiative power emission, the energy efficiency of power transmission is very low; because of this, it is not appropriate for WPT, since the power needed to charge energy storage elements is large [3].

Non-radiative wireless power transfer usually relies on the near field magnetic coupling of conductive loops (coils) and can be classified into short-range and mid-range applications [3]; WPT based on the magnetic resonance and near-field coupling of two loop resonators (coils working in resonance) was reported by Nicola Tesla a century ago [4], and it is known as inductive power transfer (IPT).

The operation of a resonant IPT system is comparable to that of an air core transformer with the leakage inductance compensated by means of capacitances; compensation is applied to both the primary and secondary of the transformer to boost power transfer as well as making operation possible. Secondary capacitor is calculated to resonate with the secondary self-inductance at the operating frequency, while the primary capacitor is either designed to have unity power factor at the input of the system, i.e. getting resistive input impedance [5], or to resonate with the primary self-inductance.

The mutual coupling within IPT systems is generally weak. To deliver the required power and ensure equipment sizes remain manageable, it is necessary to operate at high frequency.

It should be noted that wireless power transfer has been applied extensively in ac machines, which were also pioneered by Tesla [6]. Using a cage induction machine as an example, energy is transferred from the excited stator windings across the air gap to the rotor cage. Energy transfer via coupled windings is the basic principle used in electric machines; therefore, wireless power systems can be mathematically described by electric circuit theory for magnetically coupled circuits. Also, [3] WPT has been an active research topic for transcutaneous energy systems for medical implants since 1960's [7]-[11] and induction heaters [12] since 1970's. For modern short-range applications, the inductive power transfer (IPT) systems [13]-[17] and the wireless charging systems for portable equipment such as mobile phones [10], [11], [20]-[23] have attracted much attention since 1990's and 2000's respectively. Short-range wireless charging technology for portable electronic devices has reached commercialization stage through the launch of the "Qi" Standard by the Wireless Power Consortium [1], now comprising over 135 companies worldwide.

The combined use of magnetic induction, tuned circuits and resonance operating frequency has been a common theme in wireless power and radio investigations. Some of these features are referred to as "non-radiative", "magneto-inductive" and "magnetic resonance" in recent mid-range wireless power research.

1.2. CLASSIFICATION OF WIRELESS POWER TRANSFER SYSTEMS

WPT systems can be classified depending on the parameter considered. According to the distance from the radiating source, they can be divided into

- Near field.
- Mid field.
- Far field.

Each one has its own electromagnetic properties and propagation characteristics; near field takes place when the transmission distance is less than one wavelength, mid field between one and two wavelengths and far field applies when the distance between the source and the receiver is bigger than two wavelengths.

According to the coupling mode employed, WPT systems can be classified as: electromagnetic radiation, electric induction or magnetic induction. Figure 1.1 shows a block diagram using this classification method [24]:

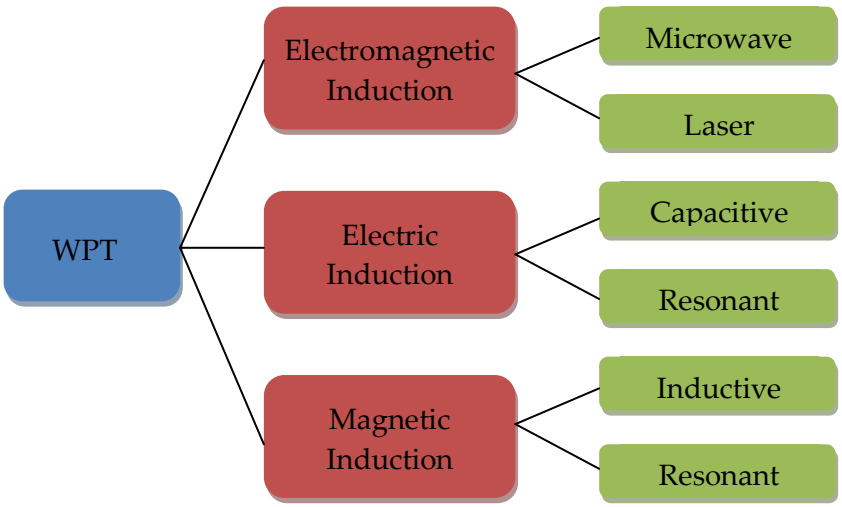

Figure 1.1. Types of wireless transmission [24]

1.2.1. Electromagnetic radiation

The WPT by electromagnetic radiation is commonly transmitted as microwaves or laser rays, which are considered as far field since the inductive and magnetic field are orthogonal and related through the impedance of the medium of propagation. It has promising applications on satellites and others when the distance from the WPT emitter is large [25]. On the other hand, both WPT by electric induction and WPT by magnetic induction work in near field.

WPT by using electromagnetic energy is not a new idea, and several experiments, even in recent times, have proved its feasibility. The starting idea was the proposal concerning transmission of energy from space down to the Earth, as suggested by Peter Glaser (1969) in his project, namely *Solar Power Satellite*, along three steps. First, D.C. electric energy is collected by solar cells displaced in space by a satellite on a geostationary orbit. Then, the collected D.C. electric energy is converted to microwave field energy that is transmitted as a wave beam down to the Earth. Finally, the microwave field energy is collected by a receiving antenna array at the receiver site over the ground, and converted back to D.C. energy by loading the elements of the array over a rectifying circuitry. For this reason the receiving antenna is named *rectenna*.

This solar energy concept has been (theoretically) explored, mainly in the US and Japan, essentially along the lines originally envisaged by Glaser. However, the subsequent steps, i.e., going from the theoretical analysis at paper work level to executive projects, requires a deep, convincing analysis of technological, as well as economical points. Construction, localization, and long-term operation (tens of years) of huge complex space systems over prescribed (not necessarily geo-stationary) orbits is the first issue. Collection of huge amount of solar energy, and its subsequent transmission as a microwave beam to the ground station, with stringent safety and efficiency requirements, is the second issue. Above two points should comply with usually contrasting stringent cost requirements and environmental safety rules. For instance, limitation of the density power levels in the accessible area around the rectenna, to comply with the population safety exposure level to microwave radiation, sets an upper bound to the total allowed transmitted power by the microwave beam. This is just one example out of a large category of others.

Laser Power Transfer (LPT) systems are based on lasers as the energy transport media. Lasers generate phase-coherent electromagnetic radiation by the principle of population inversion and the most commonly used type of lasers is solid state lasers. Direct solar pumping lasers involve the concentration of solar energy before being injected into the laser medium.

1.2.2. Electric induction

The WPT by electric induction is known as Capacitive Power Transfer (CPT) [26]; since it causes more danger to the human body than WPT by magnetic induction, little research on this topic has been done.

CPT is a novel technique used to transfer power wirelessly between the two electrodes of a capacitor assembly [27]. It is based on the fact that when high frequency ac voltage source is applied to the plates of the capacitor that are placed close to each other, electric fields are formed and displacement current maintains the current continuity. Thus, in this case the energy carrier media is the electric field and hence the dual of IPT. Some of the features that CPT has compared to IPT are [27]:

1. Energy transfer can still continue even on the introduction of a metal barrier as it would result in a structure consisting of two capacitors in series.

2. Most electric fields are confined within the gap between the capacitors and hence EMI radiated and power losses are low.

3. The requirement for bulky and expensive coils doesn't exist and hence, the circuit can be made small.

1.2.3. Magnetic induction

The WPT by means of magnetic induction depending on the resonance and the way the field is generated can be divided into: magnetically coupled inductive WPT and magnetically coupled resonant WPT [24]. The first one is sometimes known as inductive coupling power transfer (ICPT), which has become a focus point to applications from few microwatts up to kilowatts, with efficiencies higher than 90% [29]-[31]. Usually, in this way of transmitting energy the distance between coils is lower than their diameters. In figure 1.2, its working principle is shown.

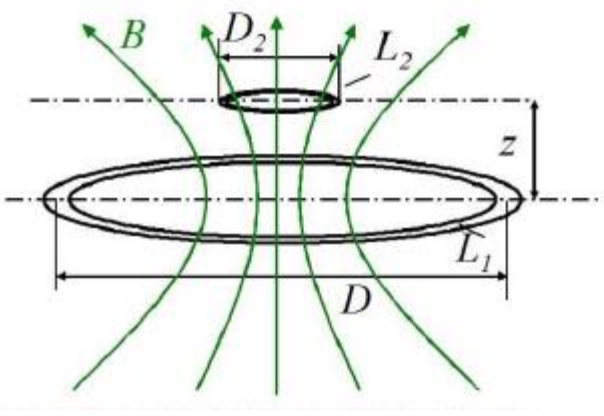

Figure 1.2. Magnetically coupled inductive WPT [32]

Where D is the emitter diameter.
L_1 is the emitter coil.
L_2 is the receiver coil.
D_2 is the receiver diameter.
z is the distance between coils.
B is the magnetic field.

The magnetic field generated by the emitter produces a magnetic flux going through the receiver, this way the energy exchange is produced. This kind of energy transfer has a number of advantages, e.g., it's unaffected by dirt, dust, water, or other chemicals and is thereby environmentally inert and maintenance free [33]-[36]. With such characteristics it has found many applications, but the conditions under which such systems are stable are now of prime importance, especially in critical applications with a multiplicity of receivers [13], [37]-[39].

As said before, magnetic induction WPT can be divided into "Magnetically Coupled WPT" and "Magnetically Coupled Resonant WPT" considering either capacitive compensation is carried out or not; and into "Short-range" or "Mid-range" depending on the distance between the transmitter and the receiver.

1.2.3.1. Magnetically Coupled WPT

The ICPT systems have been studied in applications such as electric vehicles, which includes movable inductors applications [40], [41], and fixed inductors applications [42], [43]. For movable inductors, the receiver moves along the transmitter, and the energy transmission is made by the horizontal component of the magnetic flux [44]. In the second case, both emitter and receiver are fixed, in this case the energy transmission is made by the vertical component of the magnetic flux [42].

In some papers, what are called ICPT systems are resonant but designed for high power transfer; in order to design this type of systems, a compensation topology must be selected (as later can be seen). The compensation topology helps to improve the energy transfer between coils; to use a compensation topology the power ratio and the control technique must be taken into account [45]-[48].

1.2.3.2. Magnetically Coupled Resonant WPT

Unlike ICPT, in resonant systems (IPT systems from now on) there is a resonance and the distance between coils is usually higher than their diameters. It was introduced by Massachusetts Institute of Technology (MIT) in 2007 [49]. Since then, there have been many publications related to this topic.

Literature describes four basic topologies: Series-Series (SS), Series-Parallel (SP), Parallel-Series (PS) and Parallel-Parallel (PP) depending on the position of the compensation capacitor with respect to the coils; each one has its advantages and drawbacks depending, among other factors, on the efficiency, currents and voltage implied and tolerances to deviation from the operating frequency [5]; in figure 1.3 these topologies are seen.

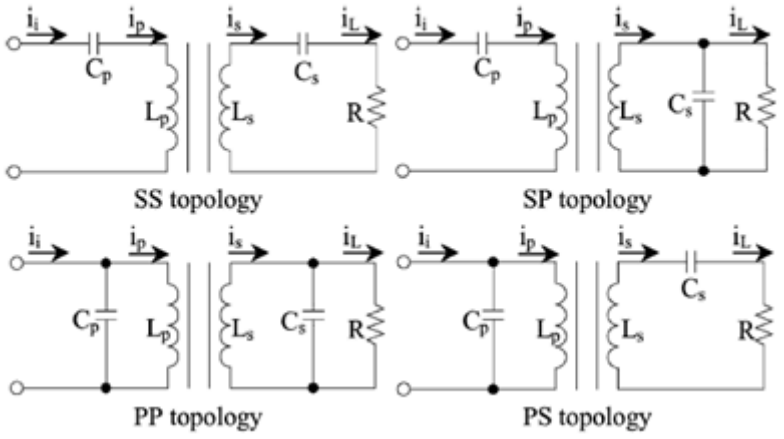

Figure 1.3. Basic resonant IPT topologies

1.2.3.3. Short-range magnetic induction

The first step in near-field transmission involves short distances. Strongly coupled contactless charging systems have been used for many years in devices such as electric toothbrushes. These use ferrite cores and require precise alignment, via mechanical constraints in the device such as projections or slots, to achieve strong coupling. The design goal is increased safety, as opposed to additional freedom of movement. As a result, there is no conductive path between the charger and the device and no additional freedom of movement. The challenge for a device suitable for portable electronics is to maintain high efficiency while allowing freedom of movement and reducing or eliminating the use of bulky magnetic materials.

1.2.3.4. Mid-range magnetic induction

The same concepts which work in the contactless charging system can be extended so that longer transfer distances are possible. Similar to using large antennas to improve the power transfer efficiency in a far-field system, a large inductive coil can be used to efficiently transfer energy over distances on the order of the size of the coil to a few times this size (since the coupling factor depends on the area of the coils). Two factors will tend to limit the maximum transmission distance for any magnetic-field-based near-field wireless power transfer system (for a given minimum efficiency): the mutual inductance between the transmitting coil and the receiving coil, and the parasitic resistance of the coils.

1.3. STATE OF THE ART FOR MID-RANGE MAGNETICALLY COUPLED RESONANT WPT

1.3.1. Introduction

For the two-coil system (just one transmitter and receiver), the resonant capacitor, along with the inductance of the coils, determines the operating frequency, which can then be tuned via mechanically or electrically adjustable capacitors. One disadvantage of this technique is that the coils must be operated at a frequency well below their self resonant frequency (SRF), which tends to decrease the maximum efficiency of a system with a fixed coil configuration, as can be seen in [50]–[52].

For the ICPT applications of several kilowatts such as charge of electric vehicles, energy efficiency higher than 90% is possible for small transmission distances and large coils. For the low-power wireless charging of mobile phones (up to 5W), a typical system energy efficiency exceeding 70% can be achieved. For these modern short-range domestic and industrial applications, the operating frequency is usually in the range of 20 kHz to a few megahertz. Such a frequency range is chosen because the power processing circuits (which are power electronics based switched mode power converters) with this operating frequency range are commercially available and economical. This frequency range is often neglected in recent mid-range wireless power research, but is a very important factor affecting the overall system energy efficiency and costs in both short-range and mid-range wireless power transfer systems, particularly when the power level is high. For non-radiative mid-range wireless power transfer, operating frequency ranging from 10 kHz in Tesla's work [6] to almost 200 MHz [53] has been reported. Using an operating frequency in excess of 10 MHz, for example, would substantially increase the costs and switching losses of the driving circuits, in addition to the radiation losses.

Although in this work a two coil system with small coils will be used, other configurations from literature are below explained.

1.3.2. Four-coil configuration

Many coil configurations are possible for midrange transfer; Kurs et al. [49] used a four-coil approach, utilizing two resonant structures, in this case cylindrical helices, both tuned to the same resonant frequency, as well as two additional coils that each couples to a resonator, serving the function of a matching network, as can be seen in figure 1.4.

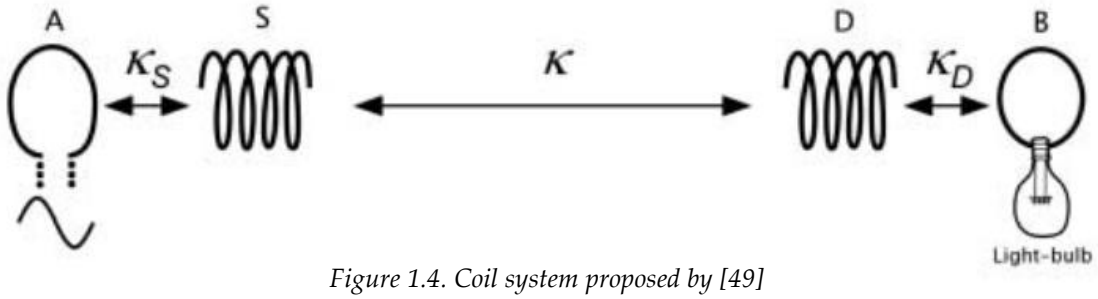

Figure 1.4. Coil system proposed by [49]

The following system has 4 coils, the primary (A), which is connected directly to an AC source, the coupling coil (S), which transmits the energy to high distance, the other coupling coil (D), which is the receiver of the energy, and the output coil (B), which supplies the load. It is important to notice that the couplings between coils A and D, A and B, and S and B are neglected because very weak coupling exists. In figures 1.5 and 1.6 this configuration and its electric equivalent circuit are shown.

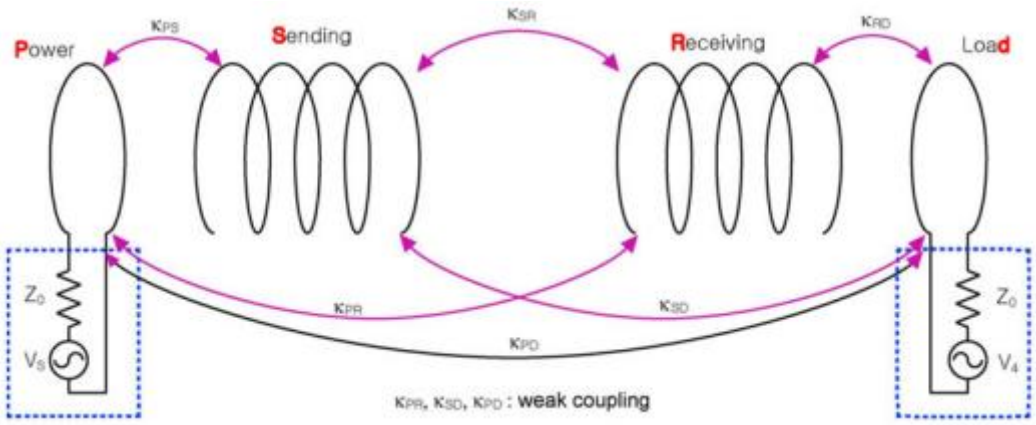

Figure 1.5. Another example of a 4-coil system [54]

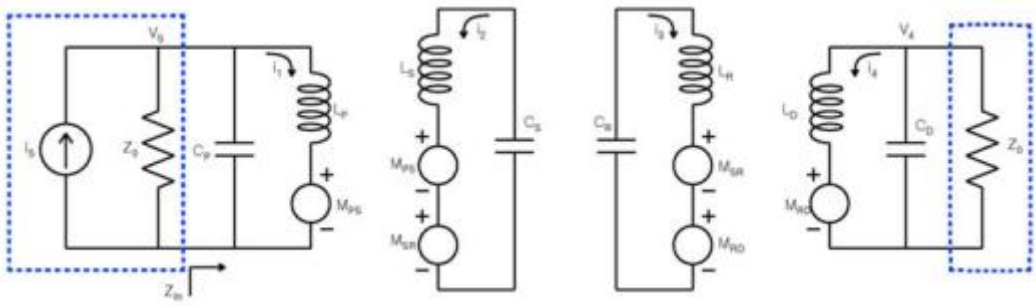

Figure 1.6. Equivalent circuit of a 4-coil system [54]

The use of the power driving coil and the load coil offer two extra mutual coupling coefficients for impedance matching (assuming that the mutual coupling of the driving loop and the load loop is negligible). In addition to the mutual coupling coefficient between the Sending resonator and the Receiver resonator ($\varkappa_{SR}$), the two extra coefficients are the mutual coupling coefficient between the Power driving coil and the Sending resonator ($\varkappa_{PS}$), and that between the Receiving resonator and the loaD coil ($\varkappa_{RD}$). Reference [54] contains a detailed circuit analysis of this 4-coil system and step-by-step explanations on how to match impedances in various stages in order to maximize power transfer. The 4-coil system provides 3 mutual coupling coefficients $\varkappa_{PS}$, $\varkappa_{SR}$ and $\varkappa_{RD}$ which can be utilized to maximize the power transfer if the following condition is met:

$$\frac{\kappa_{PS}\kappa_{RD}}{\kappa_{SR}} = 1$$

The 4-coil system provides a mechanism to extend the transmission distance compared with the basic two-coil system since the two extra mutual coupling coefficients (κ_{PS} and κ_{RD}) in the 4-coil systems provide extra freedom by minimizing κ_{SR} through the use of the previous equation. However, the impedance matching requirement also implies that such system has its overall energy efficiency not higher than 50%, because it uses the maximum power transfer principle, which is explained in section 1.3.3. This inherent limitation could form a bottleneck of this 4-coil approach for mid- and high-power applications, unless energy efficiency is not a primary concern. Due to this drawback, the difficulty of adjusting κ_{PS} and κ_{RD}, and also its complexity (it adds two resonators), the 2-coil system has been adopted for this work.

1.3.3. Transmission issues

The operating principles can be summarized as the maximum power transfer and maximum energy efficiency principles: if the WPT system is simplified in a circuit like that of figure 1.7, maximum power transfer will occur when $Z_L=Z_S^*$; however maximum energy efficiency will take place as the power of the load increases respect to that of the source impedance. This work is oriented to achieve maximum energy efficiency and proposes a method for it.

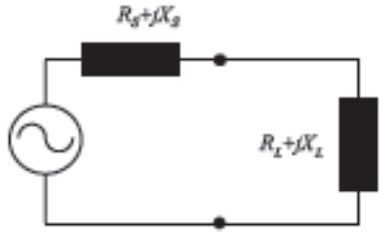

Figure 1.7. Equivalent circuit of a WPT system

An interesting phenomenon affecting WPT is frequency splitting, as can be seen in figure 1.8. When multiple receivers are powered, coupled mode frequency splitting occurs if two receivers are in close enough proximity that their magnetic fields are relatively strongly coupled, causing the peak frequency be divided into two peaks. Control circuitry to track the resonant frequency shifts and retuning the receiving coil capacitances is a potentially viable strategy for addressing this issue.

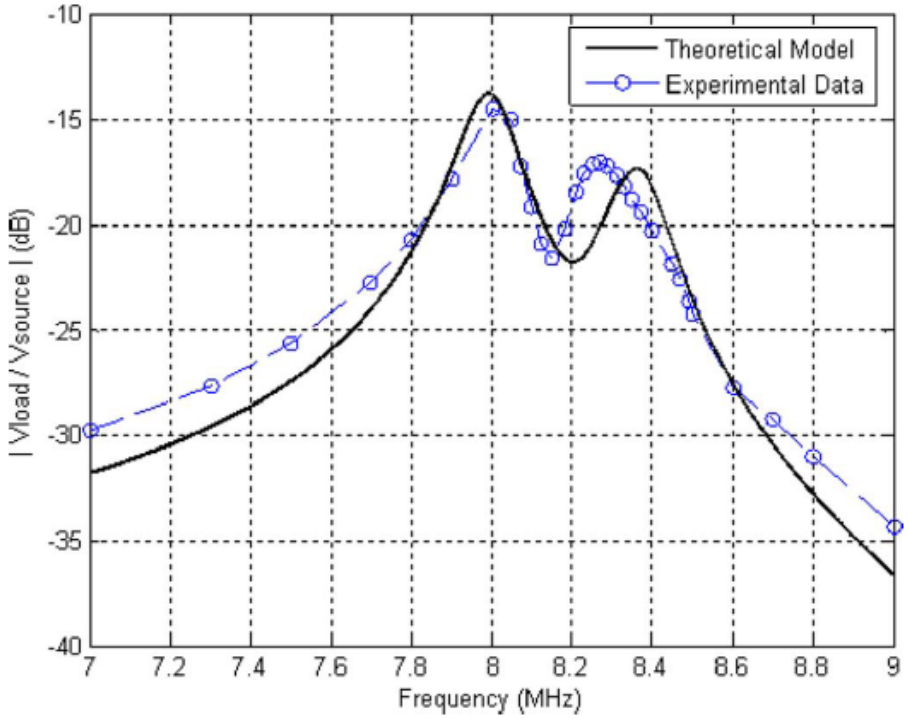

Figure 1.8. Frequency splitting example [80]

Another interesting application of WPT seen in literature [3] is domino resonators like that one shown in figure 1.9. By means of connecting several resonators between the transmitter and the receiver, the efficiency achieved is higher and the distance of transmission boosted. The demonstration of its better efficiency is done in appendix D of this document.

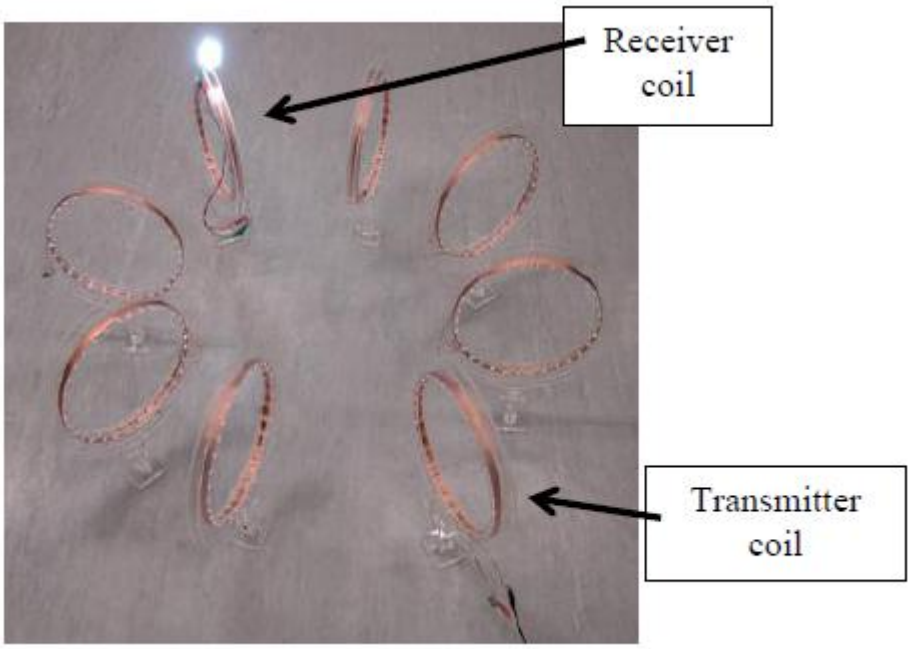

Figure 1.9. Domino resonator

1.3.4. Safety issues

With increasing transmitted power level and transmission distance for mid-range wireless power transfer, one obvious concern are the safety issues related to human exposure of electric, magnetic and electromagnetic fields (EMF). Established adverse effects on health depend on the frequency and intensity of the EMF. In general, 100 kHz is a crossover frequency below which the electro stimulation effects dominate, and above which the heating effects dominate [3]. For short-range and low-power applications such as wireless charging pads for portable electronics (5W), the human exposure problems can be mitigated by using localized charging principle together with the use of the EM shields [22]. For short-range high-power applications such as wireless charging of electric vehicles (2kW), special magnetic designs can be adopted to guide the magnetic flux in order to minimize the leakage flux [56]. So as to comply with the human exposure regulations, an idea of detecting the presence of humans and lowering the power level when humans are in the very close vicinity has been suggested [57]. For short-range applications, only the leakage flux is of concern and therefore the EMF issues are less severe.

For mid-range wireless power transfer, the two guiding regulatory documents are a) the ICNIRP Guidelines for Limiting Exposure to Time-varying Electric, Magnetic and Electromagnetic fields (1Hz to 100kHz) [58] and (up to 300GHz) [59] and b) IEEE Standard for Safety Levels with Respect to Human Exposure to Radio Frequency Electromagnetic Fields 3kHz to 300 GHz [60]. The typical human exposure limits of the ICNIRP and IEEE standards are shown in figures 1.10 and 1.11, respectively. The ICNIRP regulations provide two different sets of limits for occupational exposure and for general public exposure, while the IEEE standard provides only one set of limits. For mid-range wireless power transfer, the majority of the work is conducted at or below 13.56 MHz; within this frequency range, it can be observed from figures 1.10 and 1.11 that the maximum EMF levels for both the electric and magnetic fields become more stringent as the frequency increases.

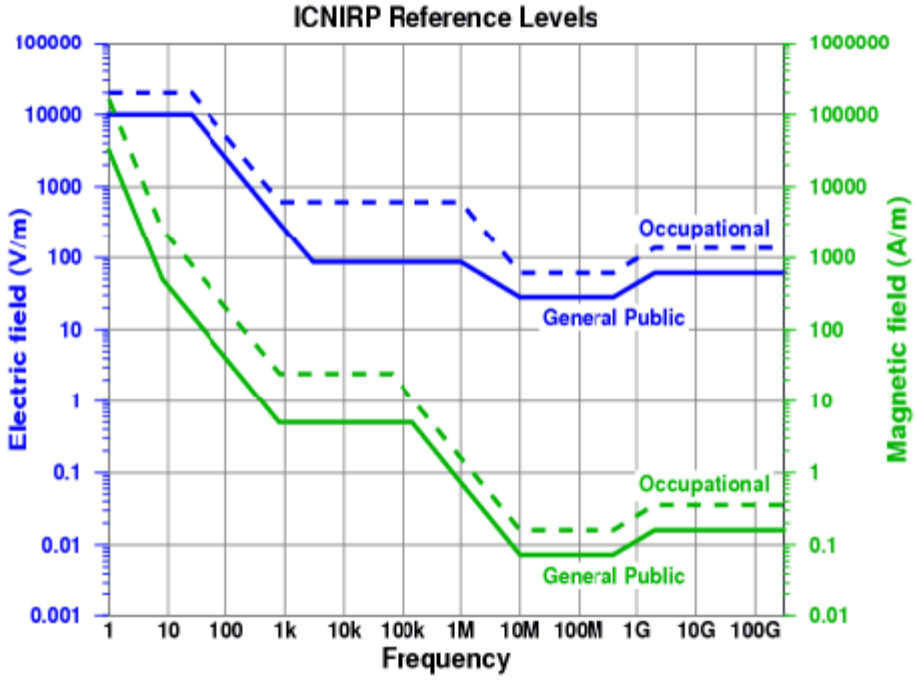

Figure 1.10. ICNIRP Reference levels for exposure to time-varying electric and magnetic fields

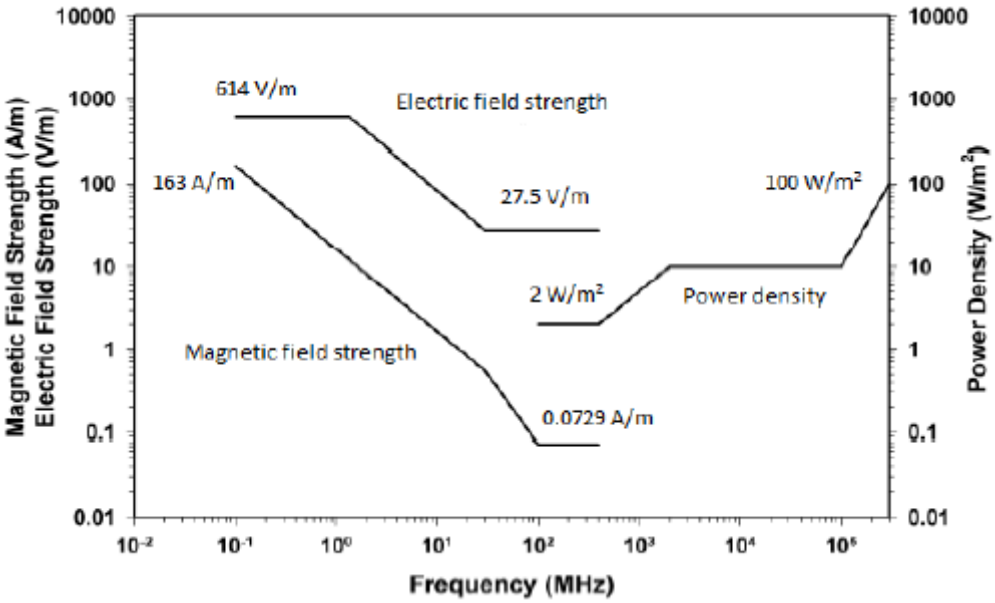

Figure 1.11. IEEE Reference levels for exposure to time-varying electric and magnetic fields

Several tests have been reported to evaluate the EMF issues of mid-range wireless power transfer for the 4-coil systems. The report in [61] in fact sheds some light on the EMF issues of the 4-coil system reported in [49]. When 60W is transferred over 2m between the sending resonator and the receiving resonator under an operating frequency of 10MHz, the electric field in the position halfway between the two resonators is E_{rms}=210V/m, and the magnetic field is H_{rms}=1A/m; at the point of 20 cm from the resonator coil surface the electric field and magnetic field increase to E_{rms}=1400V/m and H_{rms}=8A/m, respectively. Under the 10 MHz operation, the electric and magnetic field exposure levels are higher than their respective limits shown in figure 1.11. In order to comply with the IEEE regulations, the author of [58] replaces the self-resonant coils with capacitively-load loops to confine the electric field in the capacitors and lowers the operating frequency to 1MHz (which further reduces the transmission efficiency).

1.3.5. Recent applications

Two examples of recent applications are shown below. Unlike this work, whose goal is making an efficient transmission using small coils for the receiver that can be embedded in a mobile device, the following employ large coils.

In [62], transmission efficiencies as high as 76% for an output power of 40W are achieved over a gap of 1m, with the set-up of figure 1.12.

Figure 1.12. Set-up used in [62]

Besides, it is shown that the coupling coefficient k is almost constant when the angular misalignment is below 60º, as exposed in figure 1.13.

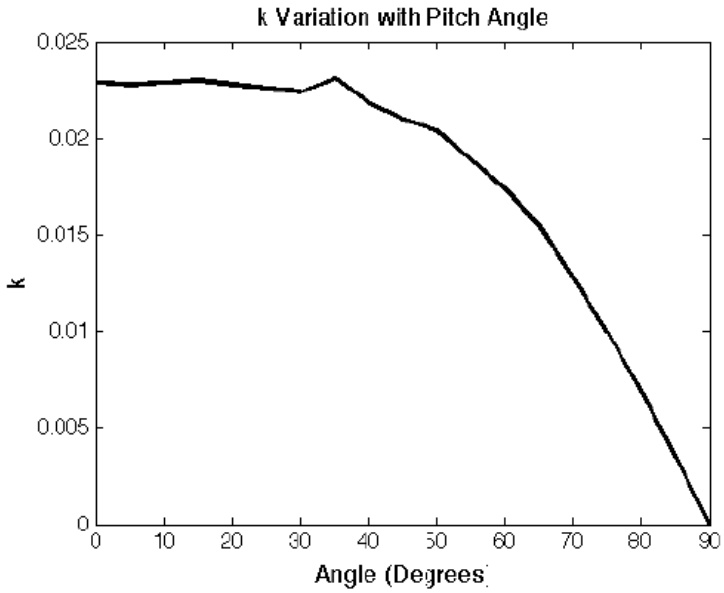

Figure 1.13. Coupling coefficient with respect to misalignment angle between coils [62]

In [63] 5m-off-distance inductive power transfer systems that have optimally shaped cores in the primary and secondary coils are proposed, and schematized in figure 1.14. Instead of conventional-loop-type coils for magnetic resonance scheme, magnetic dipole type coils with cores are used for drastic reduction in deployment space and quite long wireless power transfer. Experimentally obtained maximum output powers and primary-coil-to-load-power efficiencies for 3m, 4m, and 5m at 20 kHz were 1403W, 471W, 209W, and 29%, 16%, 8%, respectively.

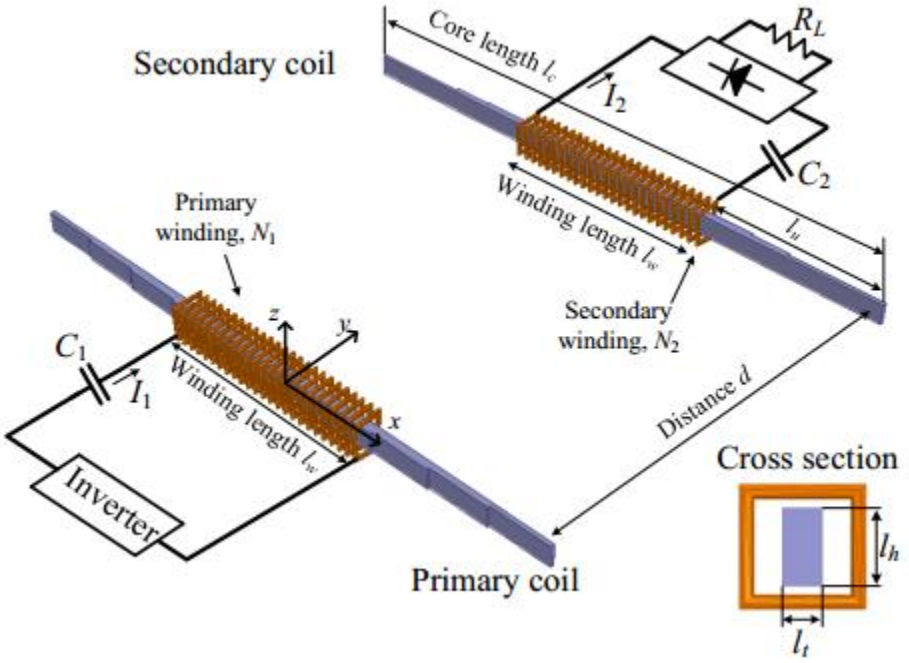

Figure 1.14. Configuration scheme used in [63]

1.4. OBJECTIVES AND PROPOSED SOLUTION

Many studies have appeared the last years about WPT, however, only a few of them tackle its real implementation and optimization. The main goal of this work is the study and implementation of an optimized resonant inductive power transfer system, particularly for a low power application in which the transmission distance is about the coil diameter (mid-range transmission). To reach this goal, the following steps will be carried out:

- Understanding the influence of the geometric and physical parameters of the coil on the performance of the WPT:
  With the purpose of having a primary and a secondary which improve the energy transmission and also considering practical issues like size, cost, shape..., physical and electrical simulations will be done, besides using analytical models from literature and a specially designed tool (appendix C). Real effects like parasitic resistances, deviation from the operating frequency, misalignment, etc, will be taken into account for the better comprehension of the energy transmission mechanism and to identify the sources of power losses.

- Optimization of the wireless link:
  Several methods to optimize the magnetic link depending on the circuit constraints will be proposed. This will allow improving the efficiency of the transmission reducing the losses, making this way possible to solve partially one of the main drawbacks of the WPT due to its low coupling.
- Optimization of the coils and transmission parameters:
  Thanks to the knowledge of the coils and with the aid of a software to extract their RLC parameters, a special software will be developed to select the geometrical parameters of the coils and the operating frequency which allows maximizing the mutual inductance and so the power transferred to the load and the efficiency.
- Validation with experimental results:
  The method proposed in chapter 3.3 will be validated with a novel mid-range configuration in chapter 5, unlike chapter 3.3.1 where it will be validated for a short-range transmission. So, the versatility of this optimization method is proven.

The future deployment of WPT systems for low power mobiles devices can be closer and the knowledge from this work may help it to occur.

2. STUDY AND ANALYSIS OF THE WIRELESS LINK

2.1. INTRODUCTION

In this chapter, with the help of the tool explained in appendix C, many tests are carried out in order to deeply understand all the parameters involved in the resonant WPT between two coils.

The conclusions for each test will be also explained and taken into account to improve the geometrical design of the coils.

2.2. MAGNETIC DIPOLE APPROXIMATION

In this section, it will be evaluated if the mutual inductance between two coils can be obtained by means of the magnetic dipole [78] approximation (2.1):

$$M = \frac{\mu_0 N_1 N_2 A_1 A_2}{2\pi d^3} \tag{2.1}$$

In the following figures, the curves for the mutual reactance $X_m = 2*\pi*f*M$, will be plotted for several configurations depending on the distance between the coils, calculated through (2.1) and using FastHenry (with the tool explained in Appendix C). This way, it can be seen when complex and time-consuming simulations could be substituted by the simpler formula (2.1).

The results for 2 coaxial square coils of $1m^2$, one turn each one, and at 500kHz are shown in figure 2.1; its visual representation is presented in figure 2.0:

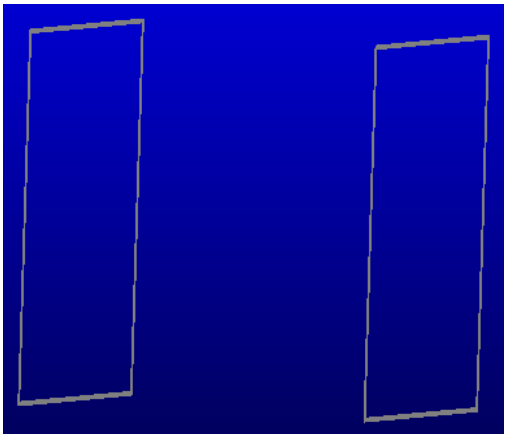

Figure 2.0. Visual representation of the coils in FastHenry

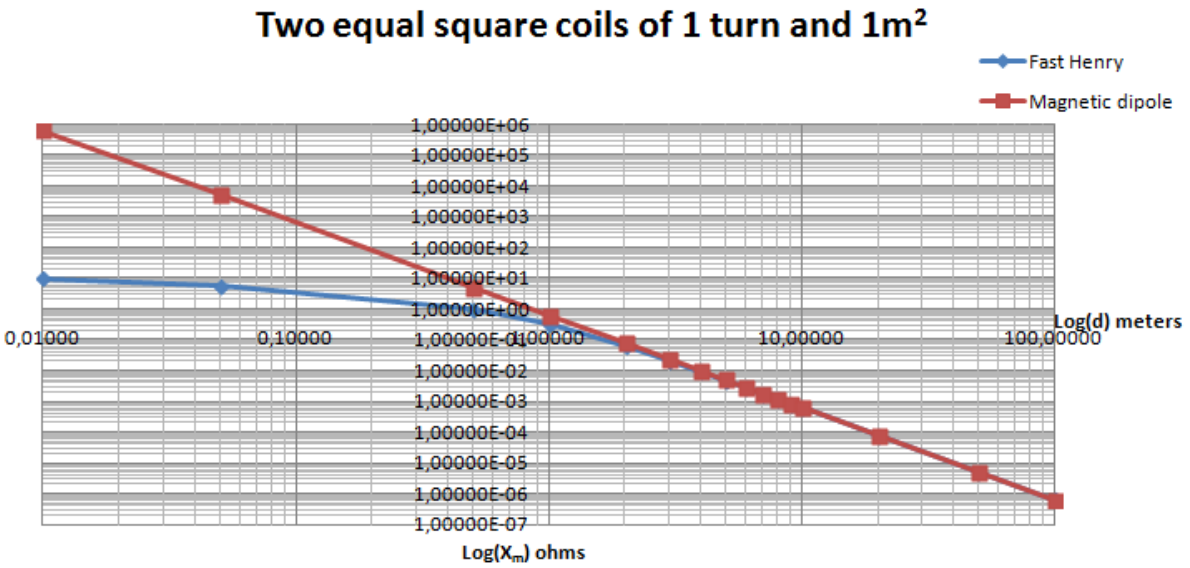

Figure 2.1. Two equal square coils of 1 turn and 1m²

Also, for two coaxial square coils of 6 turns and 1m² in figure 2.2; for two coaxial square coils of one turn with different areas of 1m² and 25cm² in figure 2.3; and for two coaxial square coils of one turn with areas of 1m² and 1cm² in figure 2.4:

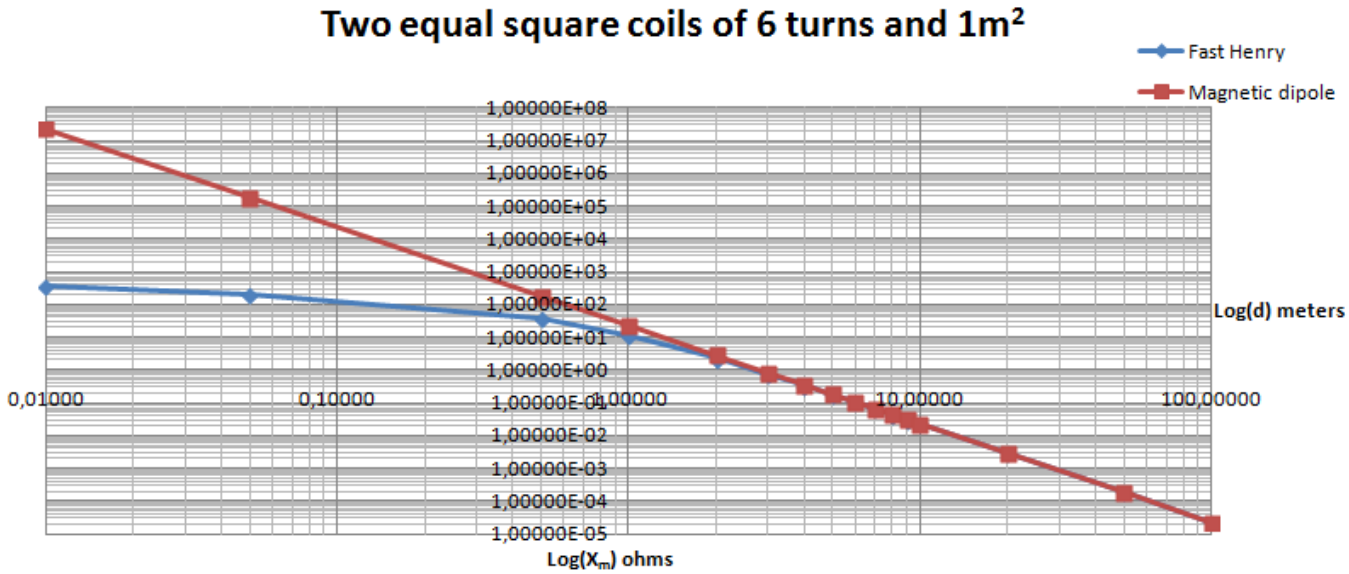

Figure 2.2. Two equal square coils of 6 turns and 1m²

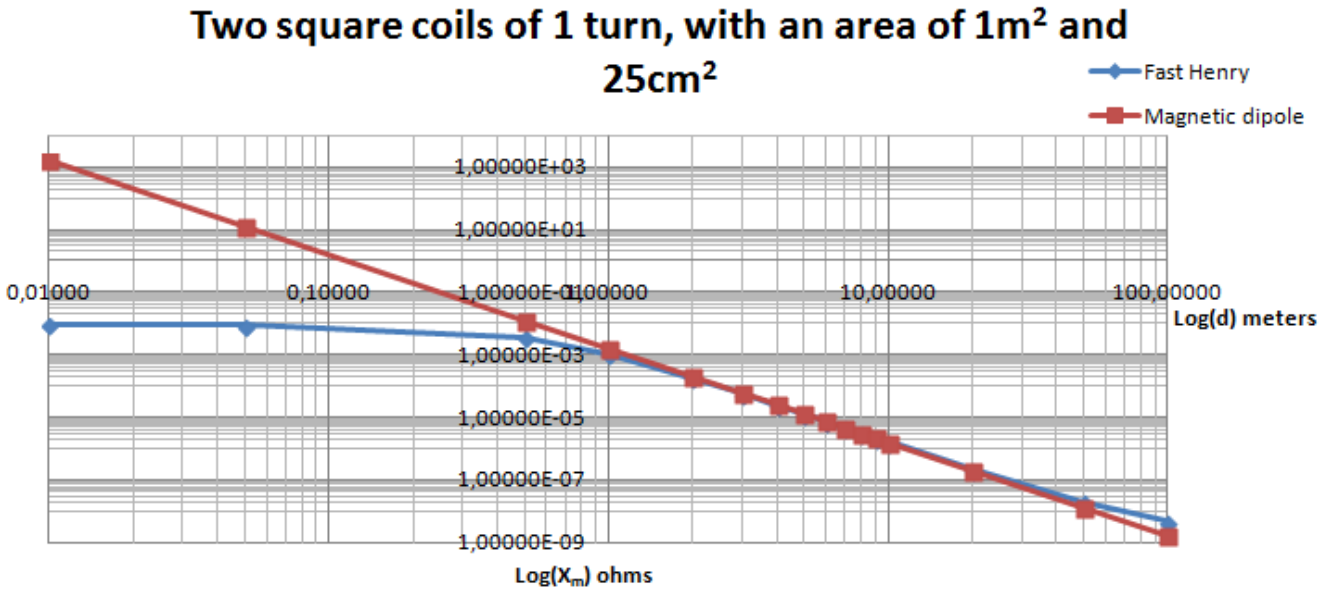

Figure 2.3. Two square coils of 1 turn with different areas, 1m² and 25cm²

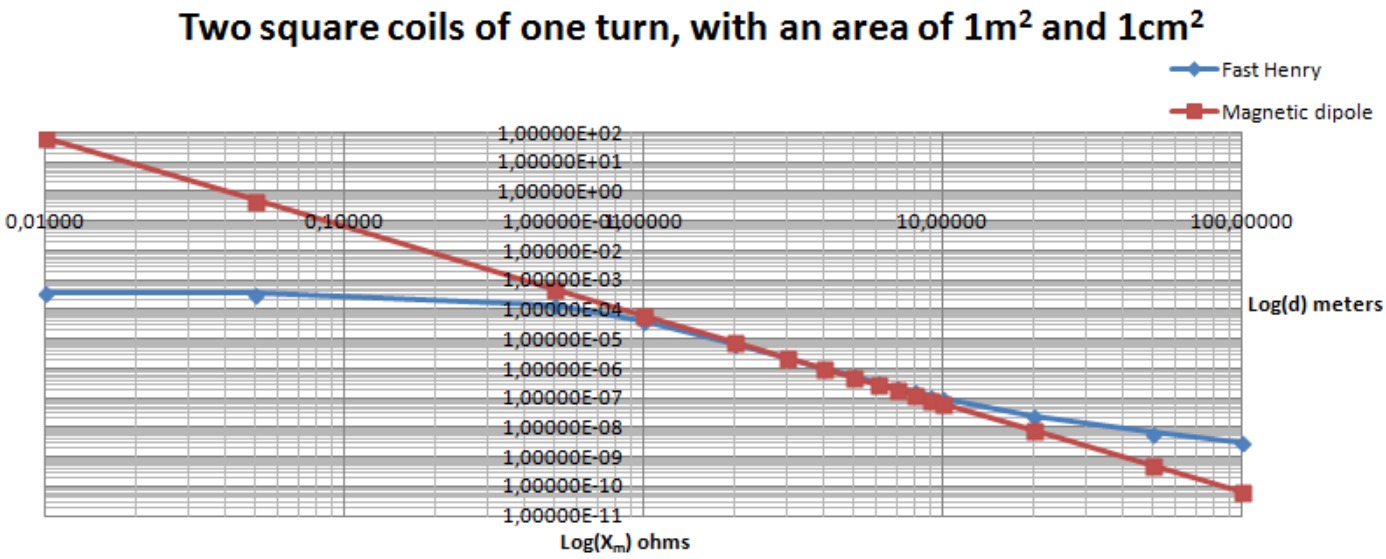

Figure 2.4. Two square coils of 1 turn with different areas, 1m² and 1cm²

From the above figures, comparing the mutual reactance using (2.1) and the extremely accurate simulation software FastHenry, it can be determined that when the separation distance is larger than three times the side of the larger coil, the error produced using (2.1) is less than 10%, and both curves seem overlapped.

The linear appearance of the curve which represents the magnetic dipole approximation is because in (2.1) M is proportional to ($1/d^3$) and in the previous figures, both X_m and distance d are represented logarithmically.

In figures 2.5 and 2.6 it is shown how X_m varies depending on the area of the transmitter and on the receiver (both have 1 turn), respectively, using FastHenry software:

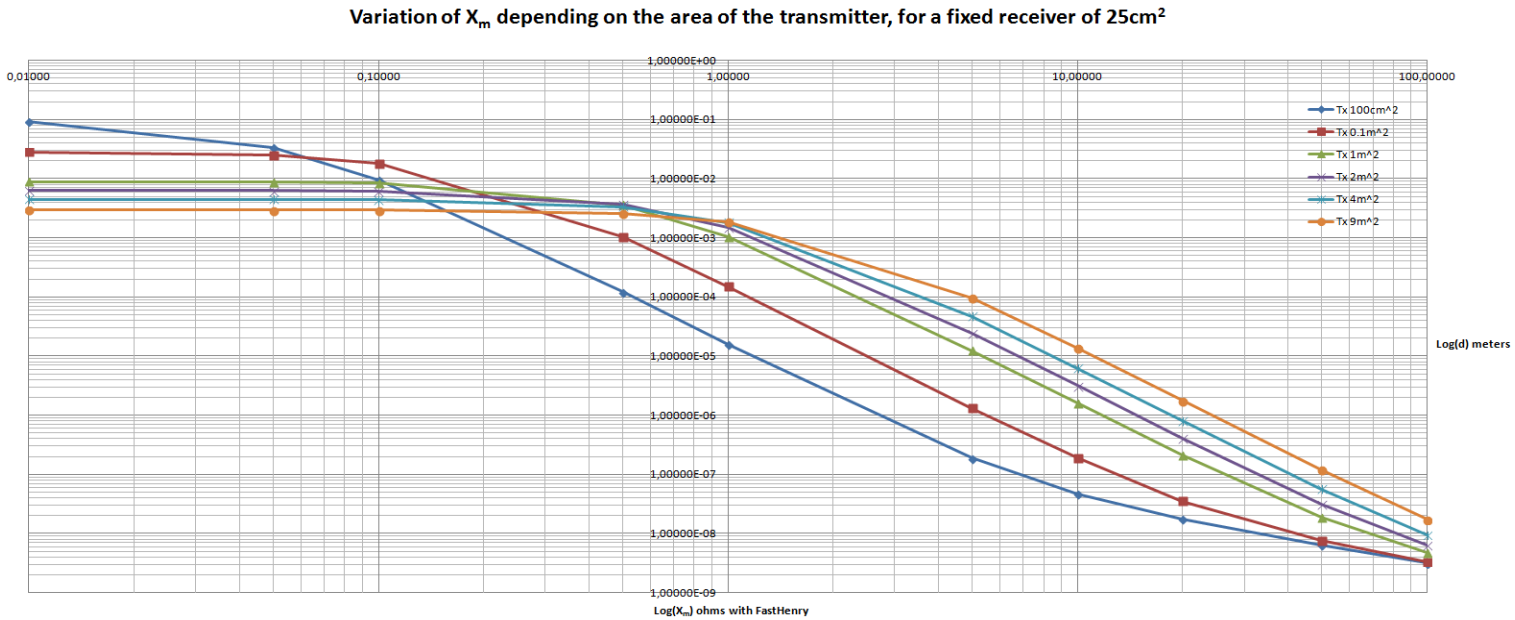

Figure 2.5. Calculation of X_m for different transmitter areas, with a receiver area fixed to 25cm²

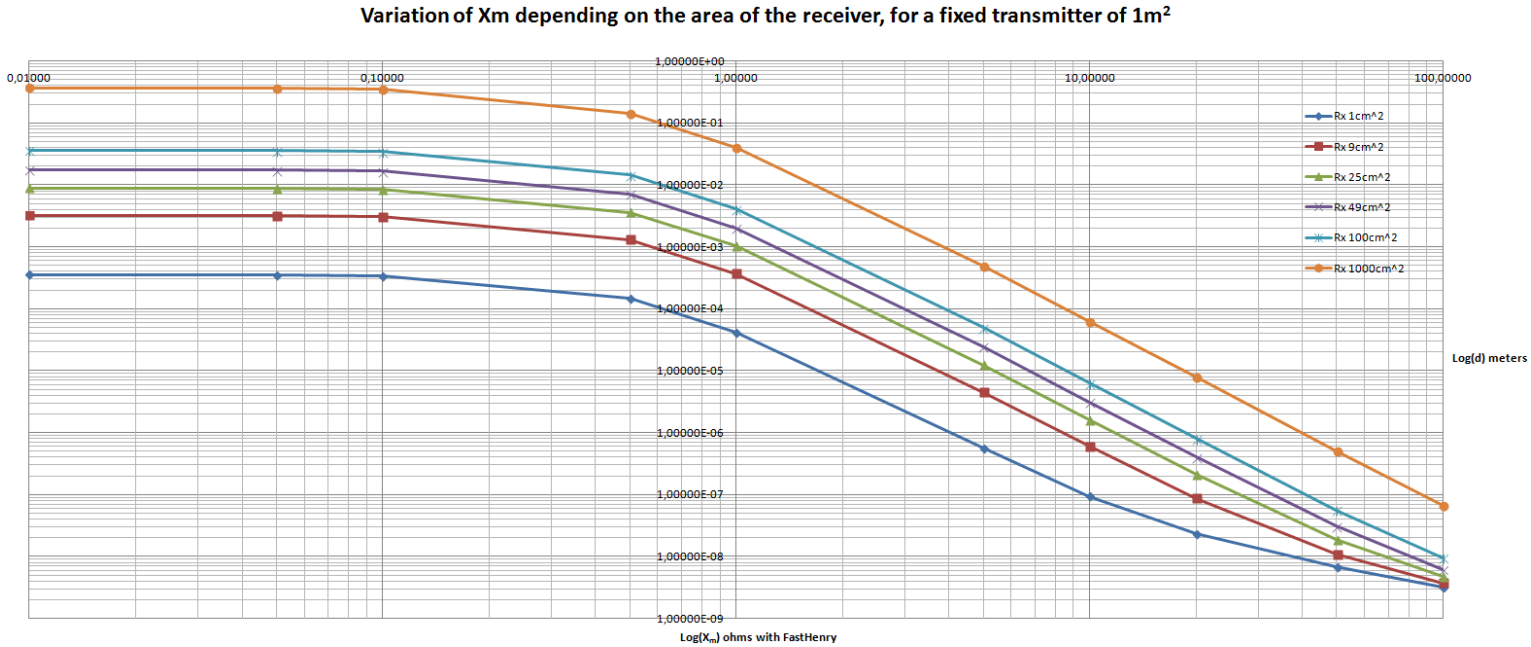

Figure 2.6. Calculation of X_m for different receiver areas, with a transmitter area fixed to 1m²

From the last two figures, it would be easy to choose the area of the coils needed to have a particular X_m value. If X_m value were negative would mean that the electromotive force (emf) induced in one coil by a change of current in the other coil is in the opposite direction than the emf resulting from the same change in current when the loops are arranged in a coaxial position [79].

Other analytical accurate ways of calculating the mutual inductance between coils with different shapes apart from magnetic dipole approximation are introduced in [78] and [79], and they are valid for every distance between coils, unlike magnetic dipole approximation. [79] is more accurate and doesn't need very large tables like [78]; however, it is more complicated since it involves the resolution of elliptic integrals of the first and second kind to solve the following formula:

$$M = \frac{\mu_0 R_S}{\pi} \int_0^{2\pi} \frac{[p_1 \cos\varphi + p_2 \sin\varphi + p_3]\Psi(k)}{k\sqrt{V_0^3}} d\varphi$$

Nevertheless, all magnetic dipole, [78] and [79] become quite inaccurate when the area occupied by the turns is significant compared to the total area of the coil; for that reason, the calculation of the mutual inductance from simulation through FastHenry will be preferably used.

2.3. EQUIVALENT WIDTH

It has been proven, by means of the tool described in appendix C, that it is equivalent, from the efficiency point of view, whether the turns are located on the primary, or in the secondary or shared among them: for a 1mx1m primary, 5cmx5cm secondary, at 500kHz, both separated 1m, the result is equivalent in the following three cases: a primary of 49 turns and a secondary of 1 turn, a primary of 1 turn and secondary of 49 turns, or a primary and a secondary with 7 turns each one.

Since the magnetic field created by a coil with N turns and current I is equivalent to that of a coil with 1 turn and current N*I, it is studied which of both configurations is preferable:

Two 1mx1m coils, with 10 turns each one, 0.1mm width, separation between turns 0.1mm, and separated 1m, have an efficiency of 4.78%; while if these coils have an equivalent width of 1.9mm (10*0.1+9*0.1) and just one turn, its efficiency is 9.11%. So, it is better, as for the efficiency, having 1 turn with a current of value N*I than N turns with a circulating current I.

This test has been also carried out in other scenarios and the results show that there is not noticeable difference, as Ampere's law predicts $\int Hdl = Number\ of\ turns * current$, in terms of efficiency, between both configurations. However, these tests were made without considering the power stage, whose losses are bigger as the current it manages is increased.

2.4. INFLUENCE OF THE AREA, THE NUMBER OF TURNS AND THE FREQUENCY ON THE EFFICIENCY

In this section, several analysis are carried out (using the tool described in appendix C) depending on some factors and in each case the voltages, currents and efficiencies will be shown; these values were calculated using the formulas from section 3.3 for a series-series configuration, which cause the optimum case to take place. In all cases, the coil is implemented with just one turn and an equivalent width (explained in section 2.3) as it had n number of turns, where n will be said for each test; for this reason, the voltage values at the source ($V1_{rms}$) and at the load ($V2_{rms}$) are quite small.

2.4.1. Influence of the secondary coil size

In table 2.1 it can be seen how the efficiency increases as the secondary coil area gets larger.

Frequency 500kHz, in resonance, distance 1m	Primary 1mx1m and 400 turns (equivalent width), for different secondary areas with 100 turns (equivalent width)				
	$I1_{rms}$ (A)	$I2_{rms}$ (A)	$V1_{rms}$ (V)	$V2_{rms}$ (V)	Efficiency (%)
50x50mm	170,4566933	23,62182965	2,694103043	0,043922817	0,217863952
100x100mm	53,95547998	14,37324639	0,895461763	0,078477501	2,094146454
150x150mm	27,50979758	10,64185415	0,530258301	0,11586205	7,26324155
200x200mm	17,40701656	8,300847818	0,427790514	0,156294997	15,38649932
250x250mm	12,46004751	6,648118399	0,404477766	0,197963352	24,71847324
300x300mm	9,660928082	5,451009384	0,411519686	0,240028517	33,7448888

Table 2.1. Different results depending on the secondary coil geometry

2.4.2. Influence of the primary coil size

In table 2.2 the test is similar to the previous one, but varying the primary coil area. It is noticeable that from 1500x1500mm on, the efficiency remains practically the same.

Frequency 500kHz, in resonance, distance 1m	Secondary 200mmx200mm and 400 turns (equivalent width), for different primary areas with 400 turns (equivalent width)				
	$I1_{rms}$ (A)	$I2_{rms}$ (A)	$V1_{rms}$ (V)	$V2_{rms}$ (V)	Efficiency (%)
500x500mm	38,9029214	20,3906241	0,33432407	0,06834857	7,989132564
1000x1000mm	15,8715064	18,4792551	0,368409	0,11999238	17,66154751
1500x1500mm	10,6552179	17,5357697	0,42358542	0,16324805	22,70971836
2000x2000mm	9,07741723	17,4904838	0,48884322	0,18809353	22,95477839

Table 2.2. Different results depending on the primary coil geometry

2.4.3. Influence of the number of turns

In table 2.3 it can be seen how the efficiency increases as the number of turns grows; also, from 300 turns on, the efficiency is almost the same.

Frequency 500kHz, in resonance, distance 1m	Primary 1mx1m and secondary 200mmx200mm, depending on the number of turns in both coils				
	$I1_{rms}$ (A)	$I2_{rms}$ (A)	$V1_{rms}$ (V)	$V2_{rms}$ (V)	Efficiency (%)
100 turns (equivalent width)	15,9913598	9,13764437	1,08051037	0,16101256	5,896309496
200 turns (equivalent width)	14,1248639	12,4870265	0,58035175	0,14910103	12,58292698
300 turns (equivalent width)	14,3701267	15,4777087	0,43466349	0,13576576	16,55741402
400 turns (equivalent width)	15,8715064	18,4792551	0,368409	0,11999238	17,66154751

Table 2.3. Different results depending on the number of turns in both coils

2.4.4. Influence of the frequency

In table 2.4, the effect of incrementing the resonance frequency is seen in terms of efficiency and circuit parameters. Such effect is always positive in terms of frequency.

In resonance, distance 1m	Primary 1mx1m and secondary 200mmx200mm, 400 turns in both (equivalent width), varying the frequency				
f (Hz)	$I1_{rms}$ (A)	$I2_{rms}$ (A)	$V1_{rms}$ (V)	$V2_{rms}$ (V)	Efficiency (%)
100000	70,4078966	24,1704617	0,92538564	0,049943	1,540800262
125892,5412	56,7655015	23,6494479	0,78100524	0,05454214	2,268347905
158489,3192	45,7723468	23,0648764	0,66398864	0,06056674	3,316908839
199526,2315	36,9216784	22,3940485	0,57028833	0,06830448	4,803165775
251188,6432	29,8050482	21,6134507	0,49653121	0,07799821	6,862310937
316227,766	24,0932302	20,7037748	0,43986486	0,08981196	9,631172872
398107,1706	19,5205649	19,6564065	0,3978534	0,10381452	13,21773335
501187,2336	15,8715064	18,4792551	0,368409	0,11999238	17,66154751
630957,3445	12,9688954	17,198855	0,3497392	0,13829545	22,90117065
794328,2347	10,6654174	15,8560849	0,34034156	0,15869934	28,76631995
1000000	8,83846004	14,4970604	0,33903388	0,18125666	34,99965019

Table 2.4. Different results depending on the resonance frequency

2.5. SKIN AND PROXIMITY EFFECTS

In this section, both high frequency effects are evaluated to know their influence.

If the number of turns is big but the conductor radius is smaller than the skin depth, $\delta = \sqrt{\frac{2\rho}{\omega\mu_r\mu_0}}$, then proximity effect is negligible since the total resistance of the coil is equal to the resistance of one turn multiplied by the number of turns.

As the conductor radius increases, proximity effect becomes more important, and the error obtained calculating the total resistance through the resistance of one turn considering skin effect times the number of turns will not be negligible. For example, at 500kHz, with 5 turns, for radius r>δ, for a particular design, the calculated resistance is 3Ω while the result of multiplying the resistance of one turn times the number of turns is 1.25Ω.

Also, it has been said many times that it's not very advisable to use a conductor radius greater than the skin depth; however, as the conductor radius increases, always its resistance is slower (for example, for a conductor with a skin depth of 0.165mm at 500kHz, its resistance is 35Ω when it is 0.1mmx0.1mm, while 3Ω for 1mmx1mm); such reduction depends on the square root of the frequency.

It is also relevant to note that as the conductor radius makes bigger, the coil inductance gets reduced: for the last example resistance changed from 35Ω to 3Ω, but the inductance from 161.42μH to 113.95μH.

As will be seen in section 2.9 and according to the tests made above, proximity effect must be considered in the calculation of the coil resistance; therefore, the most accurate way of obtaining such resistances is by means of simulation (in this case using FastHenry).

2.6. ANALYSIS FOR DIFFERENT PCB COPPER THICKNESSES

Although it is obvious that, for a coil implemented in a PCB, the efficiency will be higher as the copper layer thickness increases (because it reduces the self resistance), such efficiency will be simulated for common PCB layer thicknesses (105µm, 70µm and 35µm) in two scenarios (figures 2.7 and 2.8, using the tool described in appendix C). This test has been done bearing in mind that currently low cost PCB manufacturing requires 70µm and 35µm for layer thickness (and sometimes only the last one); in addition to this, the thicker the copper the higher the cost, so it's better using 35µm layers if the efficiency doesn't penalize too much.

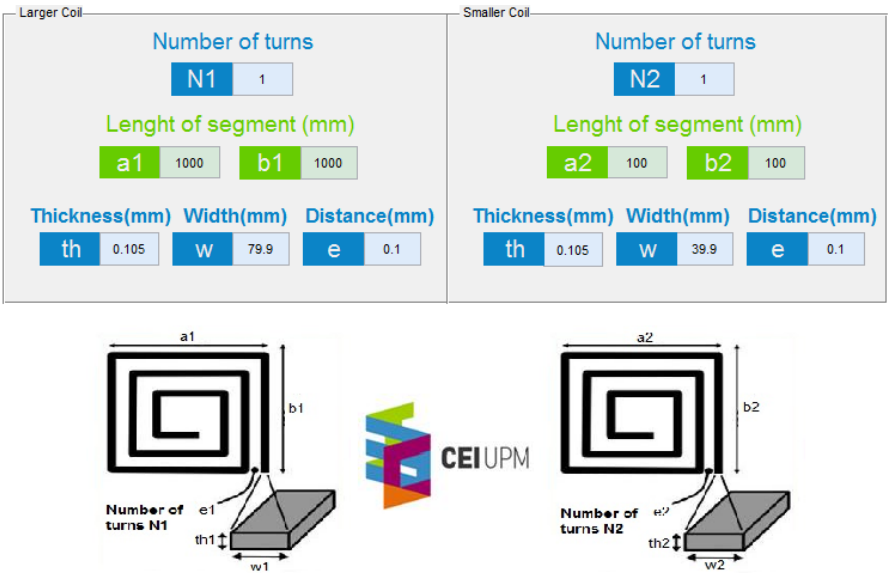

Figure 2.7. First configuration (using 105µm thickness)

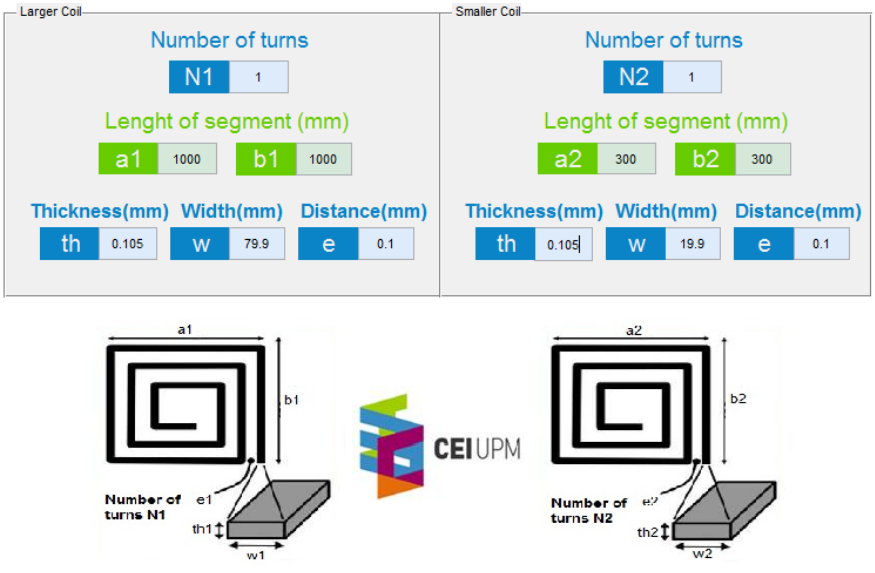

Figure 2.8. Second configuration (using 105µm thickness)

In both scenarios the operating frequency is 1MHz, the coils are coaxial and separated 1m, and the power received by the load is 1W.

For the first one, figure 2.7, the efficiency is 6.13% for 105µm layer, 4.64% for 70µm and 2.69% when 35µm technology is used. For the second one, figure 2.8, the efficiency is 53%, 48% and 38.1% for 105µm, 70µm and 35µm, respectively. With these results, it seems obvious that it is better a thicker layer, but if there is no alternative, smaller thickness can be used at the expense of the efficiency.

2.7. EQUIVALENCE BETWEEN THICKNESS AND WIDTH

The primary is intended to be implemented in a 1mx1m large structure; to do that, copper foil tapes can be utilised. Doing so, it will imply that the layer thickness (th1 in figure 2.9) is greater than the trace width (w1 in figure 2.9) of the turns, unlike how it is done for the secondary. The meaning of width and thickness can be also seen in figure 4.4.

So, to validate this method of construction for the primary, some simulations are used with the structure defined in figure 2.9, for an operating frequency of 1MHz, coaxial coils separated 1m and 1W received by the load.

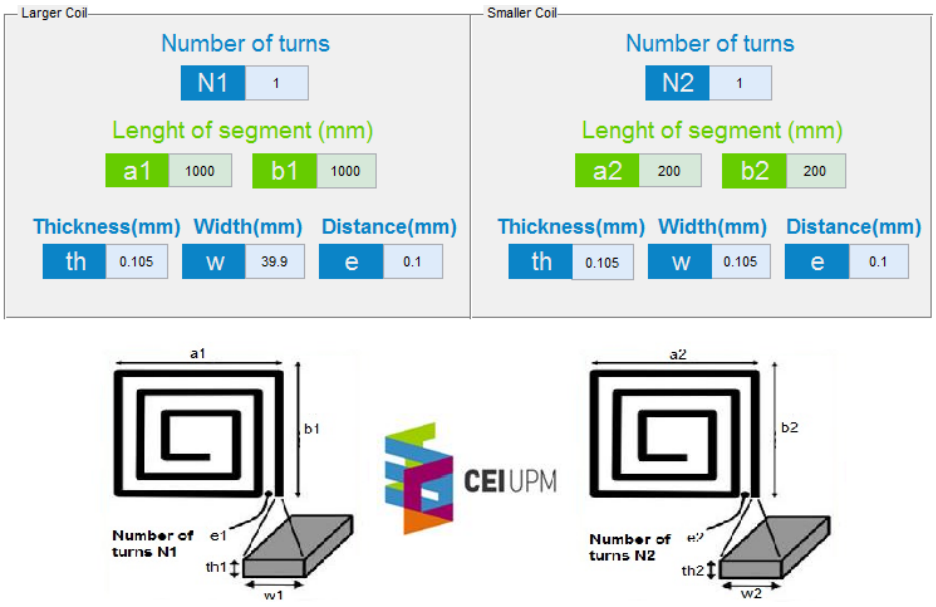

Figure 2.9. Example of primary and secondary coils used to do the simulations

If the thickness is 105µm and the widths 19.9mm, 39.9mm and 79.9mm, the efficiencies are 0.293%, 0.53% and 5.174%, respectively. However, if the width is always 105µm and the thicknesses 19.9mm, 39.9mm and 79.9% the efficiencies are 0.3%, 0.55% and 5.146%.

From the above results, almost the same when the width value is substituted by the thickness, it is concluded that a primary with a thickness higher than its width could be carried out, without affecting the efficiency of the system.

2.8. ORIGIN OF THE LOSSES

If the efficiency η is equal to P_{out}/P_{in} and given that $P_{in}=P_{out}+P_{losses}$, it results (2.2), with η expressed in %:

$$P_{losses} = P_{out}\left(\frac{100}{\eta} - 1\right) \qquad (2.2)$$

P_{losses} include the resistive losses, i.e., the power dissipated in the primary coil resistance and in the secondary coil resistance. Since the current on the primary coil must compensate the low coupling between coils, the losses of the primary will be in principle greater than the losses of the secondary; for this reason, the optimization of the primary has a bigger priority (as done in 2.9).

For example, for the scenario of figure D.2 in appendix D, the power dissipated in the primary coil is 0.311W but in the secondary coil is 0.2W, despite being the same geometrical structure for both. This difference will be incremented as the coupling factor k is reduced.

2.9. INFLUENCE OF THE PRIMARY INTERWINDING DISTANCE ON EFFICIENCY

As seen in section 2.8, the majority of the losses come from the primary coil; thus, optimizing the primary has a greater influence on efficiency than optimizing the secondary.

For a fixed secondary coil and operating at 1MHz, the interwinding distance of the primary is evaluated in order to measure its influence on the efficiency and on the primary losses; the primary is a 1x1m coil with 25 turns, with a thickness of 15mm and 0.105mm width; the power received by the load in every case is 1W. The primary resistances and inductances are also shown (R_1 and L_1, respectively):

- 0.15mm: η 13.5%, primary losses 5.67W, R_1 15Ω, L_1 2.185mH.
- 0.3mm: η 13.5%, primary losses 5.67W, R_1 14.8Ω, L_1 2.1mH.
- 1mm: η 15.44%, primary losses 4.74W, R_1 11.81Ω, L_1 1.82mH.
- 1.5mm: η 16.87%, primary losses 4.215W, R_1 10.11Ω, L_1 1.68mH.
- 2.5mm: η 19.27%, primary losses 3.51W, R_1 7.8Ω, L_1 1.47mH.
- 5mm: η 23.21%, primary losses 2.685W, R_1 4.88Ω, L_1 1.12mH.
- 8mm: η 25.39%, primary losses 2.3433W, R_1 3.3Ω, L_1 0.836mH.
- 12mm: η 25.47%, primary losses 2.33W, R_1 2.26Ω, L_1 0.58mH.

Using distances larger than 12mm the efficiency gets reduced.

From the previous results, since the resistance decreases as the interwinding distance increases, it can be said that the majority of the losses come from the proximity effect, as skin effect would make greater the primary resistance for a bigger interwinding distance.

Therefore, a special care has to be paid to the interwinding distance at the operating frequency due to its great influence on the efficiency, especially for the primary.

2.10. INFLUENCE OF THE DESIGN PARAMETERS ON THE COIL VOLTAGES

2.10.1. Introduction

The quality factor Q is shown in (2.3)

$$Q = \frac{f_0}{BW} = \frac{P_{stored}}{P_{dissipated}} = \frac{{I_{RMS}}^2 * X}{{I_{RMS}}^2 * R} \qquad (2.3)$$

Therefore I^2_{RMS} *X is equal to Q *I^2_{RMS} *R. For a series resonant circuit the power factor is equal to one, so cos(α)=1 and thus I^2_{RMS} *R=V_{RMS} *I_{RMS} => I^2_{RMS} *X=Q *V_{RMS} *I_{RMS} => V_{LRMS} = Q *V_{RMS}, and since Q is high to get high values of efficiency, V_{LRMS} will be very high, what is not desired in terms of safety.

In the following sections, the analysis is focused on the reduction of the coil voltages without affecting the efficiency, since it is not recommended to have a very high voltage in a mobile device such as a mobile phone for the matter of safety.

2.10.2. Effect of the number of turns

When two different primary coils are used, one of 25 turns and the other of 5 turns with an equivalent width, i.e. only one turn with the width corresponding to the number of turns stated, (as seen in 2.3 they should have an equivalent efficiency) the following results are obtained (the subscript 1 refers to primary and 2 to secondary). The structure in figure 2.10 has been used with the following conditions:

- Operating frequency of 1MHz.
- Distance between the coaxial coils of 1m.
- Power received at the load of 1W.

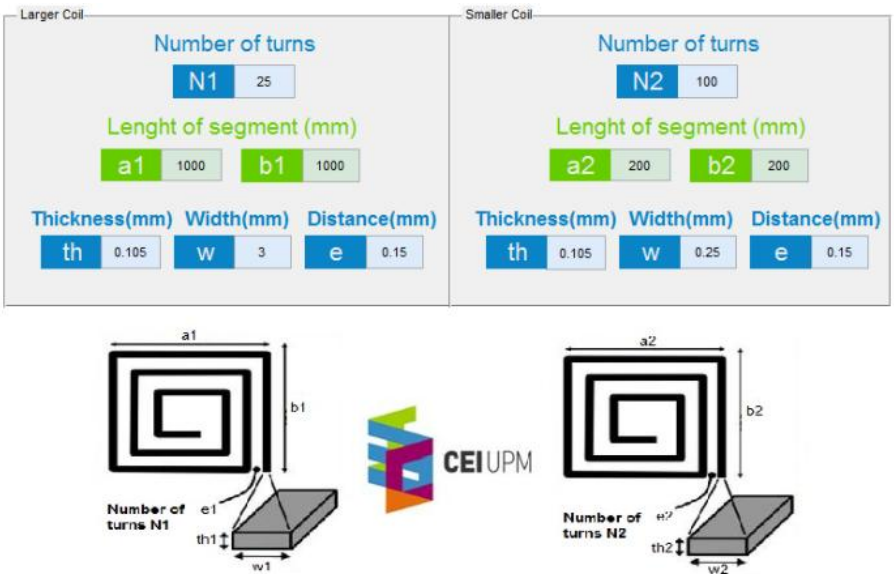

Figure 2.10. Configuration used with a 25-turns primary

For a 25-turns primary: V_{1rms} = 11.4V, V_{2rms} = 9.55V, V_{L1} = 4kV, V_{L2} = 2.6kV, η = 28.18%.

For a 5-turns primary: V_{1rms} = 2.179V, V_{2rms} = 9.67V, V_{L1} = 800V, V_{L2} = 2.6kV, η = 29.35%.

Looking at the results, the efficiency of both structures is very similar but the voltage across the primary coil is 5 times less when the number of turns is also 5-times less. This is of course preferable, however, V_{1rms} is also reduced and considering the voltage drop across the MOSFETS of the power stage, the efficiency could be penalized. For this reason, it is recommended to find a reasonable relation between the applied voltage and the voltage across the coil.

2.10.3. Dependence on the frequency

Now, the effect of changing the operating frequency will be analyzed based on its influence on the voltage coils. The compensation capacitances are changed, in such a way that the operating frequency is the resonant frequency.

Two different configurations are used to carry this test out (the power received and the relative position between coils will be the same than in section 2.10.2). The first one includes a 10x10cm secondary coil while the second one has a 20x20cm secondary coil.

- For the 10cmx10cm coil:
  - Operating frequency of 500kHz: V_{L1} 8.6kV, V_{L2} 4.35kV, η 3.6%.
  - Operating frequency of 1MHz: V_{L1} 8.6kV, V_{L2} 8.05kV, η 8.91%.
- For the 20cmx20cm coil:
  - Operating frequency of 500kHz: V_{L1} 3.15kV, V_{L2} 3.57kV, η 19%.
  - Operating frequency of 1MHz: V_{L1} 3.4kV, V_{L2} 5.8kV, η 34.36%.

Apart from the effect that the higher the frequency the higher the efficiency, due to the fact that the increase on mutual inductance is larger than that of the increase on the parasitic resistance, it can be seen that elevating the frequency causes the secondary coil voltage to go up considerably. As for V_{1rms} and V_{2rms} (voltage source and voltage at the load, respectively), their values hardly change with the frequency, for that reason they were not included in the previous results.

2.11. IMPACT OF THE QUALITY FACTOR Q

For a 1x1m primary and a 20x20cm secondary, like that of figure 2.11, the quality factor of the primary Q_p is 191.5, while that of the secondary Q_s is 259.825.

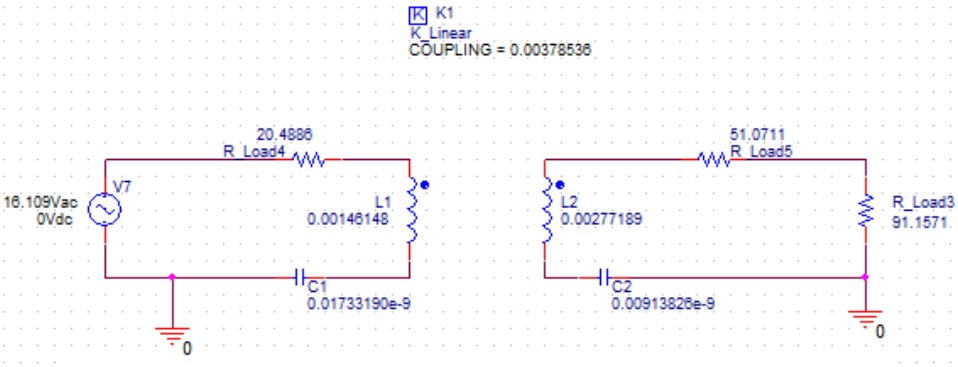

Figure 2.11. Electrical circuit representing the 2-coil scenario

In figures 2.12 and 2.13 such quality factors can be seen by means of $I_{primary}$ and $I_{secondary}$ with respect to frequency. Their shapes are quite narrow due to the high Q:

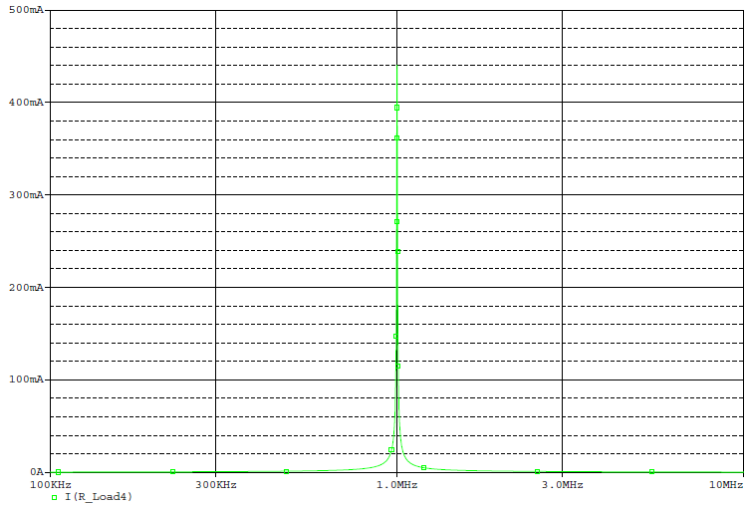

Figure 2.12. $I_{primary}$ in mA with respect to frequency

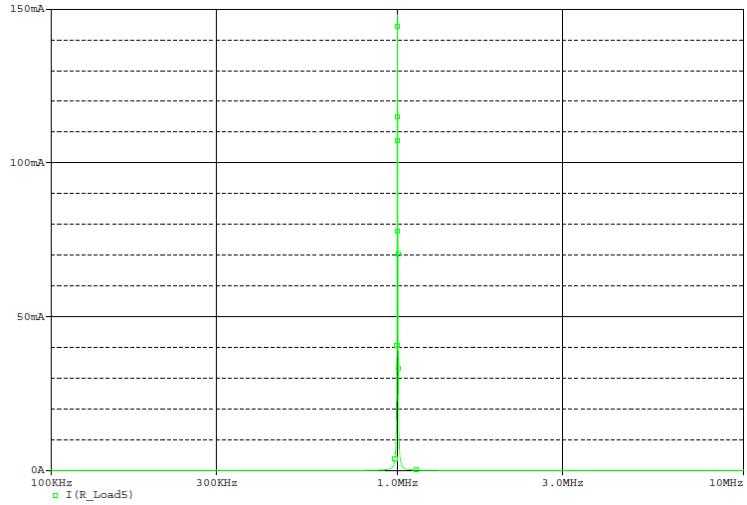

Figure 2.13. $I_{secondary}$ in mA with respect to frequency

In figures 2.14 and 2.15 $I_{primary}$ is represented as a function of the compensation capacitances of primary and secondary respectively:

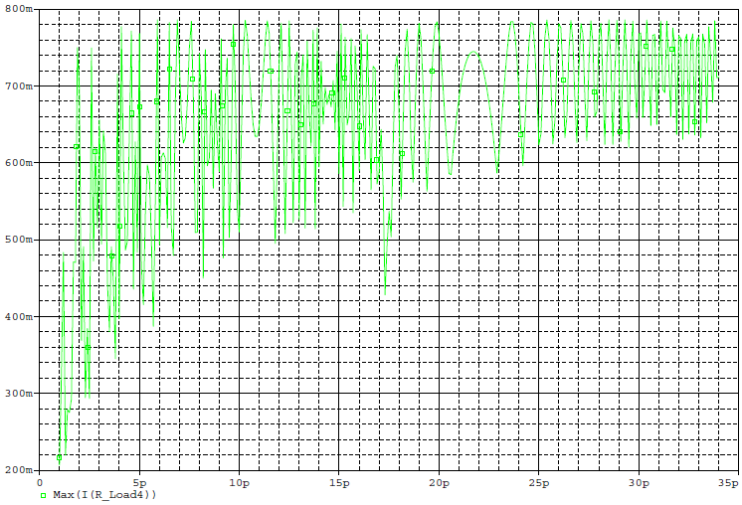

Figure 2.14. $I_{primary}$ in mA with respect to primary compensation

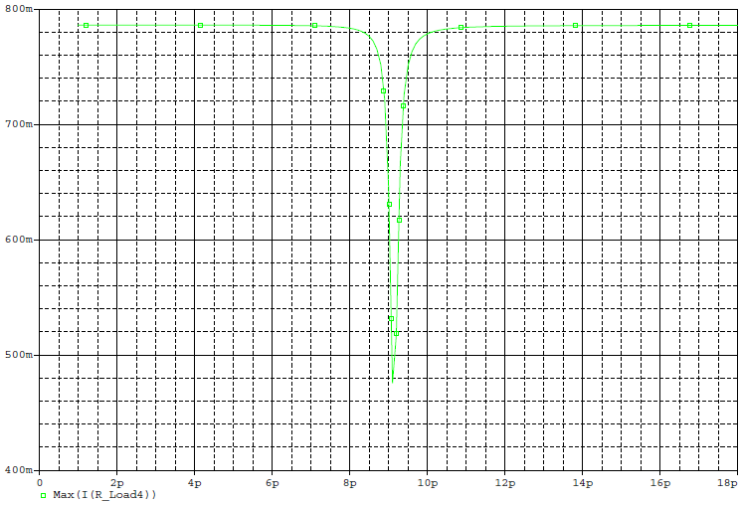

Figure 2.15. $I_{primary}$ in mA with respect to secondary compensation

In figures 2.16 and 2.17, $I_{secondary}$ is shown as a function of, again, the compensation capacitances:

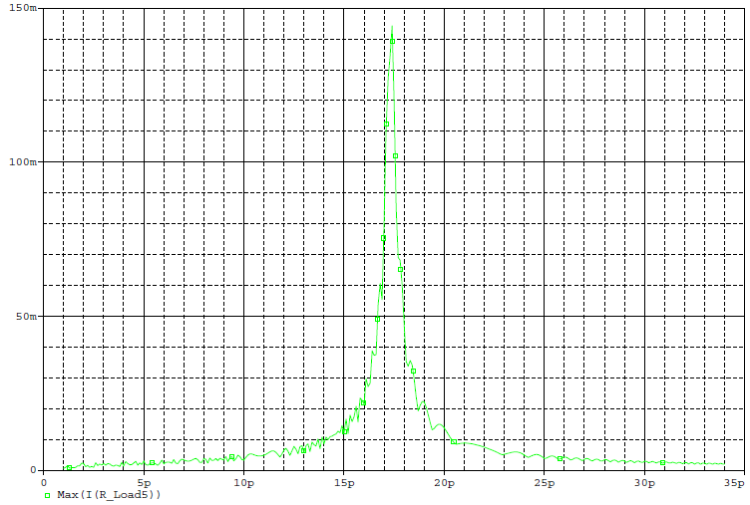

Figure 2.16. $I_{secondary}$ in mA with respect to primary compensation

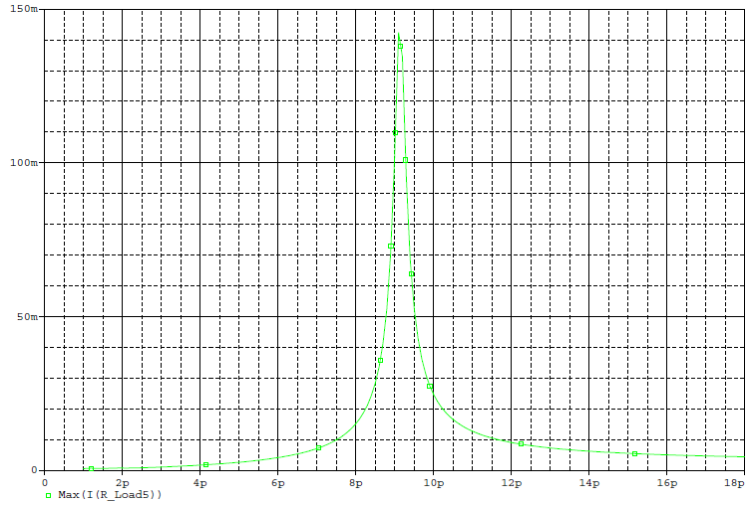

Figure 2.17. $I_{secondary}$ in mA with respect to secondary compensation

If, e.g., the primary compensation capacitance is 17pF instead of the optimum 17.33190pF, the power received at the load is 300mW instead of 1W; therefore, when the coils are designed with such a great values of Q, compensation capacitances must be carefully chosen to accomplish maximum efficiency principle or designing a control mechanism becomes fundamental to tune properly such capacitances. This is due to the high sensitivity of the coils to small variations in the compensation capacitances, what produces large variations in the power received.

2.12. IMPACT OF THE TYPE OF WINDING: LAYERS IN PARALLEL OR IN SERIES

Since designing stacked PCB layers is easy thanks to CAD programs like Altium [19] and available multilayer PCB technology, the effect on the efficiency of placing printed multilayer coils in series or in parallel will be evaluated.

If the layers from a PCB are connected in series (connecting the end of the coil on one layer to the beginning of the coil on the next layer, figure 2.18) or in parallel (connecting both ends of the coils belonging to different layers through shared vias) produce an improvement in the efficiency, better as the coupling factor between layers increases, and also as the number of layers is bigger.

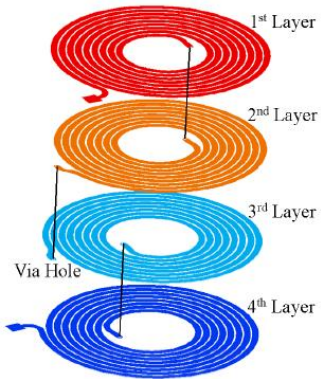

Figure 2.18. Example of four layers connected in series [28]

Connecting the layers in series fundamentally provokes an increment in the parasitic resistance but also in the self inductance; connecting them in parallel has as primary consequence the reduction of the coil parasitic resistance. Also, the addition of layers in series or parallel produces the optimum voltages and currents in the circuit to change their values. In (2.4) to (2.7) these effects are formulated assuming a perfect coupling between layers:

It has been proven analytically that, using (2.4) to (2.7), connecting the layers in series or in parallel implies a very similar increment of the efficiency, using (3.25); however, the adoption of one or the other will be taken depending on the voltages and currents expected.

$$R_{series} = R * number\ of\ layers \quad (2.4)$$

$$L_{series} = L * number\ of\ layers^2 \quad (2.5)$$

$$M_{series} = M * number\ of\ layers \quad (2.6)$$

$$R_{parallel} = R/number\ of\ layers \quad (2.7)$$

2.13. INFLUENCE OF THE FORM FACTOR ON EFFICIENCY

Since one of the goals of this work is the implementation of mid-range charging on mobile phones, the influence of the form factor on the efficiency is studied, taking into account that mobile phones have a rectangular shape instead of square, for a fixed 1x1m primary and an operating frequency of 1MHz:

For a square coil in the secondary of 141x141mm (200cm^2), the efficiency obtained is 24.68%. If the coil shape of the secondary is rectangular with dimensions 200x100mm (same equivalent area 200cm^2), the efficiency is 21.426%, while if it is 100x200mm its efficiency is 21.35% (almost the same).

As for the value of the resistances and inductances, the 20x10cm coil has an inductance of 1.40867mH and an equivalent parasitic resistance of 194.76Ω. On the other hand, for the square coil, the inductance is 1.41948mH and the resistance 176.54Ω. The larger inductance and slower resistance of the square coil explain its slightly superior efficiency.

Thus, implementing a rectangular coil has very little influence on the efficiency and so it is perfectly valid. E.g., *Google nexus 5* is 69.17x137.84mm and *Lg G2* 70.9x138.5mm, both very close to 100m^2.

2.14. RADIATION RESISTANCE

According to [77], the radiation resistance R_r of a coil with N turns and radius α, at source frequency f and corresponding free space wavelength λ=c/f is

$$R_r = 20\left(\frac{2\pi}{\lambda}\right)^4 (\pi\alpha^2 N)^2 \qquad (2.8)$$

At 1MHz, in vacuum, the planned coils:

For an expected 1mx1m primary, its radiation resistance for 25 turns is 2.4mΩ.

For a 10x10cm secondary with 400 turns, R_r is 0.0615mΩ.

For a 20x20cm secondary with 200 turns, R_r is 0.246mΩ.

In every case, the radiation resistance of the coil is far too small in comparison with its ohmic resistance; therefore radiation losses are negligible with respect to the ohmic ones, but they should be considered if the frequency is incremented since it is raised to the fourth in (2.8).

3. OPTIMIZATION OF THE WIRELESS LINK

3.1. INTRODUCTION

Depending on the constraints of the circuits involved, different kinds of optimization methods can be done; in our university working group, the following presented in sections 3.2 and 3.3 have been carried out, and already included in another master thesis [64] and end of degree project [65], both proved experimentally for short-range transmission.

The first one, commented in 3.2, allows optimizing the efficiency of the system thanks to the control of the load impedance when the input voltage is fixed. To achieve different power levels at the load, this impedance is changed, but the optimization relies on the values of the resistive and reactive parts of the load to get that power.

The second one, explained in 3.3, allows optimizing the efficiency of the system by means of controlling the module and phase of the currents travelling through the transmitter and receiver coils. The optimum load impedance remains constant and the required power at the load is obtained by means of the variation of the input voltage exciting the primary.

Below, these methods will be explained; and the last one will be experimentally tested in chapter 5 for mid-range transmission using the test circuit described in appendix A and the coils included in appendix B.

3.2. OPTIMIZATION THROUGH CHANGES ON THE LOAD IMPEDANCE

The basic resonant WPT system is shown in figure 3.1

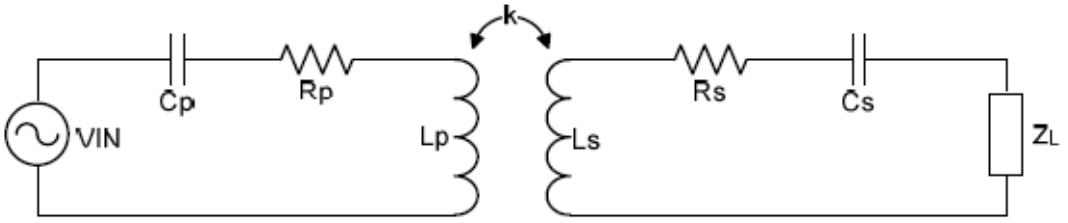

Figure 3.1. Basic resonant WPT system

In figure 3.2, figure 0.1 is repeated, which separates coil inductances into leakage and mutual.

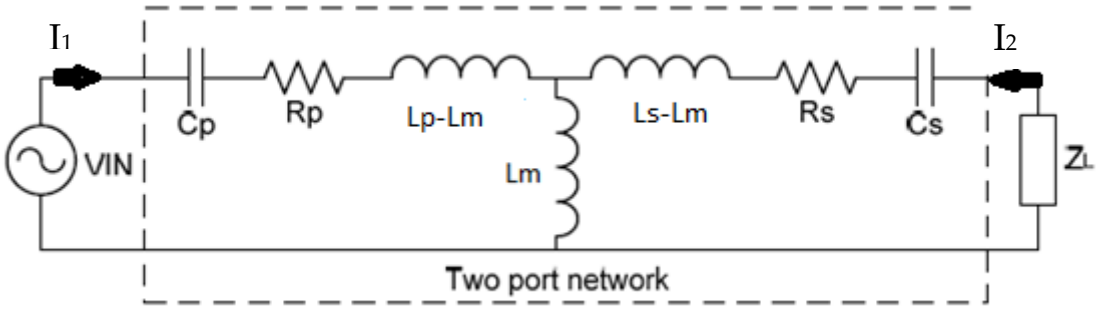

Figure 3.2. Basic resonant WPT system mutual inductance model

So, mutual inductance L_m can be calculated if coupling constant k is known, since $L_m = k\sqrt{L_p L_s}$. Apart from L_m, it is necessary to find mutual impedance X_m, primary impedance Z_1 and secondary impedance Z_2.

$$X_m = L_m \omega_s \tag{3.1}$$

$$Z_1 = R_p + jX_1 = R_p + jL_p\omega_s - \frac{1}{jC_p\omega_s} \tag{3.2}$$

$$Z_2 = R_s + jX_2 = R_s + jL_s\omega_s - \frac{1}{jC_s\omega_s} \tag{3.3}$$

ω_s is the operating frequency. The load can be seen as the addition of a resistive and a reactive part:

$$Z_L = R_L + jX_L \tag{3.4}$$

If the currents through the primary and secondary go out from the source and load, respectively, as seen in figure 3.1:

$$\begin{pmatrix} V_1 \\ V_2 \end{pmatrix} = \begin{pmatrix} Z_1 & jX_m \\ X_m j & Z_2 \end{pmatrix} \cdot \begin{pmatrix} I_1 \\ I_2 \end{pmatrix} \tag{3.5}$$

$$\begin{pmatrix} I_1 \\ I_2 \end{pmatrix} = \begin{pmatrix} Y_{11} & -Y_{12} \\ -Y_{12} & Y_{22} \end{pmatrix} \cdot \begin{pmatrix} V_1 \\ V_2 \end{pmatrix} \tag{3.6}$$

Being the admittance matrix the inverse of the impedance matrix.

$$I_2 = \left| -Y_{21}V_1 + Y_{22}V_2 e^{j\alpha} \right| \tag{3.7}$$

Where α is the phase angle between secondary voltage and current. In order to calculate the powers, the following equations are used:

$$P_1 = Re[V_1 I_1{}^*] = Re[V_1 \left(Y_{11}V_1 - Y_{12}V_2 e^{j\alpha}\right)^*] \tag{3.8}$$

$$P_2 = Re[-V_2 e^{j\alpha} \left(Y_{11}V_1 + Y_{22}V_2 e^{j\alpha}\right)^*] \tag{3.9}$$

With the previous equations the efficiency can be determined, and also the power required as a function of the load:

$$\eta(R_L, X_L) = \frac{R_L}{R_p[(R_L + R_s)^2 + (X_L + X_2)^2] + X_m^2(R_L + R_s)} \qquad (3.10)$$

$$P_{ZL}(R_L, X_L) = V_g^2 X_m^2 \frac{R_L}{[R_p(R_L + R_s) - X_1(X_L + X_2) + X_m^2]^2 + [X_1(R_L + R_s) + R_p(X_L + X_2)]^2} \qquad (3.11)$$

3.2.1. Experimental validation

The validation of this method proposed was done in [64], although the following results are included here for clarity.

This optimization method supposes a technique that allows improving both the efficiency and the maximum power delivered to the load. This technique consists in controlling the active rectifier (figure 3.6) with a phase shift in the control signals compared to the control signals of the inverter, and also controlling the output voltage set by the output load.

The following figures summarize how the efficiency and the load impedance in different circumstances are:

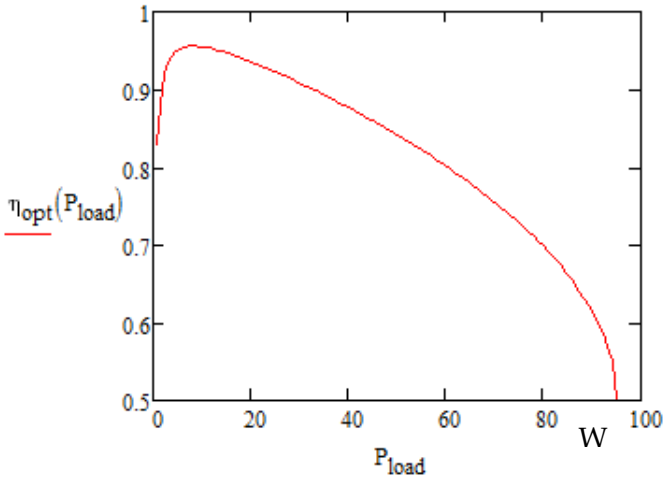

Figure 3.3. Optimum efficiency as a function of the load power

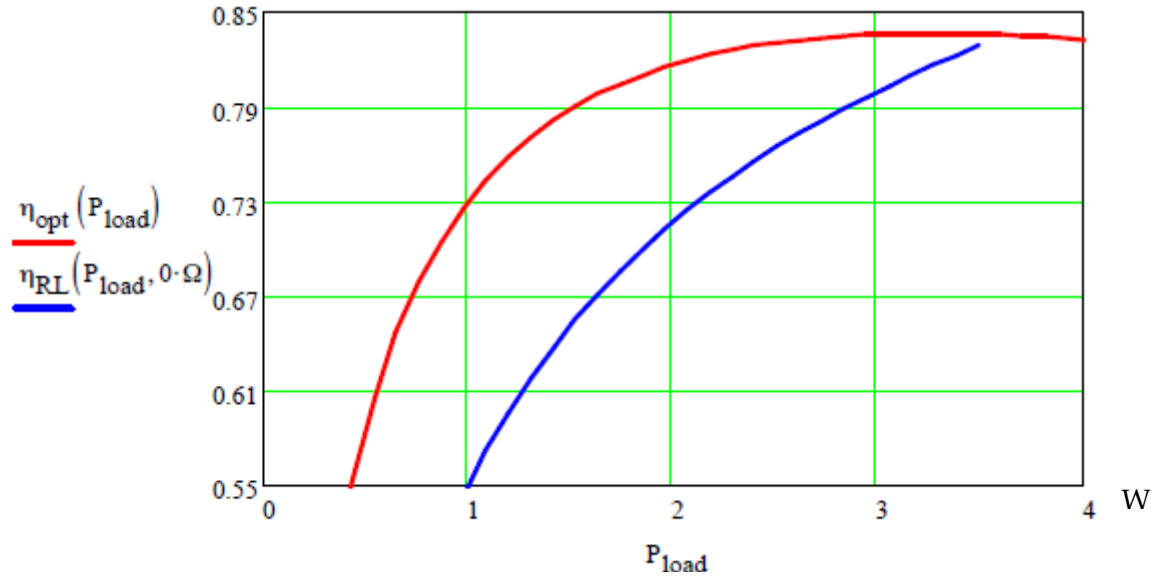

Figure 3.4. Optimum efficiency when the load has reactive part vs when is purely resistive

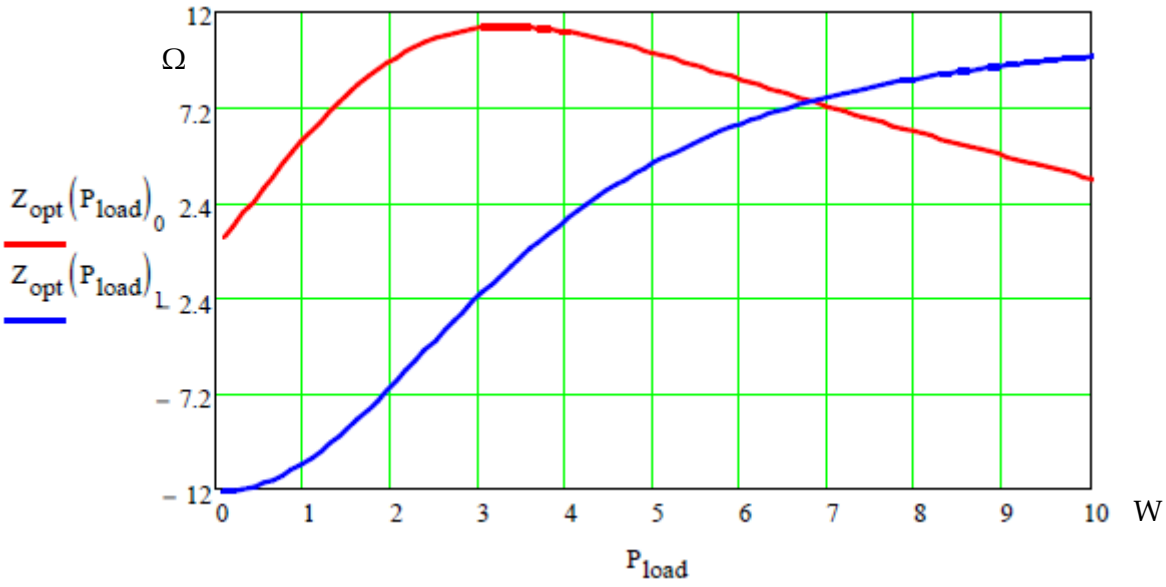

Figure 3.5. Optimum load (resistive and reactive part) for each output (load) power

In figure 3.5, the red curve corresponds to the resistive part and the blue one to the reactive part.

So as to control this wished impedance, Polytechnic University of Madrid (UPM), in collaboration with Infineon, has proposed an idea recently patented. Such proposal suggests carrying out a control of the value of the load impedance by coupling a rectifier at the secondary in such a way that for each output voltage, the α which optimizes the efficiency is obtained, since changing it the reactive part of the impedance is modified; its resistive part is changed by modifying the output voltage. With this method, a precise control over the impedance is achieved, making possible the optimization of the efficiency.

In figure 3.6 appears the simplified scheme of the set up used; it corresponds to one of those proposed in Qi standard [1].

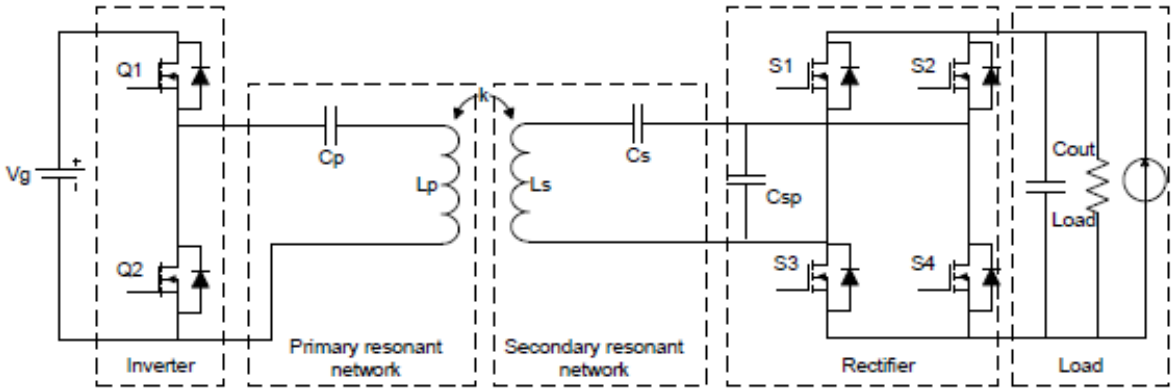

Figure 3.6. Electric scheme of the circuit used to test the optimization method

3.3. OPTIMIZATION THROUGH THE ESTABLISHMENT OF PRIMARY AND SECONDARY CURRENTS

The following model proposed, since it has two degrees of freedom unlike the previous one, gets an efficiency curve as function of the power with a flat shape. It means that the efficiency doesn't depend on the requested power and thereby there won't be an optimum operating power which maximizes the efficiency. Therefore, it is not necessary to establish a control system at the secondary which modifies the impedance depending on the requested power, since it is always the same under equivalent conditions of coupling and frequency.

The goal is trying to obtain an efficiency equation depending only on known parameters and the currents. For this, it begins from known equations using figure 3.2, with I_2 positive when it goes towards the load:

$$V_{Lm} = jX_m(I_1 - I_2) \qquad (3.12)$$

$$P_2 = Re[V_{Lm}I_2^*] - R_2|I_2|^2 \qquad (3.13)$$

$$P_1 = P_2 + R_1|I_1|^2 + R_2|I_2|^2 \qquad (3.13')$$

Where V_{Lm} is the voltage drop in L_m, which represents the mutual inductance, i.e., the lines of magnetic field which come out from the primary and link it with the secondary.

Some parameters from the earlier equations are expanded:

$$V_{Lm}I_2^* = jX_m I_1 I_2^* - jX_m|I_2|^2$$

$$Re[V_{Lm}I_2^*] = -X_m Im[I_1 I_2^*] = X_m Im[I_2 I_1^*] = X_m|I_1||I_2|\sin\varphi_{21}$$

φ_{21} is the angle which I_2 is ahead with respect to I_1.

If the efficiency is defined as equation 3.14 shows,

$$\eta = \frac{P_2}{P_1} = \frac{X_m|I_1||I_2|\sin\varphi_{21} - R_2|I_2|^2}{X_m|I_1||I_2|\sin\varphi_{21} + R_1|I_1|^2} \qquad (3.14)$$

to optimize it, it is essential to obtain the values of the modules of I_1 and I_2, and the phase between them.

If I_1 and I_2 are fixed, and partially differentiating with respect to φ_{21} and making it equal to 0:

$$\frac{\partial\eta}{\partial\varphi_{21}} = 0 \rightarrow R_1|I_1|^3|I_2|X_m\cos\varphi_{21} + R_2|I_2|^3|I_1|X_m\cos\varphi_{21} = 0 \qquad (3.15)$$

To comply with the previous equation:

$$\cos\varphi_{21} = 0 \rightarrow \varphi_{21} = \pm\frac{\pi}{2}$$

As a conclusion, for I_2 to consume power, its phase must be ahead $\pi/2$ with respect to I_1. This way, the efficiency equation is simplified to:

$$\eta = \frac{P_2}{P_1} = \frac{X_m|I_1||I_2| - R_2|I_2|^2}{X_m|I_1||I_2| + R_1|I_1|^2} \qquad (3.16)$$

To keep on with this development, an optimization problem must be solved in which the maximization of the efficiency is pursued, with the constraint of transferring a determined power P_2.

$$\text{Max}\ \eta(I_1, I_2) \rightarrow \text{Min}\ P_1$$

$$P_2 = X_m|I_1||I_2| - R_2|I_2|^2$$

This optimization problem can be solved through Lagrangians, defining the Lagrange function L as:

$$L = (X_m|I_1||I_2| + R_1|I_1|^2) - \lambda(X_m|I_1||I_2| - R_2|I_2|^2) \quad (3.17)$$

$$\frac{\partial L}{\partial I_1} = 0 \Rightarrow X_m|I_2| + 2R_1|I_1| - \lambda X_m|I_2| = 0 \quad (3.18)$$

$$\frac{\partial L}{\partial I_2} = 0 \Rightarrow X_m|I_1| + 2R_2\lambda|I_2| - \lambda X_m|I_1| = 0 \quad (3.19)$$

$$P_2 = X_m|I_1||I_2| - R_2|I_2|^2 \quad (3.20)$$

Therefore, it results a system of 3 equations (3.18), (3.19) and (3.20) with 3 unknowns λ, $|I_1|\ and\ |I_2|$. Since such system is non-linear, it will be solved with MathCAD®, obtaining the corresponding solutions as a function of the parameters R_1, R_2 and X_m:

$$|I_2|(P_2) = \left(\frac{P_2^2 R_1}{R_1 R_2^2 + R_2 X_m^2}\right)^{\frac{1}{4}} \quad (3.21)$$

$$|I_1|(P_2) = \frac{P_2 + R_2\sqrt{\frac{P_2^2 R_1}{R_1 R_2^2 + R_2 X_m^2}}}{X_m\left(\frac{P_2^2 R_1}{R_1 R_2^2 + R_2 X_m^2}\right)^{\frac{1}{4}}} \quad (3.22)$$

Once the currents are expressed as functions of the output power and known parameters from the circuit, the curve of how the efficiency evolves depending of such power can be represented through MathCAD®. The result is surprising as the efficiency is a constant which not depends on the output power, as seen in figure 3.8.

Below, that constant efficiency is validated analytically. Doing a change of variable, and from the last equations:

$$p_2 = \frac{P_2}{X_m} \quad r_1 = \frac{R_1}{X_m} \quad r_2 = \frac{R_2}{X_m}$$

$$|I_2|(p_2) = \left(\frac{p_2^2 r_1}{r_1 r_2^2 + r_2}\right)^{\frac{1}{4}} \qquad |I_1|(p_2) = \frac{p_2 + r_2\sqrt{\frac{p_2^2 r_1}{r_1 r_2^2 + r_2}}}{X_m\left(\frac{p_2^2 r_1}{r_1 r_2^2 + r_2}\right)^{\frac{1}{4}}} \qquad (3.23) \quad (3.24)$$

$$\eta = \frac{\sqrt{\frac{p_2^2 r_1}{r_1 r_2^2 + r_2}}}{2p_2 r_1 + \sqrt{\frac{p_2^2 r_1}{r_1 r_2^2 + r_2}} + 2r_1 r_2\sqrt{\frac{p_2^2 r_1}{r_1 r_2^2 + r_2}}} = \frac{\sqrt{\frac{r_1}{r_1 r_2^2 + r_2}}}{2r_1 + \sqrt{\frac{r_1}{r_1 r_2^2 + r_2}} + 2r_1 r_2\sqrt{\frac{r_1}{r_1 r_2^2 + r_2}}}$$

In the last step, the efficiency doesn't depend on the output power. To finish, an approximation of the efficiency equation is addressed to work with a simpler formula:

$$\eta = \frac{1}{2\frac{r_1}{\sqrt{\frac{r_1}{r_1 r_2^2 + r_2}}} + 1 + 2r_1 r_2} = \frac{1}{1 + 2r_1 r_2\left[1 + \sqrt{\left(1 + \frac{1}{r_1 r_2}\right)}\right]} \qquad (3.25)$$

If $r_1 \ll 1$ and $r_2 \ll 1$, it can be assumed:

$$\eta aprox = \frac{1}{1 + 2\sqrt{r_1 r_2}} \qquad (3.26)$$

Values commonly obtained for r_1 and r_2 shows that this simplification is not valid many times and it won't be enough precise to be used in the efficiency calculation; however, it serves to get an appropriate order of magnitude of that efficiency.

To conclude, I_1 is controlled through a voltage source V_1, and I_2 by means of the load impedance, as it is a good approximation of the prototype used for the experimental validation.

From figure 3.2, the following analysis is developed:

$$I_1(P_2) = |I_1|e^{j0} \qquad I_2(P_2) = |I_2|e^{j\frac{\Pi}{2}} \qquad (3.27)\ (3.28)$$

$$V_1 = V_{L1} + V_{cp} + V_{Rp} + V_{Lm} \qquad (3.29)$$

$$V_2 = -V_{L2} - V_{cs} - V_{Rs} + V_{Lm} \qquad (3.30)$$

$$V_{Lm} = jX_m(I_1(P_2) - I_2(P_2)) \qquad (3.31)$$

$$\text{From (3.29)} \Rightarrow V_1 = \left((L_p - L_m)j\omega + \frac{1}{C_p j\omega} + R_p\right) I_1(P_2) + V_{Lm}$$

$$\text{From (3.30)} \Rightarrow V_2 = -\left((L_s - L_m)j\omega + \frac{1}{C_s j\omega} + R_s\right) I_2(P_2) + V_{Lm}$$

$$Z_L = \frac{V_2}{I_2} \qquad (3.32)$$

From these equations, the evolution of the following parameters ($|V_1|, |V_2|, |Z_L|$ and $\arg(Z_L)$) with respect to the requested power can be represented. Again, an interesting result is achieved: the module and argument of the load impedance are constant for every power, i.e., they don't depend on the output power.

The optimum load keeps constant, independently of the output power, due to the following:

Firstly, if the circuit is considered as a voltage source and an admittance dependent of the load, as figure 3.7 shows,

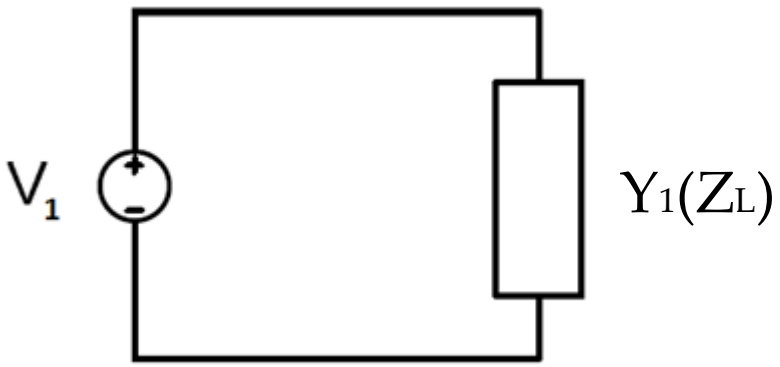

Figure 3.7. Representation of the circuit admittance

$$I_2 = Y_{21}(Z_L)V_1 \qquad (3.33)$$

$$P_2 = |I_2^2|\, Re\{Z_L\} = |I_2^2|R_L = |Y_{21}(Z_L)|^2 R_L {V_1}^2 \qquad (3.34)$$

$$P_1 = {V_1}^2 |Y_{12}(Z_L)|^2 \qquad (3.35)$$

$$\eta = \frac{P_2}{P_1} = \frac{{V_1}^2 f_2(Z_L)}{{V_1}^2 f_1(Z_L)} = \frac{f_2(Z_L)}{f_1(Z_L)} \qquad (3.36)$$

the efficiency is independent of the power and thus, an optimum Z_L which maximizes such efficiency will exist, which depends on the operating frequency, and that Z_L will be constant.

3.3.1. Experimental validation

The verification of this method was carried out in [65], but some results are copied here for a better understanding.

If, e.g., an output power of **10W** is used, and also the parameters from table 3.1, which corresponds to Qi standard,

Name	Symbol	Value	Units
Input voltage	V_g (rms)	10	V
Primary inductor	L_p	24	µH
Parasitic resistance primary	R_p	150	mΩ
Secondary inductor	L_s	10	µH
Parasitic resistance secondary	R_s	200	mΩ
Switching frequency	f_s	110	kHz
Resonance frequency	f_r	100	kHz
Coupling factor	k	0.53	

Table 3.1. Circuit element values

the following is found:

$$L_m = \sqrt{L_p L_s}\, k = 8.21 \cdot 10^{-6}\ H$$

$$X_m = 2\pi f_s L_m = 5.6748\ \Omega$$

$$|I_2|(P_2) = \left(\frac{P_2^2 R_1}{R_1 R_2^2 + R_2 X_m^2}\right)^{\frac{1}{4}} = 1.235\ A \qquad |I_1|(P_2) = \frac{P_2 + R_2\sqrt{\frac{P_2^2 R_1}{R_1 R_2^2 + R_2 X_m^2}}}{X_m\left(\frac{P_2^2 R_1}{R_1 R_2^2 + R_2 X_m^2}\right)^{\frac{1}{4}}} = 1.47\ A$$

$$\eta = \frac{\sqrt{\frac{p_2^2 r_1}{r_1 r_2^2 + r_2}}}{2P_2 r_1 + \sqrt{\frac{p_2^2 r_1}{r_1 r_2^2 + r_2}} + 2r_1 r_2\sqrt{\frac{p_2^2 r_1}{r_1 r_2^2 + r_2}}} = 0.9408 = 94.08\%$$

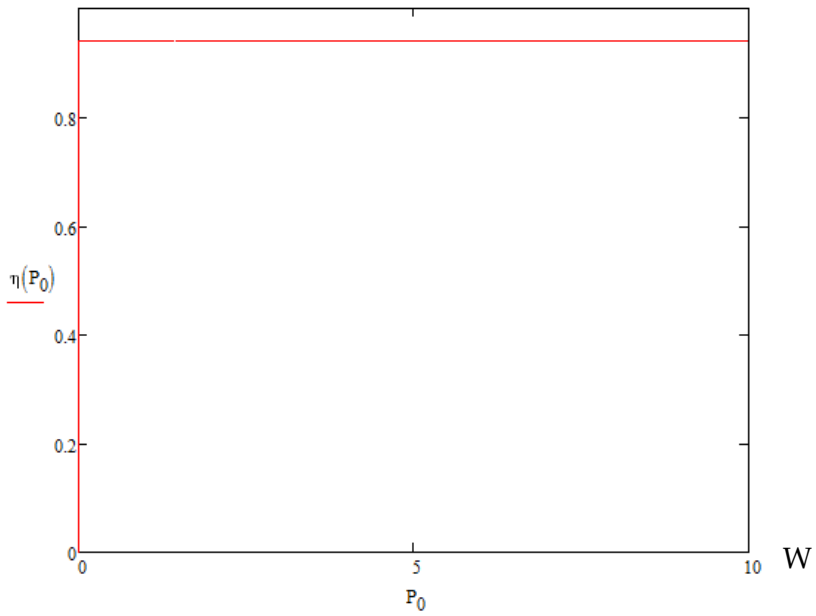

Figure 3.8. Efficiency curve as a function of P_2 (P_0 in the figures)

Also the following parameters are calculated:

$$V_{Lm} = jX_m(I_1 - I_2) = 7.008 + 8.341j\ V$$

$$V_1 = \left((L_p - L_m)j\omega + \frac{1}{C_p j\omega} + R_p\right) I_1 + V_{Lm} = 7.228 + 3.115j\ V \qquad |V_1| = 7.871\ V$$

$$V_2 = -\left((L_s - L_m)j\omega + \frac{1}{C_s j\omega} + R_s\right) I_2 + V_{Lm} = 1.388 + 8.094j\ V \qquad |V_2| = 8.212\ V$$

$$Z_L = \frac{V_2}{I_2} = 6.554 - 1.124j\ \Omega$$

$$X_L = \frac{1}{\omega C} \Rightarrow C = 1.287\ \mu F$$

As it was mentioned before, the previous results are represented with respect to the power at the load in the following figures:

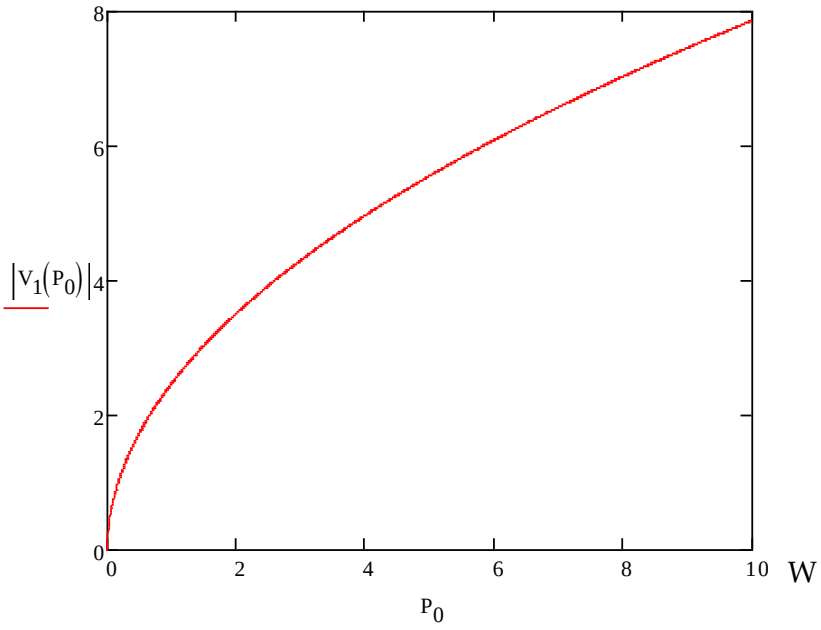

Figure 3.9. Module of the input voltage

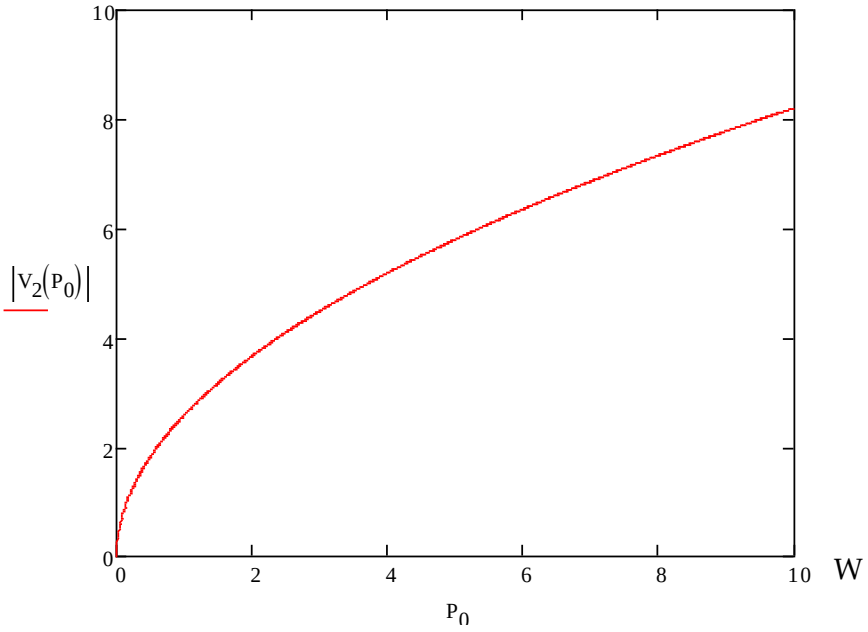

Figure 3.10. Module of the voltage at the load

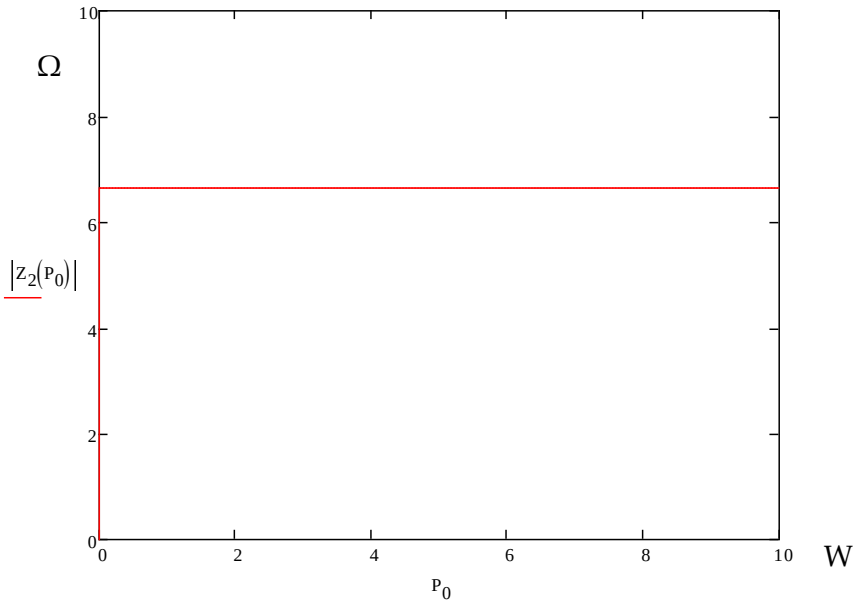

Figure 3.11. Module of the load impedance

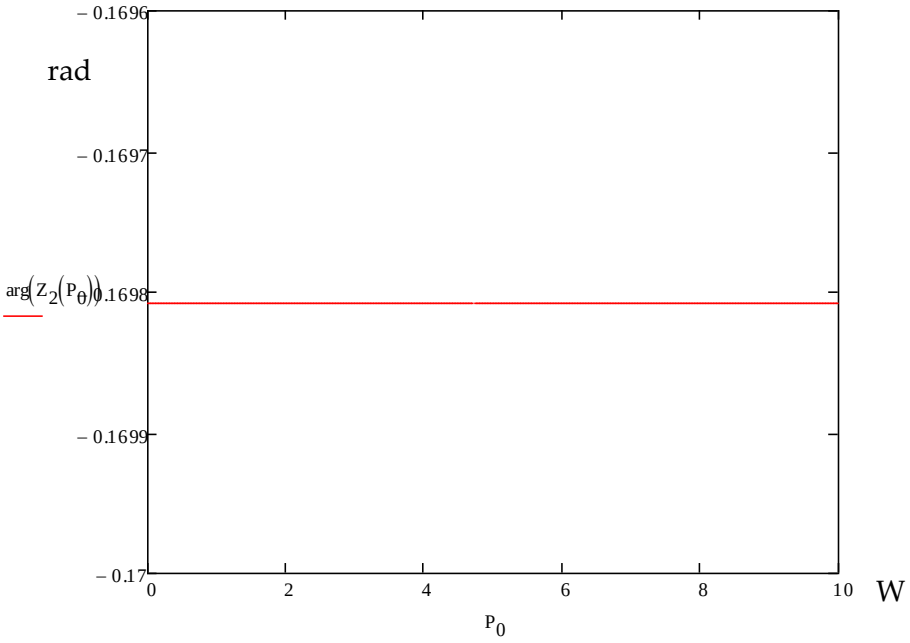

Figure 3.12. Phase of the load impedance

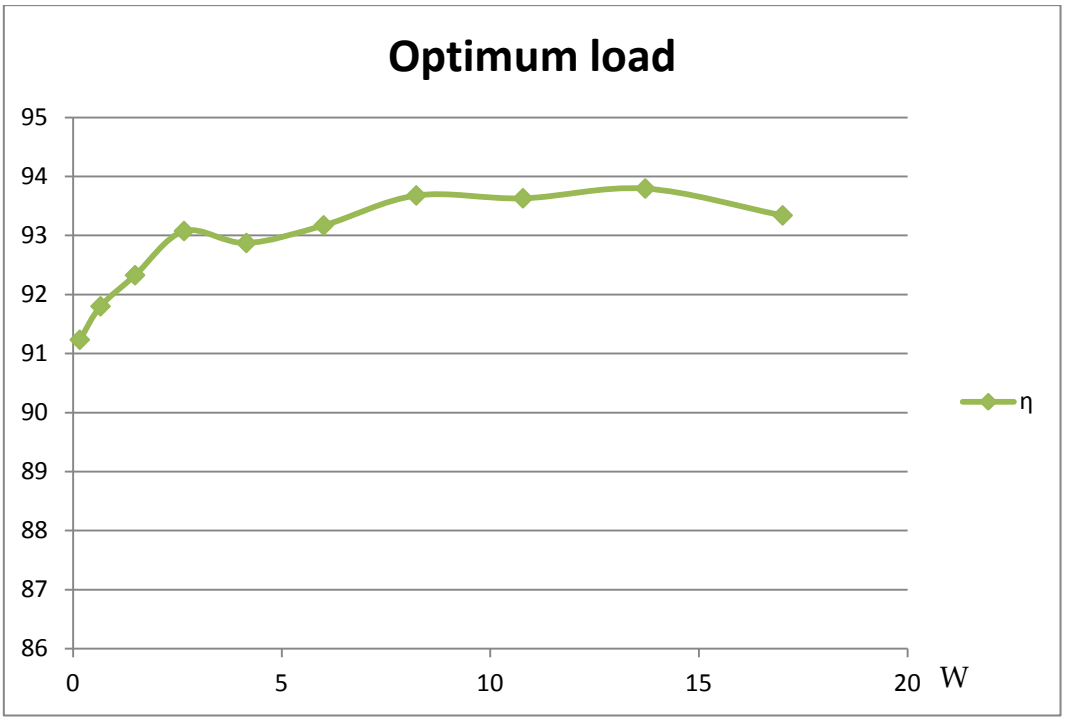

Figure 3.13. Efficiency obtained experimentally with respect to the output power

In figure 3.13, it can be seen that for low power, the losses of the mosfets from the inverter are more important, making the efficiency to decrease. In figure 3.14, the tests carried out in [65] are shown together: green curve corresponds to figure 3.13, that of higher efficiency; purple curve occurs when the reactive part of the optimum impedance is not considered; the red one shows that the output power is achieved by varying the load resistance instead of the input voltage; and the blue one is like the purple one, but mounting a resistance with a value close to the optimum.

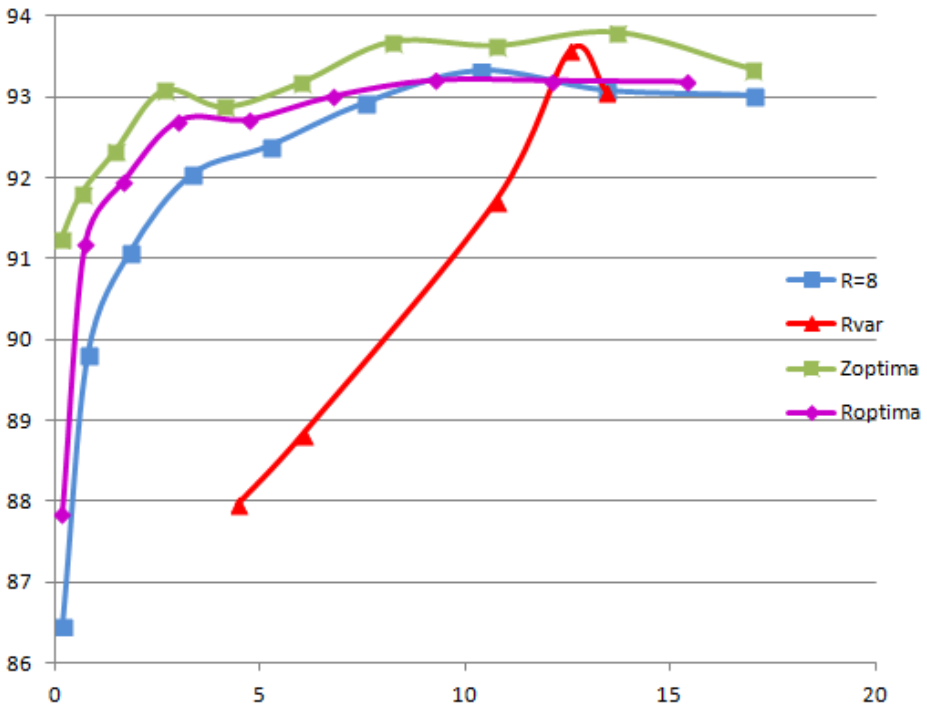

Figure 3.14. Dependency of the efficiency with the output power, comparing different tests

4. OPTIMIZATION OF THE COILS

4.1. PARASITIC CAPACITANCE ISSUE

The coils designed in appendix B to validate the optimization method from section 3.3 have a problem since their self capacitance has an unexpected large value. This capacitor has been studied in many papers [28], [55], [66] to [74], and the consequence is the reduction of the self-resonant frequency (f_{SRF}) of the coils, since according to (4.1) the increment in the undesired capacitance (C_P in 4.1) provokes that the maximum available operating frequency be reduced, as this one must be slower than f_{SRF}.

$$f_{SRF} = \frac{1}{2\pi\sqrt{LC_p}} \tag{4.1}$$

In [28], [55], [68], [72], and [74] among others, PCB multilayer coils are characterized and modelled, including more or less complex analytical methods to synthesize such coils as lumped elements, with their inductance, parasitic resistances and capacitances. Also, methods to mitigate the parasitic elements are studied and demonstrated experimentally in [28] and [66]. Examples of these models are shown in figures 4.1, 4.2 and 4.3:

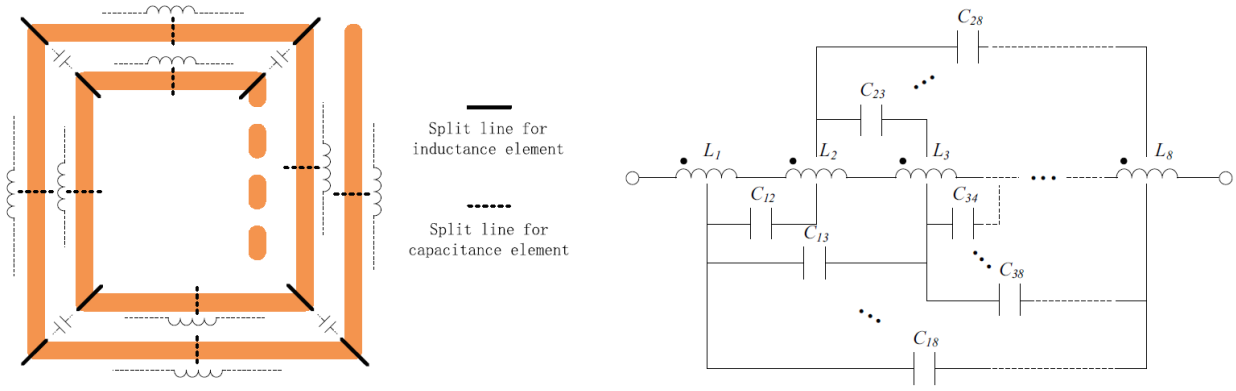

Figure 4.1. Coil model in [55]

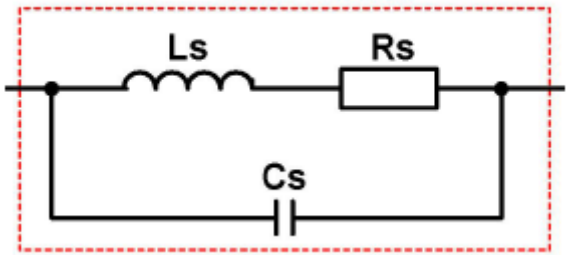

Figure 4.2. Coil model in [67]

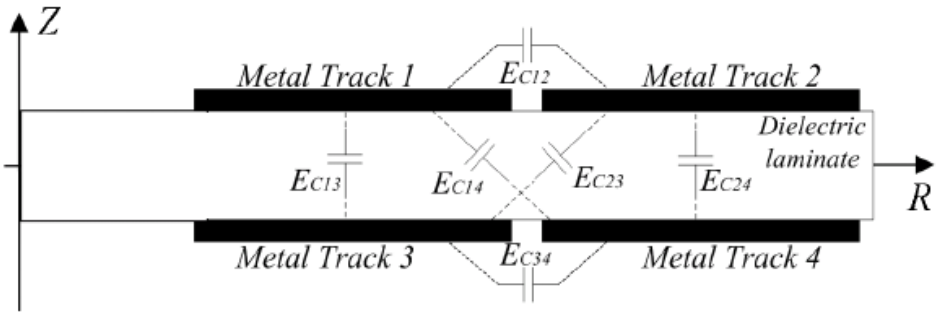

Figure 4.3. Coil model in [28]

4.2. ANALYTICAL CAPACITANCE ESTIMATION

Although the coils designed and manufactured are sufficiently good to validate the optimization method, a method to estimate the self (parasitic) capacitance of the coils is needed. Many have been seen in literature [66], [67], [68] and [72], but that of [72] has been adopted here for its simplicity and good results, and so included in the simulation tool explained in 4.3, whose goal is choosing the best coil parameters (track width, layer copper thickness, number of layers, separation between coil turns, operating frequency) in order to achieve the highest efficiency and to have a model from simulation whose results matches with the real ones obtained from a network analyzer.

The analytical method selected to estimate the self capacitance value corresponds to (4.2) [72]:

$$C_{pi} = i(C_{pc} + C_{ps}) = i(\alpha\varepsilon_{rc} + \beta\varepsilon_{rs})\varepsilon_0 \frac{t_c}{s} l_g \tag{4.2}$$

Where C_{pc} is the capacitance between metal traces through coating, C_{ps} is the capacitance between metal traces through substrate, i is the number of layers, ε_0 the dielectric constant of the vacuum, l_g is the length of the gap, ε_{rc} and ε_{rs} are the relative dielectric constants of the coating and substrate materials respectively; typically values for air and FR-4 are α=0.9 and β=0.1 [72]. From figure 4.4, t_c is the copper track thickness, w is the track width and s is the separation between parallel tracks for a planar and square coil, as those studied in this work.

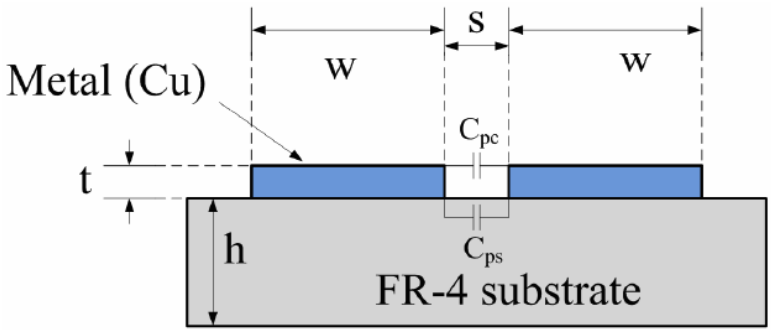

Figure 4.4. Cross-sectional view of a PCB [72]

4.3. SIMULATION TOOL

To foresee the elements of the coil model from figure 4.2, where C_s is C_{pi} in (4.2), a dedicated tool has been developed; resistance and inductance are calculated through FastHenry and the capacitor with the analytical model from (4.2). In this tool, presented in figure 4.5, the following parameters are introduced by the user: layer (track) copper thickness, external dimensions of the PCB, number of layers in series or in parallel, power desired at the output load, primary coil dimensions, relative permittivity ε_r of the PCB dielectric, distance between pcb layers and area dedicated to copper tracks in the pcb layer (equivalent width).

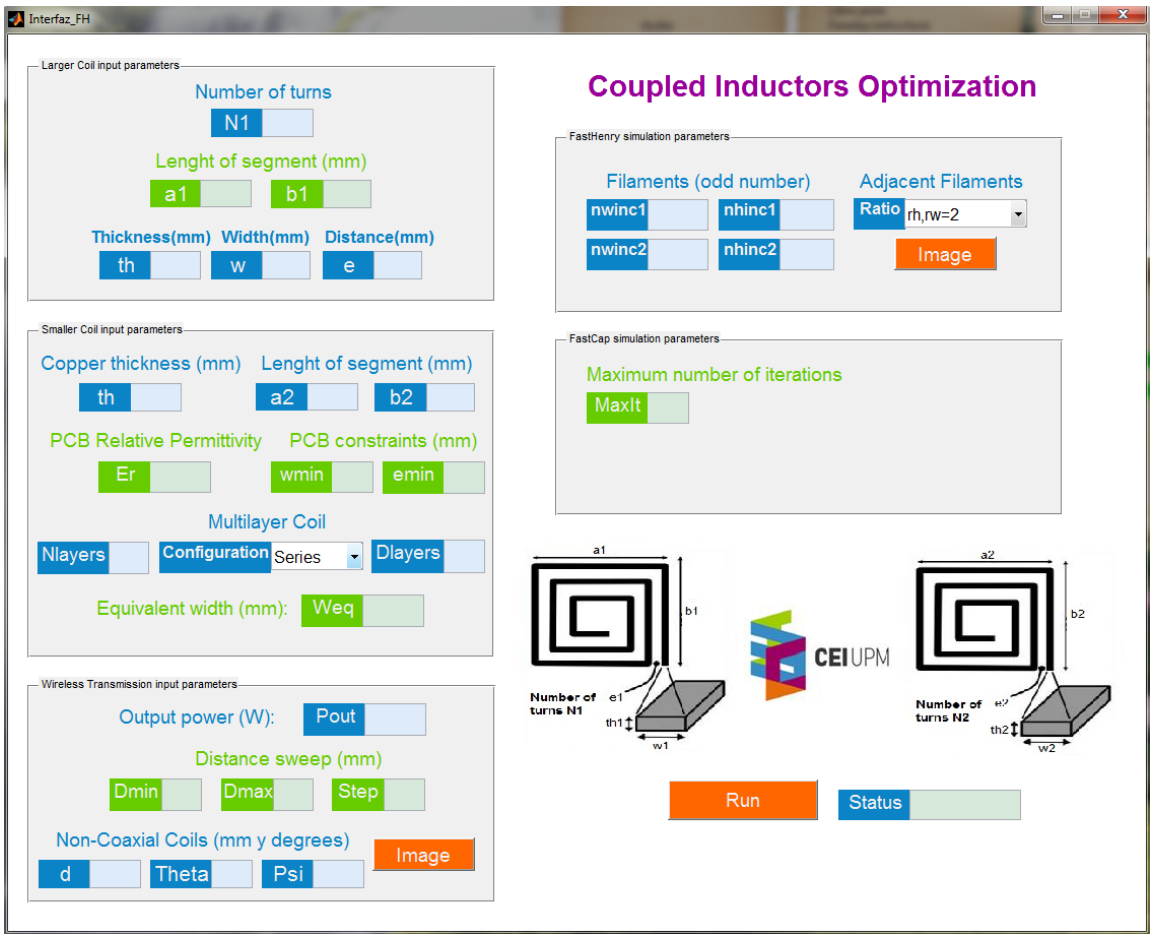

Figure 4.5. Screenshot of the optimization tool developed

As the primary is supposed to be a very large coil without restrictions, whose sides have an order of magnitude of meters, it is introduced manually in the simulation tool and it is the secondary the coil optimized.

With these parameters introduced by the user, the tool downloads in an excel sheet many results for every combination of s, w and number of turns N, where must be complied that Equivalent width = w*N + (N-1)*s. These results are: coil L, R and C; efficiency, Mutual Inductance Xm, maximum available operating frequency, which depends on the self-resonant frequency, voltages and currents in the circuit. After, in the excel sheet, it is easy to order the solutions depending on any parameter. A screenshot of an example of that excel sheet is shown in figure 4.6:

Distancia(mr	Frecuencia(H	L1(H)	L2(H)	M(ohm)	R1(ohm)	R2(ohm)	Rendimient	I1ef(A)	I1arg(Deg)	I2ef(A)	I2arg(Deg)	V1ef(V)	V1arg(Deg)	V2ef(V)	V2arg(Deg)	Cp(nF)	Cs(nF)	w2(mm)	N2	e2(mm)	Cauto(nF)
110	10000000	0,00277157	3,2834E-06	516,549548	198,348854	0,64497626	95,7155414	0,01073814	0	0,18423132	90	97,2945019	1,339E-13	5,42795883	90	9,1393E-05	0,07714587	2,25	1	0,15	0
110	10000000	0,00277157	3,1492E-06	515,203829	198,348854	0,53797285	96,0695807	0,01025667	0	0,19303415	90	101,486335	-1,2837E-13	5,18043041	90	9,1393E-05	0,08043282	2,75	1	0,15	0
110	10000000	0,00277157	3,0363E-06	513,851555	198,348854	0,46178101	96,343741	0,0098715	0	0,20081304	90	105,146095	0	4,97975628	90	9,1393E-05	0,08342451	3,25	1	0,15	0
110	10000000	0,00277157	2,9386E-06	512,492745	198,348854	0,40472795	96,5640529	0,00955319	0	0,20782107	90	108,401657	0	4,81183155	90	9,1393E-05	0,086198	3,75	1	0,15	0
110	10000000	0,00277157	2,8524E-06	511,127421	198,348854	0,36022804	96,7467119	0,00928271	0	0,21424898	90	111,349743	-1,17E-13	4,66746678	90	9,1393E-05	0,08880401	4,25	1	0,15	0
110	10000000	0,00277157	2,7751E-06	509,755604	198,348854	0,32451632	96,9013957	0,00904855	0	0,2202117	90	114,048918	0	4,54108475	90	9,1393E-05	0,0912765	4,75	1	0,15	0
110	10000000	0,00277157	2,705E-06	508,377318	198,348854	0,29512114	97,0350111	0,00884221	0	0,22580818	90	116,5496	0	4,42853749	90	9,1393E-05	0,09364087	5,25	1	0,15	0
110	10000000	0,00277157	2,6409E-06	506,992586	198,348854	0,27048486	97,1519961	0,00865823	0	0,23109908	90	118,88287	0	4,32714831	90	9,1393E-05	0,09591597	5,75	1	0,15	0
110	10000000	0,00277157	2,5817E-06	505,60143	198,348854	0,24935973	97,2564747	0,00849112	0	0,23617052	90	121,092358	1,0758E-13	4,23422866	90	9,1393E-05	0,09811631	6,25	1	0,15	0
110	10000000	0,00277157	2,5266E-06	504,203876	198,348854	0,23113385	97,3500449	0,00833907	0	0,24102876	90	123,181681	0	4,14888246	90	9,1393E-05	0,10025332	6,75	1	0,15	0
110	10000000	0,00277157	2,4752E-06	502,799947	198,348854	0,21516085	97,434992	0,00819898	0	0,24572575	90	125,177154	0	4,06957752	90	9,1393E-05	0,1023362	7,25	1	0,15	0
110	10000000	0,00277157	2,4269E-06	501,389671	198,348854	0,20107293	97,5124246	0,00806949	0	0,25027306	90	127,084902	0	3,99563579	90	9,1393E-05	0,10437249	7,75	1	0,15	0
110	10000000	0,00277157	2,3814E-06	499,973072	198,348854	0,18855122	97,5834214	0,00794918	0	0,2546892	90	128,914454	1,0106E-13	3,92635411	90	9,1393E-05	0,10636843	8,25	1	0,15	0
110	10000000	0,00277157	2,3383E-06	498,550178	198,348854	0,1773584	97,6487693	0,00783704	0	0,25898504	90	130,671507	-9,9697E-14	3,86122687	90	9,1393E-05	0,10832926	8,75	1	0,15	0
110	10000000	0,00277157	2,2973E-06	497,121016	198,348854	0,16731775	97,7090213	0,00773241	0	0,26316388	90	132,35801	0	3,79991359	90	9,1393E-05	0,11025945	9,25	1	0,15	0
110	10000000	0,00277157	2,2584E-06	495,685614	198,348854	0,1582184	97,7650957	0,00763392	0	0,26725519	90	133,988735	0	3,74174208	90	9,1393E-05	0,11216283	9,75	1	0,15	0
110	10000000	0,00277157	2,2211E-06	494,244001	198,348854	0,14997694	97,8171535	0,00754149	0	0,27124852	90	135,5588	-9,6103E-14	3,68665605	90	9,1393E-05	0,11404271	10,25	1	0,15	0
110	10000000	0,00277157	2,1855E-06	492,796206	198,348854	0,14247257	97,8656859	0,00745442	0	0,27515557	90	137,074194	0	3,63430773	90	9,1393E-05	0,11590199	10,75	1	0,15	0
110	10000000	0,00277157	2,1513E-06	491,342259	198,348854	0,13561108	97,9110685	0,00737219	0	0,27898412	90	138,538951	0	3,58443346	90	9,1393E-05	0,11774322	11,25	1	0,15	0
110	10000000	0,00277157	2,1185E-06	489,882191	198,348854	0,12931472	97,9536147	0,00729436	0	0,28274049	90	139,956357	0	3,53681217	90	9,1393E-05	0,11956866	11,75	1	0,15	0
110	10000000	0,00277157	2,0869E-06	488,416032	198,348854	0,12353146	97,9934854	0,00722075	0	0,28642236	90	141,3255	-9,2181E-14	3,49134752	90	9,1393E-05	0,12138031	12,25	1	0,15	0
110	10000000	0,00277157	2,0564E-06	486,943815	198,348854	0,1181849	98,0310764	0,00715074	0	0,29004592	90	142,654409	0	3,4477299	90	9,1393E-05	0,12317998	12,75	1	0,15	0
110	10000000	0,00277157	2,0269E-06	485,465572	198,348854	0,11324891	98,0664136	0,00708437	0	0,29360223	90	143,938951	0	3,4059687	90	9,1393E-05	0,12496929	13,25	1	0,15	0
110	10000000	0,00277157	1,9984E-06	483,981336	198,348854	0,10866378	98,0998287	0,0070211	0	0,29710634	90	145,186552	-8,973E-14	3,36579823	90	9,1393E-05	0,12674971	13,75	1	0,15	0
110	10000000	0,00277157	1,9709E-06	482,49114	198,348854	0,10440017	98,1314266	0,00696081	0	0,30055765	90	146,397073	0	3,32714867	90	9,1393E-05	0,12852259	14,25	1	0,15	0
110	10000000	0,00277157	1,9442E-06	480,99502	198,348854	0,10042684	98,1613485	0,00690327	0	0,30395923	90	147,572134	0	3,28991487	90	9,1393E-05	0,13028915	14,75	1	0,15	0
110	10000000	0,00277157	1,9182E-06	479,493009	198,348854	0,09671692	98,1897157	0,00684833	0	0,30731348	90	148,713025	0	3,25400629	90	9,1393E-05	0,13205051	15,25	1	0,15	0
110	10000000	0,00277157	1,893E-06	478,030112	198,348854	0,09324398	98,2168292	0,00679545	0	0,31061027	90	149,82893	0	3,21946861	90	9,1393E-05	0,13380771	15,75	1	0,15	0

Figure 4.6. Screenshot of a resulting excel sheet from an optimization process

Also, the minimum width w and minimum s, since they are constraints in the PCB manufacturing process, are taken into account; therefore, that solutions with w and s smaller than min w and min s are automatically discarded.

[69] states that the operating frequency must be much lower than the self-resonant frequency in order to neglect the parasitic capacitance; however, since these kinds of coils have a high quality factor Q, for this work the maximum operating frequency given by the tool is the self-resonant frequency of the secondary coil divided by two.

4.4. CONCLUSIONS

In appendix E, the results for the simulation corresponding to figure 4.7 are shown.

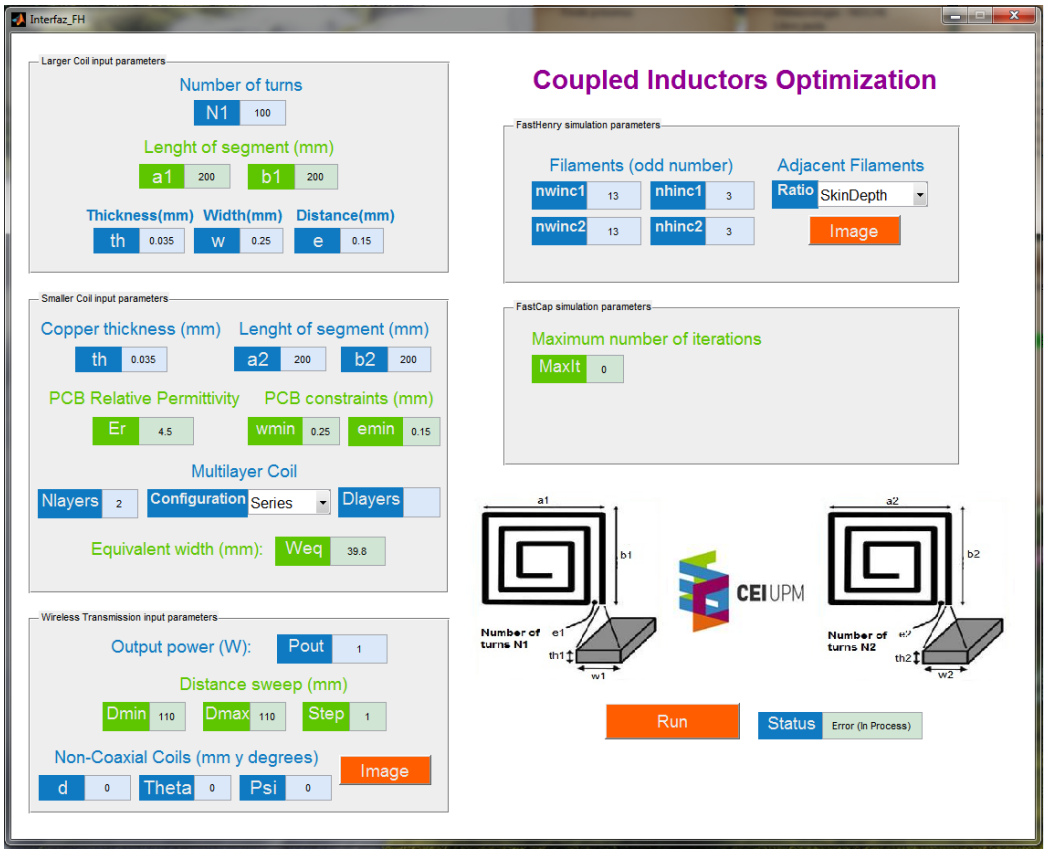

Figure 4.7. Screenshot of the parameters introduced to run the simulation

The geometrical dimensions from figure 4.7 are equivalent to that of 20x20cm designed coils in appendix B, which are used in the experimental results in chapter 5. The goal of this simulation test is to find the optimum geometrical design of the coils which would have produced the best results in terms of efficiency and power transferred.

From results in appendix E, as the number of turns is increased, the maximum available operating frequency is reduced since the self-capacitance is increased, what minimizes both efficiency and mutual impedance. For this reason, the best option is to choose the highest number of turns that allows selecting the maximum operating frequency, which is usually determined from the power stage.

The same occurs for a fixed number of turns; the best is to use thinner copper tracks and increasing the separation between them to minimize the self-capacitance; however, as the maximum operating frequency is limited, the thicker width, of those that give a maximum operating frequency, will be choose since it produces the reduction of the coil parasitic resistance.

Therefore, the minimum number of turns, minimum track width and maximum separation between tracks make the maximum operating frequency be higher, and so the mutual impedance and the efficiency as seen in the results from appendix E.

4.5. FINAL CIRCUIT

In this section, the process between the original circuit and the final one to validate the experiment is covered. This circuit, which includes the compensation capacitances to operate in resonance, series-parallel transformations, and impedance matching among others, is used in chapter 5 to perform the experimental validation.

Initially, the circuit planned considering elements given from simulation to transmit 1W with an efficiency of 30.3% between two 20x20cm coaxial coils separated 11cm was that of figure 4.8:

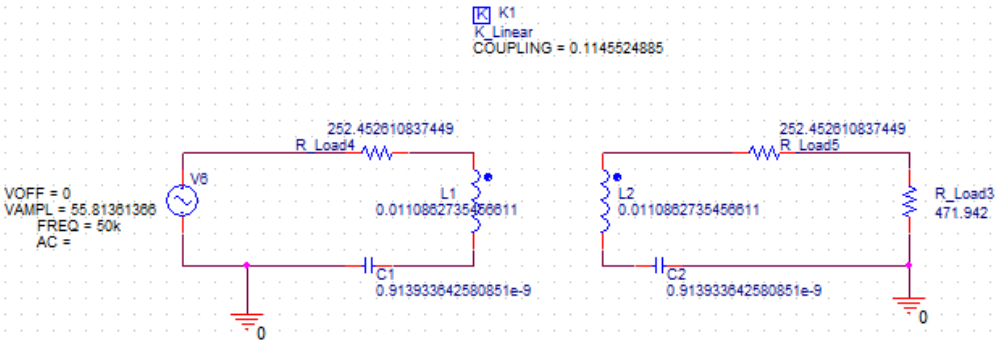

Figure 4.8. Initial test circuit

After, the self-capacitance of the coils was measured with the network analyzer, with a value of 500pF, resulting the circuit of figure 4.9, where the compensation capacitances were changed to resonate at 50kHz taking into account the self-capacitances:

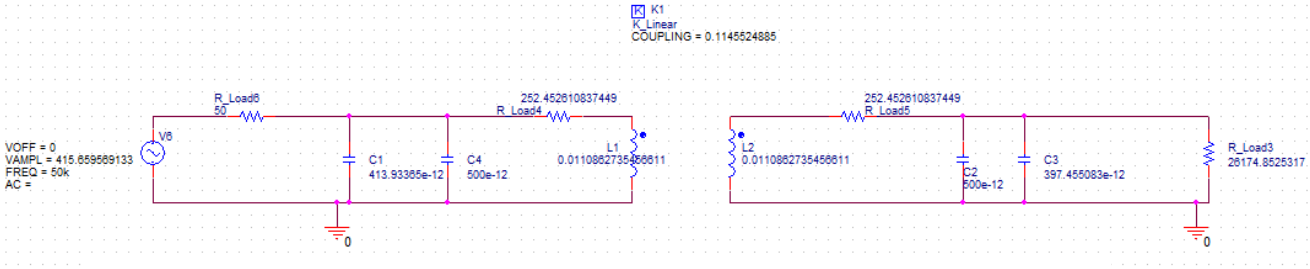

Figure 4.9. Initial circuit considering parallel self-capacitances from the coils

Since the self capacitances are modeled as capacitors in parallel with the inductors, as stated in [67], the resonant circuit becomes parallel parallel (PP) instead of series-series (SS) provoking the voltage needed at the primary input increases from 55.8V to 415V. Also, the load is converted, by means of series to parallel transformation at the resonant frequency, from 471.942Ω to 26174.852Ω.

Since there wasn't a RF amplifier in the lab able to supply 415V, a parallel to series transformation at the resonant frequency was carried out, from which resulted the circuit of figure 4.10:

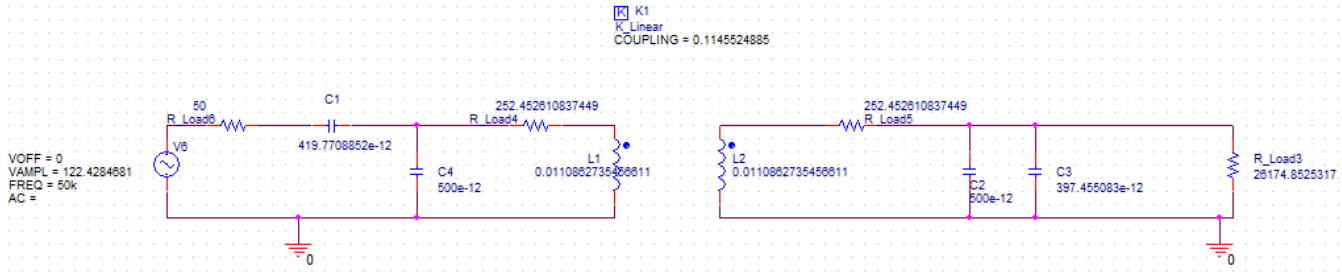

Figure 4.10. Final circuit

This is the final circuit used to do the real experiments in chapter 5; where:

C4 is the self capacitance of the primary coil, *R_Load4* its parasitic resistance, and *L1* its inductance. Self and parasitic words are used interchangeably because they mean the same.

C2 is the parasitic capacitance of the secondary coil, *R_Load5* its parasitic resistance and *L2* its inductance.

C1 is the added primary compensation capacitance and *C3* that of secondary. Both are needed for the wireless resonant transmission to occur at the operating frequency.

The coupling factor *k* between the coils was obtained by the simulation tool of appendix C and the voltage source *V6* was implemented by means of the amplifier circuit described in appendix A (it will be seen in the next chapter that this high voltage couldn't be extracted, and a lower one was used).

5. EXPERIMENTAL RESULTS

5.1. INTRODUCTION

As seen in the previous chapter, the PCBs designed, described in appendix D, didn't produce the expected results due to the large value of the parasitic capacitance of the coils.

Since this value is quite bigger than the expected one, the self resonant frequency of the coils is drastically reduced, causing the transmission distance between coils with a concrete efficiency be lower, as the maximum operating frequency must be smaller than the self-resonant.

However, validation of the analytical optimization method described in section 3.3 can be carried out, as it will be in the following section.

5.2. EXPERIMENTAL RESULTS

To perform the experiments, an operating frequency of 50kHz (the capacitors are chosen in consequence to resonate with the coils at this frequency) and a distance between coaxial coils (without misalignment) of 11 cm is used. Although this operating frequency is quite smaller than the 1MHz planned, the distance is approximately the side of the coils (20cm) and therefore it can be considered mid-range transmission. The test system explained in appendix A, corresponding to figure 5.1, is employed to perform the experiments.

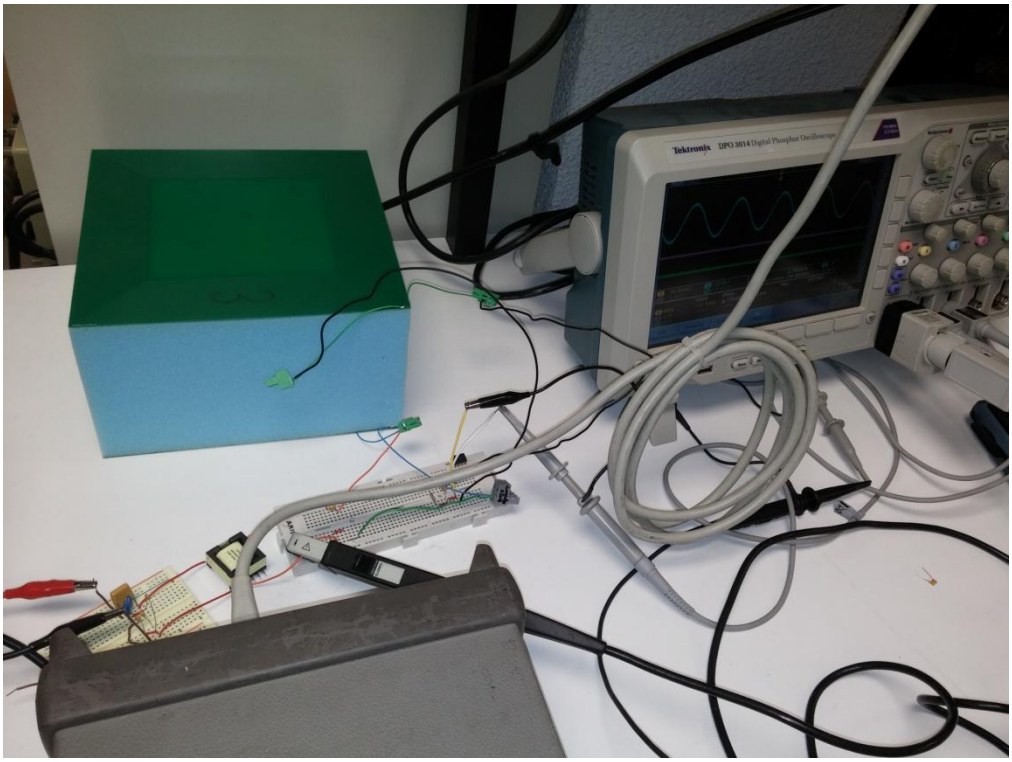

Figure 5.1. Experimental set-up: coils separated 11cm through a custom foam, scope and signal generator

5.2.1. Efficiency

By means of the software described in appendix C, the following theoretical results are obtained for the test set-up in figure 5.2 for a transmission distance of 11cm and an operating frequency of 50kHz: L = 11mH, R = 252.45Ω, efficiency = 30.3%.

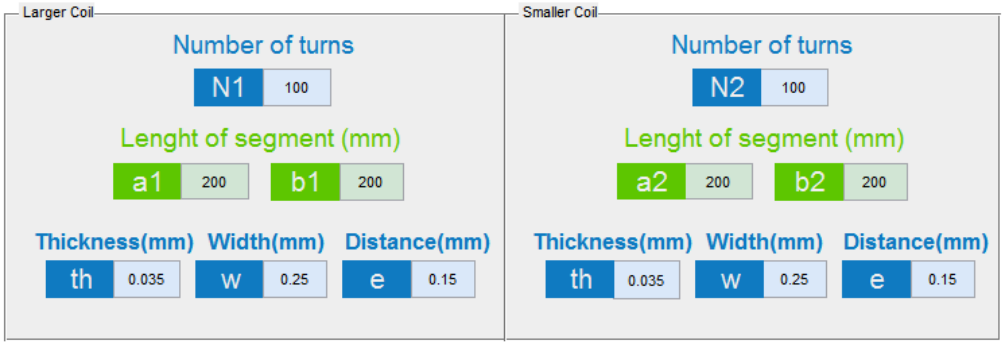

Figure 5.2. Simulated coils corresponding to real coils in figure 5.1

However, measuring the coils with a 2-port network analyzer, gave the following results: R = 320Ω, L = 10mH, what will penalize the efficiency. This difference between the real results and the simulated ones with FastHenry are due to the trace etch factor and other tolerances by the PCB manufacturer.

The efficiency obtained is 10.85%, as shown in table 5.1, lower than the theoretical one due to the reasons explained above. The R_{load} value of 27kΩ corresponds to the optimum one.

V_{1rms}	V_{2rms}	I_{1rms}	R_{load}	P_1	P_o	η
3.38V	4.18V	1.77mA	27kΩ	6mW	0.647mW	10.85%

Table 5.1. Experimental values obtained for test set-up of figure 5.1

The low power value has its origin in the limitations in the amplifier used, since extracting more power from it produced overheating of the devices. But it's a minor problem, since explained in section 3.3, the efficiency and optimum load doesn't depend on the output power.

To measure accurately the low order of magnitude of the current, a digital multimeter was employed.

5.2.2. Efficiency depending on the operating frequency

The results from table 5.2 are obtained when the frequency from the signal generator is varied, proving that the higher efficiency is achieved for the frequency at which the coils are capacitively compensated, i.e., resonating.

f_{op}	V_{1rms}	V_{2rms}	I_{1rms}	R_{load}	P_1	P_o	η
45 kHz	3.42V	1.87V	1.272mA	27kΩ	4.35mW	0.13mW	2.98%
46 kHz	4V	2.7V	1.647mA	27kΩ	6.59mW	0.27mW	4%
47 kHz	4V	3.4V	1.825mA	27kΩ	7.30mW	0.43mW	5.87%
48 kHz	3.8V	3.83V	1.876mA	27kΩ	7.13mW	0.54mW	7.62%
49 kHz	3.55V	4.1V	1.848mA	27kΩ	6.56mW	0.62mW	9.5%
50 kHz	3.37V	4.18V	1.77mA	27kΩ	5.96mW	0.65mW	10.85%
51 kHz	3.33V	4.05V	1.704mA	27kΩ	5.67mW	0.60mW	10.7%
52 kHz	3.42V	3.99V	1.639mA	27kΩ	5.61mW	0.59mW	10.51%
53 kHz	3.62V	3.9V	1.56mA	27kΩ	5.65mW	0.56mW	9.975%
54 kHz	3.81V	3.54V	1.432mA	27kΩ	5.46mW	0.46mW	8.5%
55 kHz	3.94V	3.09V	1.267mA	27kΩ	4.99mW	0.35mW	7%

Table 5.2. Experimental efficiency depending on the operating frequency

5.2.3. Efficiency depending on the input voltage

In table 5.3, the efficiency as a function of the input voltage (V_{1rms}) is shown:

V_{1rms}	V_{2rms}	I_{1rms}	R_{load}	P_1	P_o	η
1.5V	1.8V	0.759mA	27kΩ	1.1385mW	0.12mW	10.54%
2V	2.46V	1.038mA	27kΩ	2.076mW	0.224mW	10.79%
2.5V	3.1V	1.306mA	27kΩ	3.265mW	0.356mW	10.9%
3V	3.69V	1.558mA	27kΩ	4.674mW	0.5043mW	10.79%
3.5V	4.33V	1.845mA	27kΩ	6.458mW	0.6944mW	10.75%

Table 5.3. Experimental efficiency depending on the input voltage

As was predicted in section 3.3, the above results confirm the optimization method since the efficiency is constant, with a minimum error due to the tolerance in the measurements, independently of the input voltage.

5.2.4. Efficiency depending on the load

In table 5.4, the efficiency for different loads is studied; this test was carried out employing a commercial RF amplifier, instead of the described in appendix A. It corresponds to figure 5.3:

Figure 5.3. Set-up used to test the variations in the output load

V_{1rms}	V_{2rms}	I_{1rms}	R_{load}	P_1	P_o	η
3.28V	3.26V	1.798mA	15kΩ	5.90mW	0.71mW	12%
3.34V	4.03V	1.754mA	24kΩ	5.86mW	0.68mW	11.55%
3.44V	4.64V	1.732mA	**27kΩ**	5.96mW	0.80mW	13.38%
3.42V	4.92V	1.701mA	33kΩ	5.82mW	0.73mW	12.6%
3.51V	5.7V	1.681mA	47kΩ	5.90mW	0.69mW	11.72%
3.57V	6.03V	1.671mA	56kΩ	5.97mW	0.65mW	10.9%
3.63V	6.42V	1.659mA	68kΩ	6.02mW	0.61mW	10%
3.65V	6.75V	1.641mA	82kΩ	5.99mW	0.56mW	9.27%

Table 5.4. Experimental efficiency depending on the output load

As demonstrated above and foreseen by the optimization method, the maximum efficiency is achieved when $Z=Z_{opt}$, which occurs for $R_{load}=27k\Omega$. Such efficiency is calculated through:

$$\eta = \frac{P_o}{P_1} = \frac{\frac{V_{2rms}{}^2}{R_{load}}}{V_{1rms} * I_{1rms}} \qquad (5.1)$$

Also, in figure 5.4, appear the waveforms of V_1 and V_2 (purple and green curves respectively), for Rload=27kΩ.

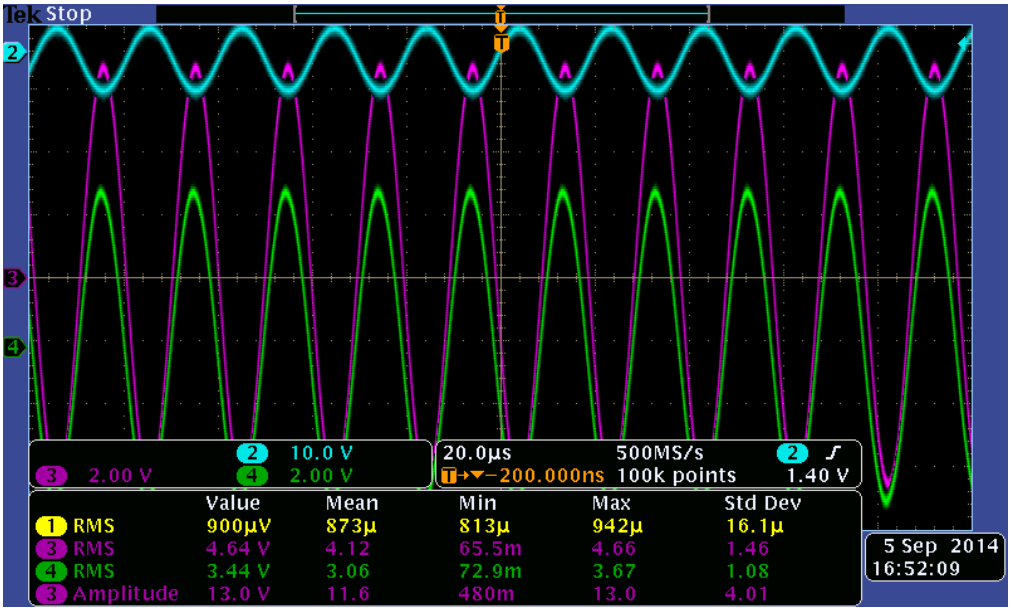

Figure 5.4. V_1 and V_2 waveforms for Rload=27kΩ (optimum)

6. CONCLUSIONS AND FUTURE WORK

6.1. CONCLUSIONS

Wireless power transfer will see a rapid boost these days due to the increment of mobile devices in the market and the need of charging them continuously. It is being currently standardized for short-distances [1], however, its drawbacks for mid- and far distances must be solved yet.

During the execution of this work, the goals pursued have been satisfied. In the following lines, a summary appears covering the work developed:

Firstly, the wireless power transfer mechanisms are studied and analysed, choosing the resonant inductive coupling as the means to transfer considerable energy when relatively long distances are present. Next, the parameters affecting the transmission and the coils are studied and considered, although the appearance of a large parasitic capacitance will limit the operating frequency in the experiments.

Several optimization methods in chapter 3 are exposed and that of section 3.3 has been validated in chapter 5 for mid-range distances, whereof it can be concluded than if the input voltage can be varied, the maximum efficiency can be achieved independently of the output power if the optimum load is used.

To conclude, an optimization program has been developed to build the coils that, for a determined geometry, produce the highest efficiency and power transfer.

In summary, a better understanding from wireless power transfer by means of resonant inductive coupling has been carried out, apart from developing optimization methods for the efficiency and the geometrical design of the coils, validating experimentally the theory with success.

6.2. FUTURE WORK

From the studied in this work, many open investigations arise in this research topic:

- The influence of numerous receivers should be studied for an application where many of them must be charged simultaneously in, e.g., a room.
- Establishing a control algorithm to tune automatically the compensation capacitances, to operate always in resonance and for the optimum load.
- Building an inverter with minimum losses able to work at different frequencies to supply the voltage to the primary inductance and whose range of output voltages allows obtaining bigger power at the load, instead of the miliwatts from this work.
- Studying the effects of high frequency magnetic fields for the health, in order to limit the power transfer in presence of people.
- Implementing the receiver coil in a mobile device, to study if exist undesired couplings between the phone and the coil.
- Constructing a large primary, like those theoretically studied in chapter 2 of, e.g., 1mx1m, since this primary allows obtaining higher levels of coupling factors, what implies more power transferred to the secondary and efficiency.

- Studying all the compensation topologies, choosing the appropriate depending on the application.
- Designing new geometrically optimized coils according to the results from chapter 4.

References

Wireless Power Transfer

[1] *(2014, Jan.). Wireless power consortium [Online]. Available: http://www.wirelesspowerconsortium.com/.*

[3] *Hui, S.Y.R.; Zhong, W.X.; Lee, C.K.;, "A Critical Review of Recent Progress in Mid-Range Wireless Power Transfer," IEEE Trans. Power Electronics, vol. 29, no. 9, pp. 4500-4511, Mar. 2013.*

[4] *N. Tesla, "Apparatus for transmitting electrical energy," U.S. Patent 1,119,732, Dec. 1, 1914.*

[5] *Venugopal Prasanth, "Wireless Power Transfer for E-mobility", Master Thesis, July 2011.*

[6] *Robert Lomas, The man who invented the twentieth century – Nikola Tesla – Forgotten Genius of Electricity. Headline 1999, ISBN 0 7472 6265 9, p. 146.*

[7] *J. C. Schuder, H. E. Stephenson, and J. F. Townsend, "High level electromagnetic energy transfer through a closed chestwall," IRE Int. Conv. Rec., pt.9, vol.9, pp. 119-126, 1961.*

[8] *W. H. Ko, S. P. Liang, and C.D.F. Fung, "Design of rf-powered coils for implant instruments," Med. Biol. Eng. Comput., vol. 15, pp. 634-640, 1977.*

[9] *E. Hochmair, "System optimization for improved accuracy in transcutaneous signal and power transmission", IEEE Trans. Biomedical Engineering, vol. BME-31, no.2, pp. 177-186, Feb. 1984.*

[10] *B. Choi, J. Nho, H. Cha, T. Ahn and S. Choi, "Design and implementation of low-profile contactless battery charger using planar printed circuit board windings as energy transfer device," IEEE Trans. Industrial Electronics, vol. 51, no. 1, pp. 140-147, Feb. 2004.*

[11] *Y. Jang and M. M. Jovanovic, "A contactless electrical energy transmission system for portable telephone battery chargers", IEEE Trans. Industrial Electronics, vol. 50, no. 3, pp. 520–527, Jun. 2003.*

[12] *W.G. Hurley and J. Kassakian, "Induction heating of circular ferromagnetic plates", IEEE Trans. Magnetics, vol. 15, no. 4, pp. 1174-1181, Jul. 1979.*

[13] *A.W. Green and J.T. Boys, "10 kHz inductively coupled power transfer-concept and control", in Proc. ICPE-VSD, 1994, pp. 694–699.*

[14] *J.T. Boys, G.A. Covic and A.W. Green, "Stability and control of inductively coupled power transfer systems", in Proc. Electric Power Applications, 2000, vol. 147, no. 1, pp. 37–43.*

[15] *J.T. Boys, A.P. Hu and G.A. Covic, "Critical Q analysis of a current-fed resonant converter for ICPT applications", Electronics Letters, vol. 36, no. 17, pp. 1440–1442, 2000.*

[16] *G.A.J. Elliott, G.A. Covic, D. Kacprzak and J.T. Boys, "A New Concept: Asymmetrical Pick- Ups for Inductively Coupled Power Transfer Monorail Systems", IEEE Trans. Magnetics, vol. 42, no. 10, pp. 3389–3391, 2006.*

[17] *M.L.G. Kissin, J.T. Boys and G.A. Covic, "Interphase Mutual Inductance in Polyphase Inductive Power Transfer Systems", IEEE Trans. Industrial Electronics, vol. 56, no. 7, pp. 2393–2400, 2009.*

[20] *C. G. Kim, D. H. Seo, J. S. You, J. H. Park and B. H. Cho, "Design of a contactless battery charger for cellular phone", IEEE Trans. Industrial Electronics, vol. 48, no. 6, pp. 1238-1247, Dec. 2001.*

[21] *S.Y.R. Hui and W.C. Ho, "A new generation of universal contactless battery charging platform for portable Consumer Electronic equipment", IEEE Trans. Power Electronics, vol. 20, no. 3, pp. 620–627, May 2005.*

[22] *X. Liu and S.Y.R. Hui, "Simulation Study and Experimental Verification of a Contactless Battery Charging Platform with Localized Charging Features," IEEE Trans. Power Electronics, vol. 22, no.6, pp. 2202–2210, Nov. 2007.*

[23] *S.Y.R. Hui, "Planar Inductive Battery Charging System", US Patent 7,576,514, 2009.*

[24] *Yiming Zhang; Zhengming Zhao; Kainan Chen, "Frequency splitting analysis of magnetically-coupled resonant wireless power transfer," Energy Conversion Congress and Exposition (ECCE), 2013 IEEE , vol., no., pp.2227,2232, 15-19 Sept. 2013.*

[25] *G. Franceschetti, V. Gervasio, "Wireless Power Transmission. A new science is borne," in Proc. IEEE MTT-S International Microwave Workshop Series on Innovative Wireless Power Transmission: Technologies, Systems, and Applications, pp. 21-23, Sep. 2012.*

[26] *L. Chao and A. P. Hu, "Steady state analysis of a capacitively coupled contactless power transfer system," in Proc. IEEE Energy Conversion Congress and Exposition, pp. 3233-3238, Sep. 2009.*

[27] *Chao Liu; Hu, A.P.; Nair, N.K.C.; Covic, G.A.; , "2-D alignment analysis of capacitively coupled contactless power transfer systems," Energy Conversion Congress and Exposition (ECCE), 2010 IEEE, pp.652-657, 12-16 Sept. 2010.*

[29] *C. Y. Huang, J. T. Boys and G. A. Covic, "LCL Pickup Circulating Current Controller for Inductive Power Transfer Systems," IEEE Transactions on Power Electronics, vol.28, pp. 2081-2093, 2013.*

[30] *L. L. Hao, A. P. Hu and G. A. Covic, "A Direct AC-AC Converter for Inductive Power-Transfer Systems," IEEE Transactions on Power Electronics, vol.27, pp. 661-668, 2012.*

[31] *D. Kurschner, C. Rathge and U. Jumar, "Design Methodology for High Efficient Inductive Power Transfer Systems with High Coil Positioning Flexibility," IEEE Transactions on Industrial Electronics, vol.60, pp. 372-381, 2013.*

[32] *Waffenschmidt, Eberhard. "Wireless power for mobile devices," Telecommunications Energy Conference (INTELEC), 2011 IEEE 33rd International. IEEE, 2011.*

[33] *Kelley, A.W., and Owens, W.R.: "Connectorless power supply for an aircraft-passenger entertainment system", IEEE Trans., 1989, PE-4, (3), pp. 348-354.*

[34] *Ross, H.R., Lechner, E.H., and Schweinberg, R.N.: "Playa Vista roadway powered electric vehicle project". Proceedings of international Electric vehicle symposium, Hong Kong, 1990, Vol. 10, pp. 981-992.*

[35] *Klontz, K.W., Divan, D.M., Novotny, D.W., and Lorenz , R.D.: "Contactless power delivery system for mining applications", IEEE Trans., 1995, IA-30, (1), pp. 27-35.*

[36] *Green, A.W., and Boys, J.T.: "An inductively coupled high frequency power system for material handling applications". International Power electronics conference, IPEC'93, Singapore, 1993, Vol. 2, pp. 821-826.*

[37] *Boys, J.T., and Green, A.W.: "Inductively coupled power transmission concept - design and application", IPENZ Trans., 1995, 22, (1), pp. 1-9.*

[38] *Hiraga, Y., Hirai, J., Kawamura, A., Ishoka, I., Kaku, Y., and Nitta, Y.: "Decentralised control of machines with the use of inductive transmission of power and signal". IEEE Industrial Applications Society Annual Meeting. 1994. Vol. IAS-29. pp. 875-881.*

[39] *Boys, J.T., and Green, A.W.: "Intelligent road-studs - Lighting the paths of the future", IPENZ Trans., 1997, 24, (1), pp. 33-40.*

[40] *G. Elliot, G. Covic, D. Kacprzak, and J. T. Boys, "A new concept: Asymmetrical pick-ups for inductively coupled power transfer monorail systems," IEEE Trans. Magn., vol. 42, no. 10, pp. 3389–3391, Oct. 2006.*

[41] *B. M. Sang, R. Kratz, and S. Gurol, "Contactless inductive power pickup system for Maglev applications," in Conf. Rec. IEEE IAS Annu. Meeting, Oct. 2002, vol. 3, pp. 1586–1591.*

[42] *C. S. Wang, O. H. Stielau, and G. A. Covic, "Design consideration for a contactless electric vehicle battery charger," IEEE Trans. Ind. Electron., vol. 52, no. 5, pp. 1308–1313, Oct. 2005.*

[43] *G. A. Covic, G. Elliot, O. H. Stielau, R. M. Green, and J. T. Boys, "The design of a contactless energy transfer system for a people mover system," in Proc. Int. Conf. Power Syst. Technol., Dec. 2000, vol. 1, pp. 79–84.*

[44] *G. A. Covic, J. T. Boys, M. L. G. Kissin, and H. G. Lu, "A three-phase inductive power transfer system for roadway-powered vehicles," IEEE Trans. Ind. Electron., vol. 54, no. 6, pp. 3370–3378, Dec. 2007.*

[45] *C. S. Wang, G. A. Covic, and O. H. Stielau, "Power transfer capability and bifurcation phenomena of loosely coupled inductive power transfer system," IEEE Trans. Ind. Electron., vol. 51, no. 1, pp. 148–157, Feb. 2004.*

[46] *C. Wang, G. A. Covic, and O. Stielau, "General stability criterions for zero phase angle controlled loosely coupled inductive power transfer systems," in Proc. Ind. Electron. Soc. Conf., Dec. 2001, vol. 2, pp. 1049–1054.*

[47] *Y. H. Chao, J. Shieh, C. T. Pan, and W. C. Shen, "A closed-form oriented compensator analysis for series–parallel loosely coupled inductive power transfer systems," in Proc. Power Electron. Spec. Conf., Jun. 2007, pp. 1215–1220.*

[48] *Sallan, J.; Villa, J.L.; Llombart, A.; Sanz, J.F.; "Optimal Design of ICPT Systems Applied to Electric Vehicle Battery Charge"; Industrial Electronics, IEEE Transactions on; Volume: 56; 2009; Page(s): 2140 – 2149.*

[49] *A. Kurs, A. Karalis, R. Moffatt, J. D. Joannopoulos, P. Fisher, and M. Soljacic, "Wireless power transfer via strongly coupled magnetic resonances," Science, vol. 317, no. 5834, pp. 83–86, Jul. 2007.*

[50] *W. W. Massie and C. R. Underhill, ''The future of the wireless art,'' Wireless Telegraphy Telephony, pp. 67–71, 1908.*

[51] *W. C. Brown, ''The history of power transmission by radio waves,'' IEEE Trans. Microw. Theory Tech., vol. MTT-32, no. 9, pp. 1230–1242, Sep. 1964.*

[52] *A. P. Smakhtin and V. V. Rybakov, ''Comparative analysis of wireless systems as alternative to high-voltage power lines for global terrestrial power transmission,'' in Proc. 31st Intersoc. Energy Conv. Eng. Conf., Aug. 11–16, 1996, vol. 1, pp. 485–488.*

[53] *I.J. Yoon and H. Ling, "Investigation of near-field wireless power transfer in the presence of lossy dielectric materials", IEEE Trans. Antenna and Propogation, vol. 61, no. 1, pp. 482-488, Jan. 2013.*

[54] *S. Cheon, Y.H. Kim, S.Y. Kang, M. L. Lee, J.M. Lee, and T. Zyung, "Circuit-model-based analysis of a wireless energy-transfer system via coupled magnetic resonances", IEEE Trans. Industrial Electronics, vol. 58, no. 7, pp. 2906-2914, Jul. 2011.*

[56] *M. Budhia, G. Covic and J. Boys, "Design and optimization of circular magnetic structures for lumped inductive power transfer systems", IEEE Trans. Power Electronics, vol.26, no.11, pp. 3096-3107, Nov. 2011.*

[57] *M. Budhia, J. Boys, G. Covic and C.Y. Hang, "Development of a single-sided flux magnetic coupler for electric vehicle IPT charging systems", IEEE Trans. Industrial Electronics, vol. 60, no. 1, pp. 318-328, Jan. 2013.*

[61] *A. Kurs, "Power transfer through strongly coupled resonances", M.Sc. Thesis, MIT, Sept. 2007, pp. 39-40.*

[62] *Garnica, J.; Chinga, R.A.; Jenshan Lin, "Wireless Power Transmission: From Far Field to Near Field," Proceedings of the IEEE , vol.101, no.6, pp.1321-1331, June 2013.*

[63] *Park, Changbyung; Sungwoo, Lee; Cho, Gyu-Heoyng; Rim, Chun T.;, "Innovative 5m-off-distance Inductive Power Transfer Systems with Optimally Shaped Dipole Coils," IEEE Trans. Power Electronics, vol. PP, no. 99, pp. 1, Mar. 2014.*

[64] *Carlos Alberto López Pérez, "Phase Shift Control Technique to Improve Wireless Power Transference Systems", Master Thesis, March 2014.*

[65] *Pablo Sebastián Revuelta, "Optimización del rendimiento y la potencia transmitida en sistemas de transmisión de energía inalámbrica", End of degree Project, June 2014.*

[80] *Cannon, Benjamin L.; Hoburg, James F.; Stancil, Daniel D.; Goldstein, Seth;, "Magnetic Resonant Coupling As a Potential Means for Wireless Power Transfer to Multiple Small Receivers," IEEE Trans. on Power Electronics, vol. 24, no. 7, pp. 1819-1825, July. 2009.*

Miscellaneous

[2] *FastFieldSolvers, including software FastHenry, FastCap and FastModel. Available: http://www.fastfieldsolvers.com/.*

[18] *M. K. Kazimierczuk, RF Power Amplifiers. New York, NY, USA: Wiley, 2008.*

[19] *Altium Designer. Available: http://www.altium.com/.*

[58] *"ICNIRP Guidelines for Limiting Exposure to Time-varying Electric, Magnetic and Electromagnetic fields (1Hz to 100kHz)", Health Physics, vol. 99, no. 6, pp. 818-836, Dec. 2010.*

[59] *"ICNIRP Guidelines for Limiting Exposure to Time-varying Electric, Magnetic and Electromagnetic fields (up to 300GHz)", Health Physics, vol. 74, no. 4, pp. 494-522, 1998.*

[60] *IEEE Standard for Safety Levels with Respect to Human Exposure to Radio Frequency Electromagnetic Fields 3kHz to 300 GHz, IEEE 2006.*

[77] *J. D. Kraus, Antennas. NewYork: McGraw-Hill, 1988, p.251.*

Coil design

[28] *Lee, C.K.; Su, Y.P.; Hui, S.Y.R.;, "Multilayer Stacked Coreless Printed Spiral Winding Inductor with Wide Frequency Bandwidth," ECCE 2009, Sept. 20-24, 2009, pp. 1002-1009.*

[55] *Chen, Kainan; Zhao, Zhengming;, "Analysis of the Double-Layer Printed Spiral Coil for Wireless Power Transfer," IEEE Emerging and Selected Topics in Power Electronics, vol. 1, no. 2, pp. 114-121, June. 2013.*

[66] *Schmidt, Ingo; Enders, Achim;, "Characterization and Concept for Optimization of Planar Spiral High Power High Frequency Coils," IEEE International Symposium on EMC2009, Aug. 17-21, 2009, pp. 24-28.*

[67] *Zolog, Monica; Pitică, Dan; Pop, Ovidiu;, "Characterization of Spiral Planar Inductors Built on Printed Circuit Boards," 30th International Spring Seminar on Electronics Technology, May 9-13, 2007, pp. 308-313.*

[68] *Gevorgian, S.; Berg, H.; Jacobsson, H.; Lewin, T.;, "Basic Parameters of Coplanar-Strip Waveguides on Multilayer Dielectric/Semiconductor Substrates, Part 1: High Permittivity Superstrates," IEEE Microwaves Magazine, vol. 4, no. 2, pp. 60-70, June 2003.*

[69] *Olivo, Jacopo; Sandro, Carrara; De Micheli, Giovanni;, "Modelling of Printed Spiral Inductors for Remote Powering of Implantable Biosensors," 5th ISMICT, Mar. 27-30, 2011, pp. 29-32.*

[70] *Hui, Dong; Zhu, Yisheng; Zhao, Baishan;, "Calculation and Application in RFID of the PCB Spiral Inductors," IEEE ICEBE, Oct. 21-23, 2009, pp. 460-464.*

[71] *Jow, Uei-Ming; Ghovanloo, Maysam;, "Design and Optimization of Printed Spiral Coils for Efficient Transcutaneous Inductive Power Transmission," IEEE Trans. Biomedical Circuits and Systems, vol. 1, no. 3, pp. 193-202, Sep. 2007.*

[72] *Islam, Ashram B.; Islam, Syed K.; Tulip, Fahmida S.;, "Design and Optimization of Printed Circuit Board Inductors for Wireless Power Transfer System," Circuits and Systems, vol. 4, no. 2, pp. 237-244, 2013.*

[73] *Hämmerle, Florian;, "Characterization of a Miniaturized Planar Coil," Master Thesis, Aug. 2009.*

[74] *Zhao, Jonsenser;, "A new calculation for designing multilayer planar spiral inductors," EDN, July 29, 2010.*

[75] *Mohan, Sunderarajan S.; Hershenson, Maria del Mar; Boyd, Stephen P.; Lee, Thomas H.;, "Simple Accurate Expressions for Planar Spiral Inductances," IEEE Solid-State Circuits, vol. 34, no. 10, pp. 1419-1424, Oct. 1999.*

[76] *Mohan, Sunderarajan S.;, "The Design, modelling and optimization of on-chip inductor and transformer circuits," PhD Thesis, Aug. 2000.*

[78] *F. W. Grover, Inductance Calculations. New York: Dover, 1964.*

[79] *Babic, Slobodan; Sirois, Frédéric; Akyel, Cevdet; Girardi, Claudio;, "Mutual Inductance Calculation Between Circular Filaments Arbitrarily Positioned in Space: Alternative to Grover's Formula," IEEE Trans. on Magnetics, vol. 46, no. 9, pp. 3591-3600, Sept. 2010.*

Appendix A – Test circuit

As different levels of current, voltage and frequency are needed to test the boards and proving the simulations and theory, some circuits between the signal generator and the primary coil are necessary to give some versatility, and also since the power that can be obtained from a signal generator is low.

The circuits used belong to the scheme in figure A.1:

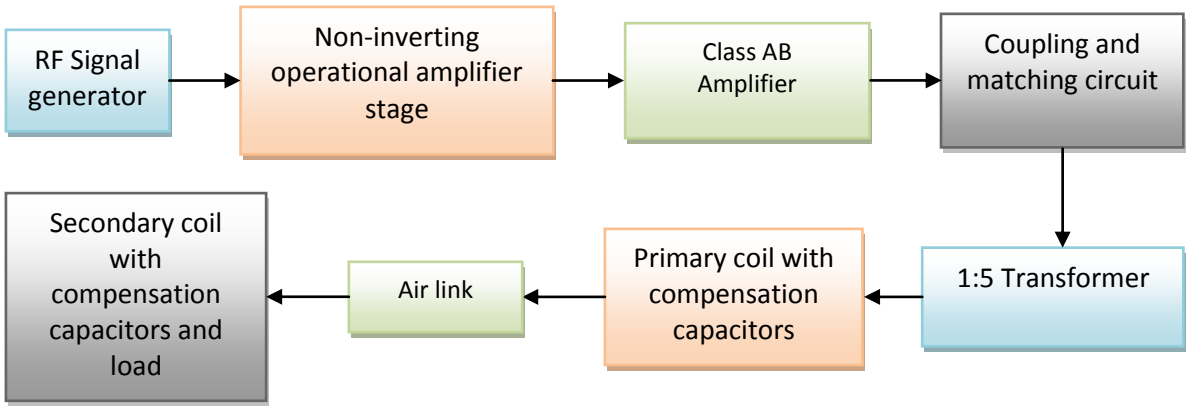

Figure A.1. Diagram of the electrical circuits used

Firstly, the RF signal generator is used to provide a low voltage and power signal with a variable RF frequency; then a non-inverting operational amplifier stage has a voltage gain such that the signal voltage at its output is several times higher than that of its input.

To avoid the complexity of triggering the mosfets in a full-bridge class D amplifier [18], despite its higher efficiency, a class AB amplifier is implemented, like that of figure A.2. Afterwards, a coupling circuit to eliminate the DC level and prevent this to reach the transformer, and a matching circuit are mounted; since the transformer is an inductive load, this matching circuit is essential to eliminate the reactive part near the operating frequency because its absence would imply very high losses in the transistors of the class AB amplifier.

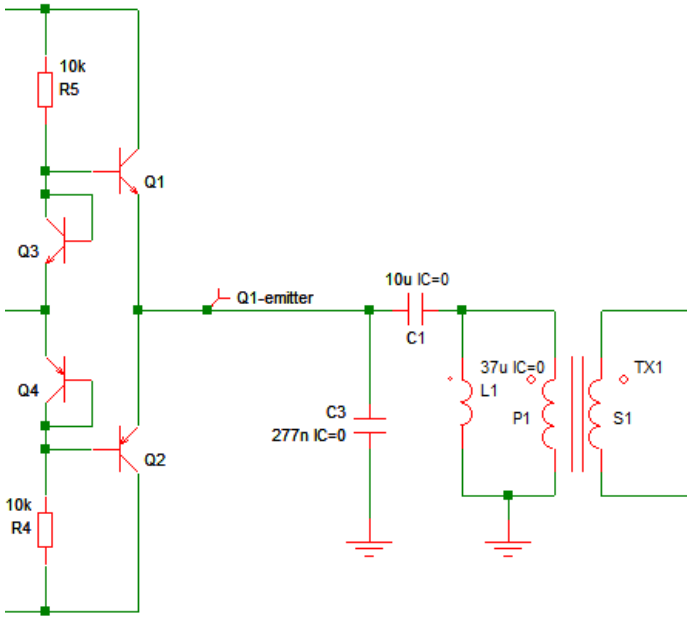

Figure A.2. Class AB amplifier, coupling and matching circuit and transformer

Then, a transformer is used to elevate the voltage of the output signal due to the voltage at the input in the primary coil must be over 100 volts. Finally, it is connected to the primary coil which is magnetically coupled with the secondary through the air.

Appendix B – PCBs designed

In order to validate the model proposed in chapter 3.3 and so as to make other tests and experiments, two printed circuit boards (PCB) were designed using Altium Designer [19].

The first one, used in the experiment described in chapter 5, corresponding to figures B.1 and B.2, is a two layer 20x20cm PCB, with 100 turns in each layer, both connected in series through vias. The width of the tracks is 0.25mm, their separation 0.15mm and the layer thickness 35um (1oz).

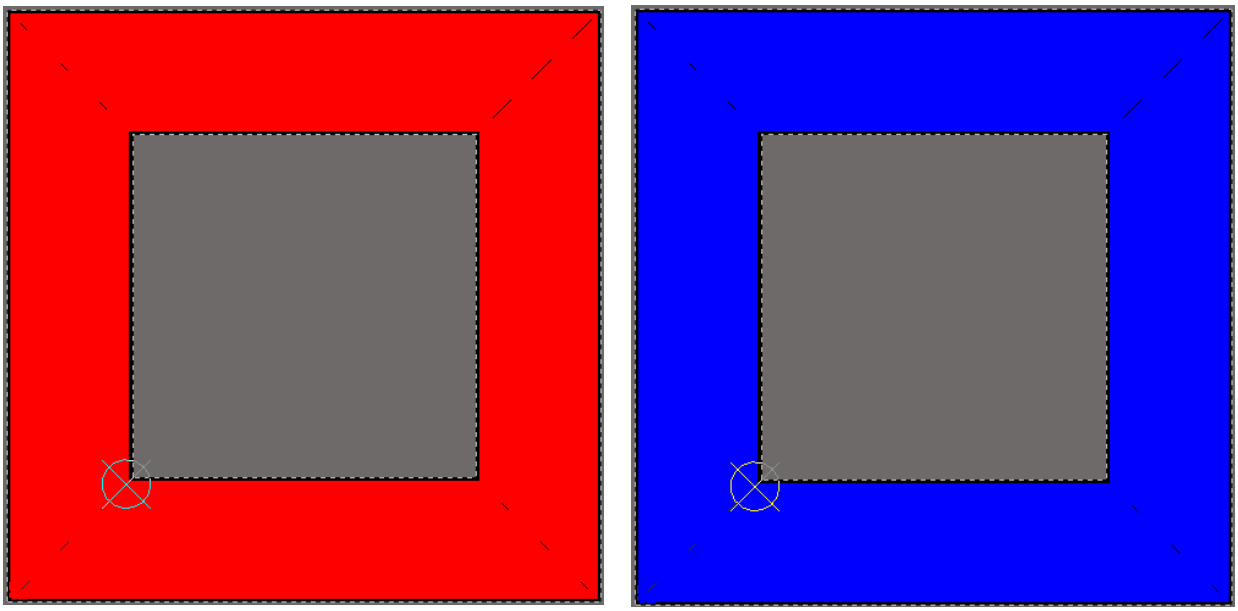

Figure B.1. 20x20cm top and bottom layers

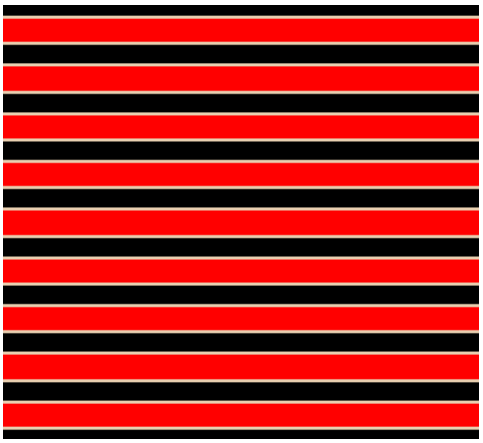

Figure B.2. TOP layer zoom

The second one, corresponding to figures B.3 and B.4, is a four layer 10x10cm PCB, with 100 turns in each layer, all connected in series through vias. The width of the tracks is 0.25mm, their separation 0.15mm and the layer thickness 35um (1oz).

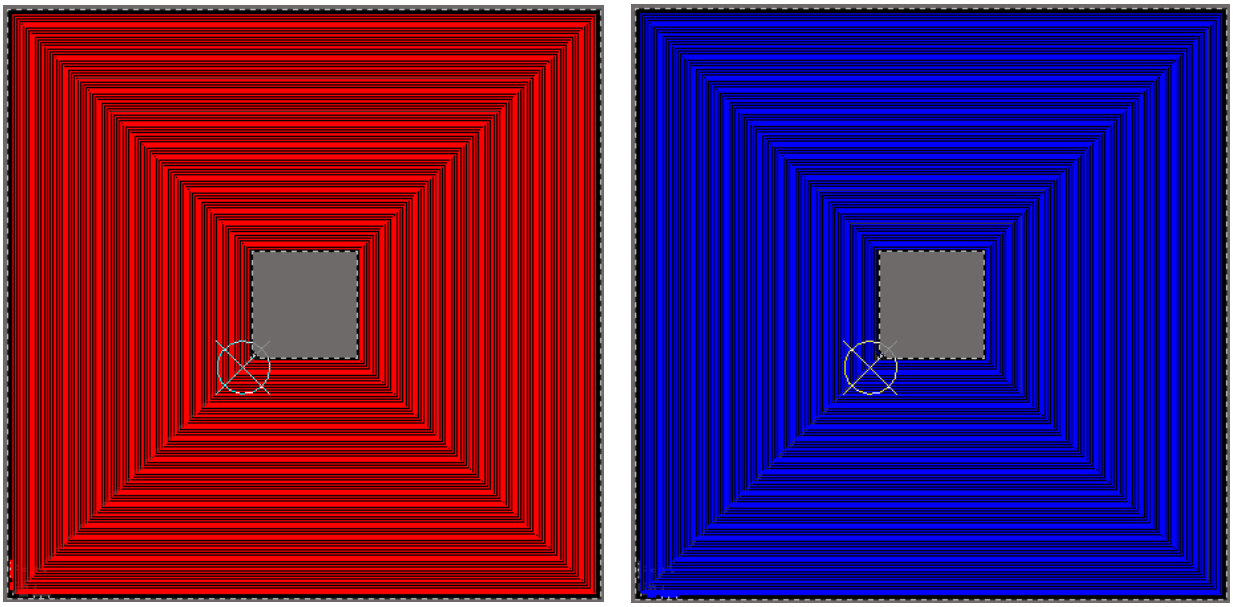

Figure B.3. 10x10cm external layers

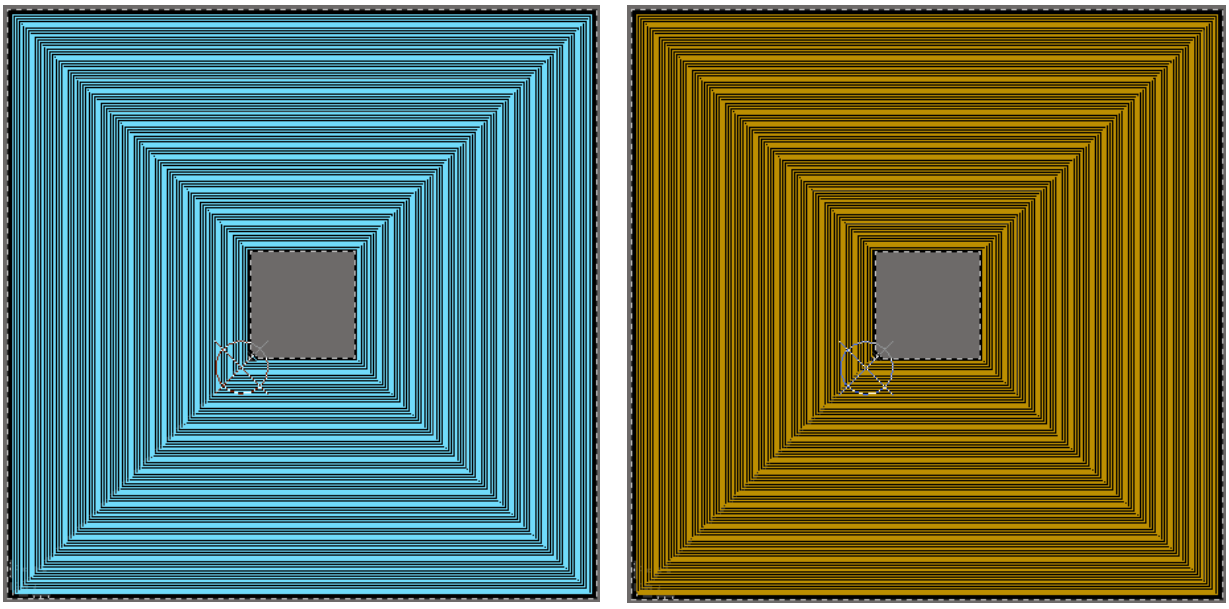

Figure B.4. 10x10cm internal layers

Appendix C – Software implemented for automated simulations

To perform the simulation tests presented in chapter two and appendix D, a Matlab® program with GUI (graphic user interface) was carried out. This software, figure C.1, once introduced some parameters of the desired scenario, is able to make up a script, figure C.2, compatible with a field solver software, containing the geometrical data about the coils, operating frequency, discretization step (a more precise step implies a slower simulation but better results), misalignment between the coils...

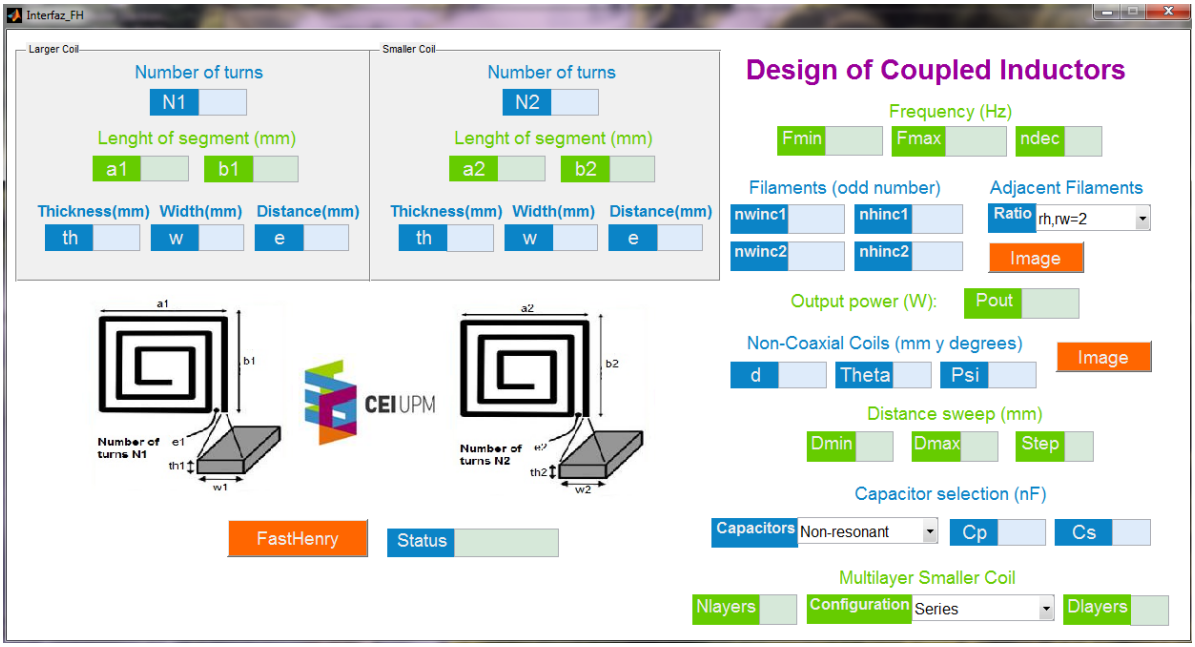

Figure C.1. Screenshot of the matlab program GUI

```
.Units MM
.Default z=0 sigma=5.8e4 w=0.25 h=0.105 nhinc=1 nwinc=11 rh=2 rw=2

* Los nodos:

N1 x=0 y=0
N2 x=980.275 y=0
N3 x=980.275 y=980.55
N4 x=-0.275 y=980.55
N5 x=-0.275 y=-0.4
N6 x=980.675 y=-0.4
N7 x=980.675 y=980.95
N8 x=-0.675 y=980.95
N9 x=-0.675 y=-0.8
N10 x=981.075 y=-0.8
N11 x=981.075 y=981.35
N12 x=-1.075 y=981.35
N13 x=-1.075 y=-1.2
N14 x=981.475 y=-1.2
N15 x=981.475 y=981.75
N16 x=-1.475 y=981.75
N17 x=-1.475 y=-1.6
N18 x=981.875 y=-1.6
N19 x=981.875 y=982.15
N20 x=-1.875 y=982.15
N21 x=-1.875 y=-2
N22 x=982.275 y=-2
N23 x=982.275 y=982.55
N24 x=-2.275 y=982.55
N25 x=-2.275 y=-2.4
N26 x=982.675 y=-2.4
N27 x=982.675 y=982.95
```

Figure C.2. Part of a FastHenry script

That field solver software is free unlike other commonly used FEA (finite element analysis) programs and faster, it is called FastHenry [2], and it solves the self- and mutual resistances and inductances of the 2-coil scenario described by the script; it also permits to see the spatial distribution of the coils for clarity (figure C.3).

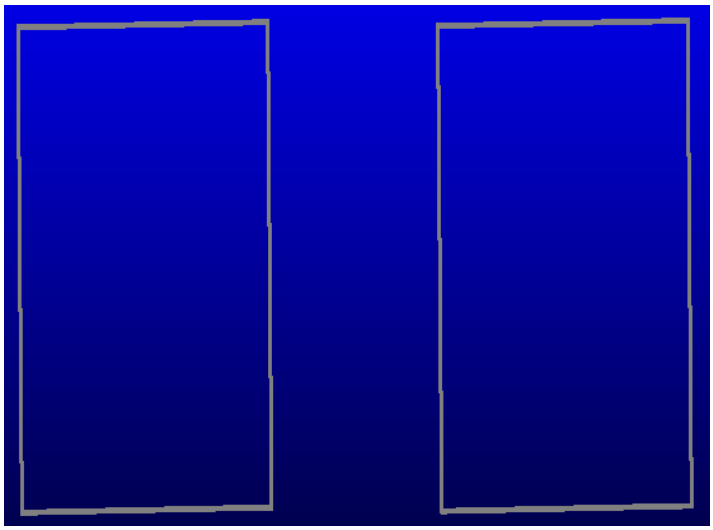

Figure C.3. Example of spatial distribution of two coils

Besides, the matlab program launches FastHenry with the script created through an automation object provided by FastHenry and receives the results calculated, to show the most interesting results after, in an excel sheet, as seen in figure C.4; these results are achieved after some mathematical processing, using equations from chapter 3, including currents, voltages, inductances, resistances and the necessary compensation capacitances to build the circuit which gets the maximum efficiency using the coils introduced.

Distancia(mm)	Frecuencia(Hz)	L1(H)	L2(H)	M(ohm)	Mbabic(ohm)	Mdipolo(ohm)	R1(ohm)	R1teor(ohm)	R2(ohm)	R2teor(ohm)	Rendimiento(%)	I1ef(A)	I1arg(Deg)	I2ef(A)	I2arg(Deg)	V1ef(V)	V1arg(Deg)	V2ef(V)	V2arg(Deg)	Cp(nF)	Cs(nF)
1000	1000000	0,00263	0,00263	386,3957	404,70457	785,398163	81,10916	123,20227	81,10916	123,20227	65,91522133	0,06199	0	0,050327	90	24,474	2,66E-13	19,87	90	0,009638	0,009638

Figure C.4. Screenshot of an example of an excel sheet with its results

The results from the excel sheet can be used then to construct an Orcad® schematic circuit in order to run electric simulations like that on figure C.5.

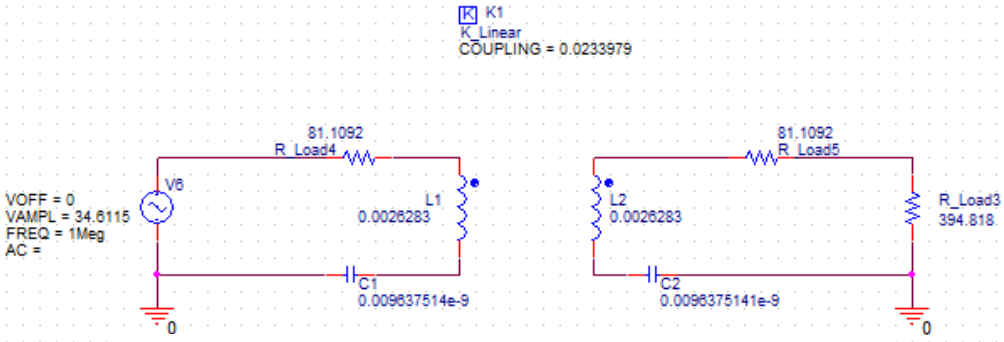

Figure C.5. Orcad circuit to simulate a 2-coil resonant WPT system

Appendix D – Intermediate resonators

In spite of not being part of the main research, the influence of intermediate resonators between the primary (transmitter) and the secondary (receiver) is simulated and proved, with the purpose of validating what is stated in many papers [3]. Two scenarios are considered, the first one is based on coils with the same dimensions, while the second one is formed by different coils; in both cases the power transferred to the load is 1W.

D.1. Equal coils

When two coaxial coils of 25 turns, 1mx1m at a resonant frequency of 1MHz are separated 1m, the calculated theoretical efficiency by means of the software described in appendix C is **65.9%** (figures D.2 and D.3); however, when another resonator is set at an intermediate distance of that of the ends (figures D.1 and D.4), the efficiency is **82.75%.**

Therefore, the intermediate resonator acts like a repeater, increasing the coupling and so the mutual inductance.

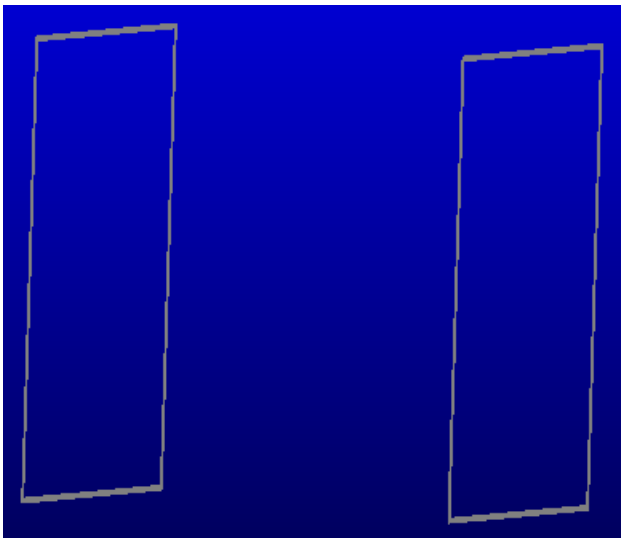

Figure D.2. Two equal resonators in FastHenry

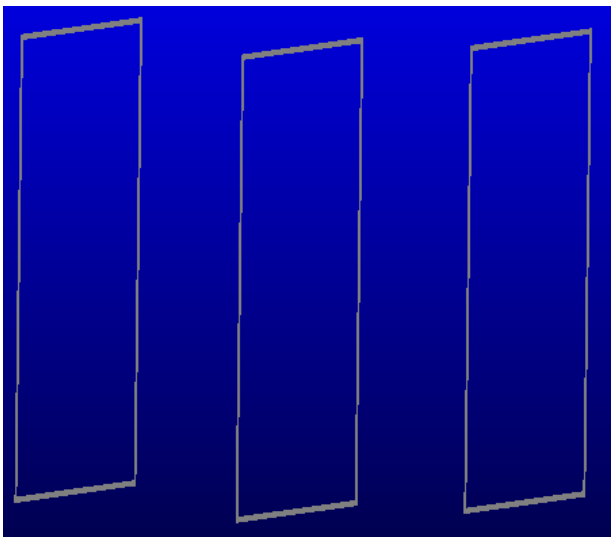

Figure D.1. Three equal resonators in FastHenry

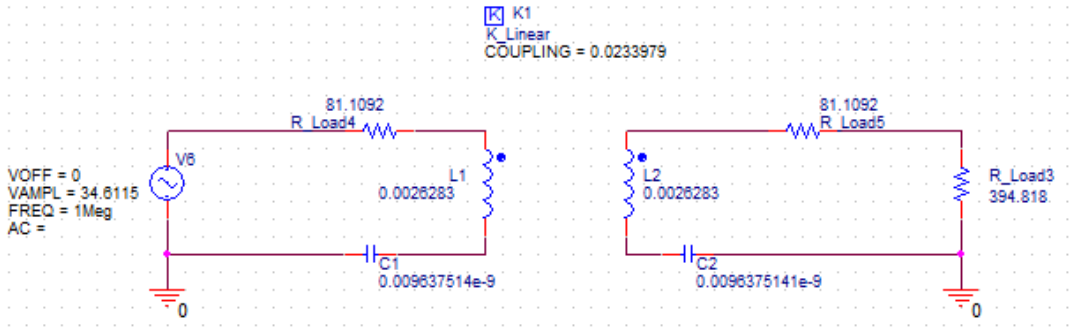

Figure D.3. Two equal resonators electrical circuit

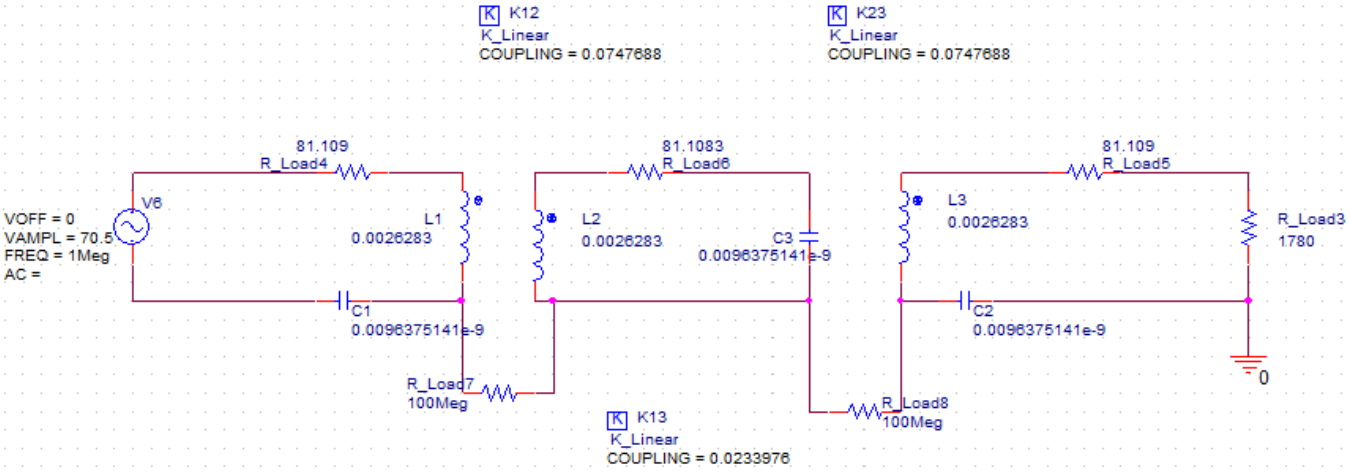

Figure D.4. Three equal resonators electrical circuit

D.2. Different coils

Now, one resonator of 25 turns, 1mx1m is separated 1m from other with 100 turns and 0.2mx0.2m (figure D.6); the efficiency turns to be **28.18%** when the operating (resonant) frequency is 1MHz. If in the middle of both a coil with the dimensions of the smaller one is placed (figures D.5 and D.7), the efficiency results to be very similar or even worse; thus, in this case the intermediate resonator isn´t very useful due to its reduced dimensions compared to that of the primary (the larger coil), therefore hampering part of the magnetic flux; this wouldn't occur if the intermediate resonator had the primary size, in which case the efficiency would be greater than the original one.

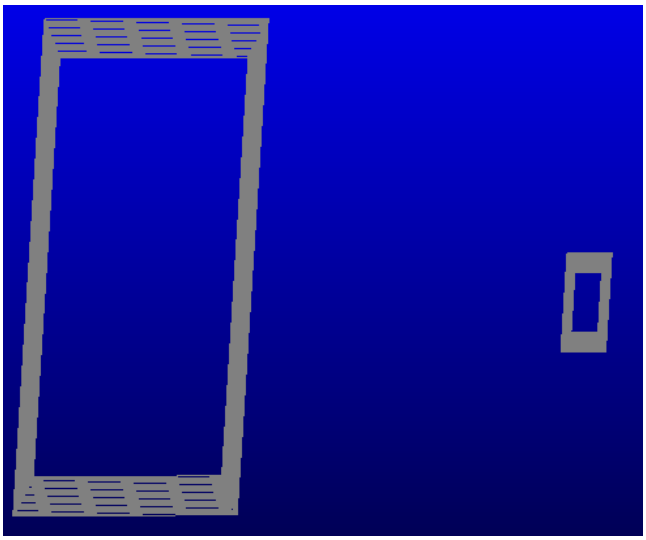

Figure D.6. Two different resonators in FastHenry

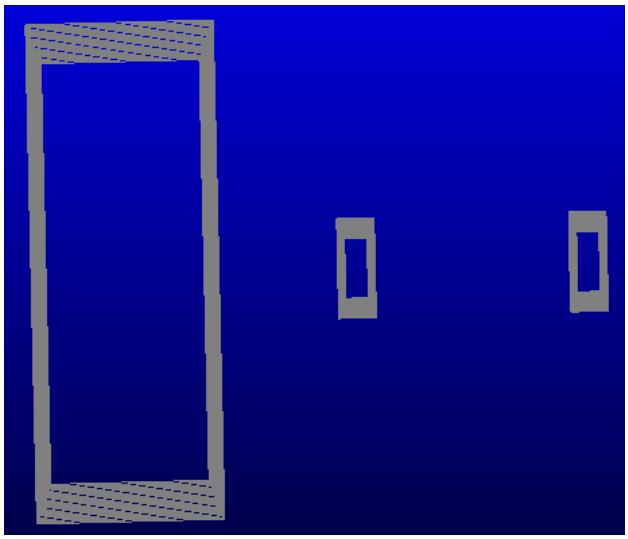

Figure D.5. Three different resonators in FastHenry

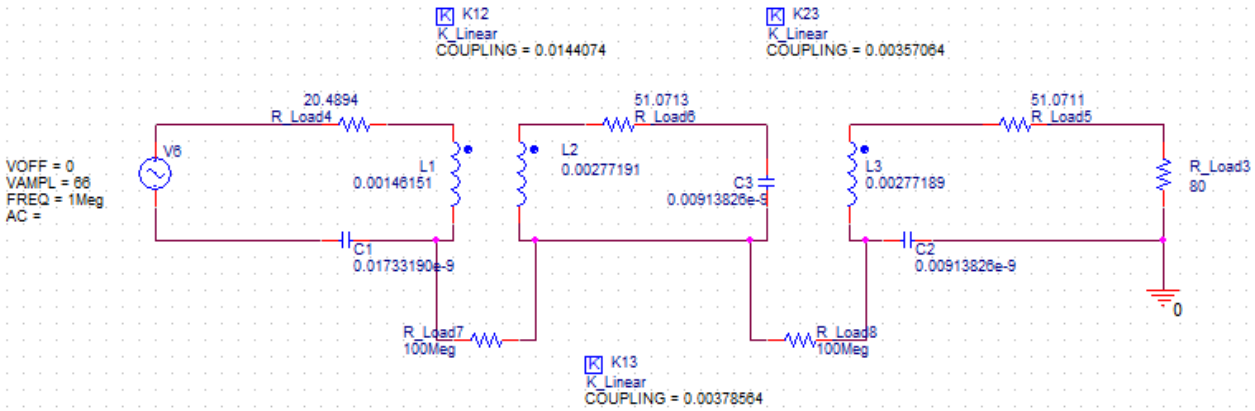

Figure D.7. Three different resonators electrical circuit

Appendix E – Simulation results

Here, the results from the simulation mentioned in section 4.4 are shown to demonstrate the conclusions explained there. They appear in figure E.1; the columns, from left to right, corresponds to: distance between coils, maximum frequency, L_1, L_2, M, R_1, R_2, efficiency, I_{1ef}, I_{1arg}, I_{2ef}, I_{2arg}, V_{1ef}, V_{1arg}, V_{2ef}, V_{2arg}, C_p, C_s, w_2, N_2, e_2, and C_{auto} (secondary self-capacitance). Subscripts 1 and p refer to the primary, while 2 and s to the secondary. C_p and C_s are the compensation capacitances needed to make the coil resonate at operating frequency.

Distancia(m	Frecuencia(I	L1(H)	L2(H)	M(ohm)	R1(ohm)	R2(ohm)	Rendiment	I1ef(A)	I1arg(Deg)	I2ef(A)	I2arg(Deg)	V1ef(V)	V1arg(Deg)	V2ef(V)	V2arg(Deg)	Cp(nF)	Cs(nF)	w2(mm)	N2	e2(mm)	Cauto(nF)
110	103079000	0,00277153	4,6415E-05	24541,9905	332,775532	49,7649778	98,9567688	0,00399036	0	0,01026477	90	253,245663	2,0577E-13	97,4206413	90	8,6017E-07	5,1362E-05	0,25	6	7,66	5,1362E-05
110	99216300	0,00277154	4,3501E-05	23633,2249	331,169024	19,7557864	99,31783	0,00322578	0	0,01316213	90	312,131789	0	75,9755616	90	9,2844E-07	5,9152E-05	0,75	6	7,06	5,9152E-05
110	93695800	0,00277155	4,219E-05	22328,3174	328,61965	12,3655912	99,4306382	0,00295591	0	0,01519465	90	340,242398	0	65,8126263	90	1,0411E-06	6,839E-05	1,25	6	6,46	6,839E-05
110	87728300	0,00277159	4,139E-05	20915,5262	325,479151	8,82714992	99,4887656	0,00281321	0	0,01703886	90	357,292383	1,4585E-13	58,6893693	90	1,1875E-06	7,9519E-05	1,75	6	5,86	7,9519E-05
110	81575000	0,0027716	4,0848E-05	19457,0661	321,750794	6,6795645	99,5246081	0,00272774	0	0,01888659	90	368,355302	0	52,9476175	90	1,3734E-06	9,3186E-05	2,25	6	5,26	9,3186E-05
110	75307700	0,00277161	4,0467E-05	17969,2623	317,350941	5,26624599	99,5460248	0,00268357	0	0,02078471	90	374,337545	0	48,1122895	90	1,6115E-06	0,00011037	2,75	6	4,66	0,00011037
110	68927700	0,0027716	4,0195E-05	16453,9787	312,136073	4,27765472	99,5568309	0,00267328	0	0,02278498	90	375,737921	-6,934E-14	43,8885712	90	1,9236E-06	0,00013264	3,25	6	4,06	0,00013264
110	62395100	0,00277159	4,0007E-05	14900,8295	305,892673	3,55235919	99,5585294	0,00269521	0	0,02495498	90	372,674406	6,9914E-14	40,0721555	90	2,3475E-06	0,00016263	3,75	6	3,46	0,00016263
110	55631200	0,00277158	3,9886E-05	13291,0166	298,304313	3,00498061	99,5504851	0,00275419	0	0,02737946	90	364,722391	-7,144E-14	36,5237353	90	2,9531E-06	0,0002052	4,25	6	2,86	0,0002052
110	48503600	0,00277157	3,9821E-05	11592,9282	288,88336	2,57812351	99,5302924	0,00286135	0	0,03021743	90	351,135094	0	33,0934826	90	3,8848E-06	0,00027038	4,75	6	2,26	0,00027038
110	40777400	0,00277157	3,9808E-05	9750,23887	276,807597	2,24888102	99,4895236	0,00304825	0	0,03373219	90	329,740692	0	29,6452732	90	5,4964E-06	0,00038268	5,25	6	1,66	0,00038268
110	31967500	0,00277157	3,9844E-05	7646,78731	260,412248	2,01478332	99,4026967	0,00340175	0	0,03855829	90	295,732913	-4,405E-14	25,9347589	90	8,9433E-06	0,0006221	5,75	6	1,06	0,0006221
110	20660100	0,00277157	3,9932E-05	4943,75328	234,287641	1,95394738	99,1381637	0,00431658	0	0,0470629	90	233,678697	0	21,2481586	90	2,1412E-05	0,00148611	6,25	6	0,46	0,00148611
110	24560700	0,00277161	0,00014267	10756,567	244,113674	48,5894769	97,9954064	0,00650559	0	0,01443492	90	156,858329	0	69,2764304	90	1,5151E-05	0,00029433	0,25	11	3,705	0,00029433
110	22630700	0,00277162	0,00013769	9914,27031	239,384942	18,8332502	98,6546383	0,00535504	0	0,01896302	90	189,286435	1,3765E-13	52,7342131	90	1,7845E-05	0,00035921	0,75	11	3,155	0,00035921
110	20334100	0,00277161	0,00013568	8910,93754	233,414483	11,7381591	98,832063	0,00504607	0	0,02237003	90	200,515739	6,497E-14	44,7026732	90	2,2103E-05	0,0004515	1,25	11	2,605	0,0004515
110	17807100	0,0027716	0,00013467	7805,97281	226,304834	8,50396102	98,882314	0,00501136	0	0,02570699	90	201,802145	0	38,8999285	90	2,8822E-05	0,00059319	1,75	11	2,055	0,00059319
110	15005400	0,00277158	0,00013418	6579,63674	217,542318	6,702693	98,8460043	0,00519508	0	0,02942517	90	194,737084	0	33,9845098	90	4,059E-05	0,00083843	2,25	11	1,505	0,00083843
110	11760700	0,00277157	0,00013405	5158,49355	205,760852	5,70864495	98,6800132	0,00572021	0	0,03411467	90	177,157306	-7,354E-14	29,3129015	90	6,6076E-05	0,00136616	2,75	11	0,955	0,00136616
110	7531110	0,00277157	0,00013423	3304,27666	186,189481	5,59844062	98,0648202	0,00731514	0	0,04177567	90	139,400382	-4,673E-14	23,9373765	90	0,00016114	0,00332722	3,25	11	0,405	0,00332722
110	10761600	0,0027716	0,00029348	6861,19652	201,660955	55,9124294	96,9522857	0,00889645	0	0,01663613	90	115,937857	0	60,1101161	90	7,8914E-05	0,00074527	0,25	16	2,38666667	0,00074527
110	9431090	0,00277159	0,0002868	6014,56196	195,755679	21,7635301	97,8529859	0,00752665	0	0,02232963	90	135,776311	0	44,7835513	90	0,00010275	0,00099298	0,75	16	1,85333333	0,00099298
110	7859990	0,00277158	0,00028456	5013,88639	187,961209	13,8694465	97,9839713	0,0074357	0	0,02709591	90	137,253447	-4,746E-14	36,9059363	90	0,00014793	0,00144085	1,25	16	1,32	0,00144085
110	5978880	0,00277157	0,00028389	3814,95927	176,948249	10,6805537	97,7467403	0,00811665	0	0,03266285	90	126,043668	-5,168E-14	30,6158221	90	0,00025567	0,00249602	1,75	16	0,78666667	0,00249602
110	3339020	0,00277157	0,00028421	2131,09883	155,79415	10,4280191	96,2881593	0,01122757	0	0,04258402	90	92,499954	7,0419E-14	23,4829847	90	0,00081974	0,00799401	2,25	16	0,25333333	0,00799401
110	5963260	0,00277159	0,00049925	4991,91962	176,846355	64,687143	95,8056467	0,01124414	0	0,01819747	90	92,8287721	0	54,9527066	90	0,00025701	0,00142676	0,25	21	1,7275	0,00142676
110	4935580	0,00277158	0,00049129	4132,62538	169,631462	25,4034533	96,8731628	0,00983115	0	0,0250042	90	105,000673	-6,204E-14	39,9932777	90	0,00037518	0,00211653	0,75	21	1,2025	0,00211653
110	3654650	0,00277157	0,00048937	3060,8669	158,836681	16,9404164	96,6675522	0,01050508	0	0,03162666	90	98,4735785	-6,615E-14	31,6188973	90	0,00068426	0,00387534	1,25	21	0,6775	0,00387534
110	1707050	0,00277157	0,00048989	1430,0575	138,034575	15,5220404	93,7325614	0,01581265	0	0,045653	90	67,4691078	4,8272E-14	21,9043652	90	0,00313633	0,01774394	1,75	21	0,1525	0,01774394
110	2902550	0,00277158	0,00075141	3009,58995	151,322211	29,2718318	95,6739083	0,01235758	0	0,02748251	90	84,5810717	0	36,3867739	90	0,00108481	0,00400133	0,75	26	0,812	0,00400133
110	1715620	0,00277157	0,00075051	1779,3065	138,12952	21,1141025	94,1111652	0,01527656	0	0,03790558	90	69,5557839	0	26,3813421	90	0,00310507	0,01146676	1,25	26	0,292	0,01146676
110	2560450	0,00277159	0,00107647	3165,06697	147,621408	83,9665068	93,2079438	0,01598406	0	0,02046139	90	67,1212541	0	48,8725384	90	0,00139405	0,00358928	0,25	31	1,06833333	0,00358928
110	1819990	0,00277158	0,00106733	2250,2742	139,293447	33,4365977	94,1156058	0,01520633	0	0,03010992	90	69,8737204	0	33,2116449	90	0,00275916	0,00716481	0,75	31	0,55166667	0,00716481
110	1845610	0,00277158	0,00144812	2649,63745	139,580968	94,9359626	91,6802566	0,01841685	0	0,02138213	90	59,2255246	-1,1E-13	46,7680329	90	0,00268309	0,00513522	0,25	36	0,88	0,00513522
110	1175800	0,00277157	0,0014392	1688,40728	132,496851	37,5248897	91,9890621	0,01850259	0	0,033346	90	58,7531619	0	29,9886057	90	0,00661075	0,01273083	0,75	36	0,36571429	0,01273083
110	1384860	0,00277158	0,00187522	2264,43517	134,573198	106,466632	89,9720982	0,02087983	0	0,02226657	90	53,2310747	6,1184E-14	44,9103698	90	0,00476545	0,00704335	0,25	41	0,73875	0,00704335
110	756810	0,00277157	0,00186713	1237,76475	129,003984	40,8417223	88,9390671	0,02258849	0	0,03786021	90	49,776033	6,5431E-14	26,4129573	90	0,01595661	0,02368596	0,75	41	0,22625	0,02368596
110	1071240	0,00277158	0,00235782	1965,34579	131,530157	118,356943	88,0835224	0,02338506	0	0,02313672	90	48,5474874	-6,709E-14	43,2213467	90	0,00796411	0,00936168	0,25	46	0,62888889	0,00936168
110	848907	0,00277158	0,00289367	1726,78642	129,677151	130,476537	86,0264929	0,02594881	0	0,0239938	90	44,7971423	-7,27E-14	41,6774269	90	0,01268211	0,01214706	0,25	51	0,541	0,01214706
110	685464	0,00277158	0,00348541	1531,06659	128,52541	142,742834	83,8029057	0,02860344	0	0,0248465	90	41,7179147	7,8069E-14	40,2471181	90	0,01945103	0,01546739	0,25	56	0,46909091	0,01546739
110	562019	0,00277159	0,00413274	1367,45747	127,79299	155,105332	81,4198891	0,0313735	0	0,02569617	90	39,1477279	-8,319E-14	38,9163107	90	0,02893404	0,01940437	0,25	61	0,40916667	0,01940437
110	466581	0,00277158	0,00483659	1228,33105	127,31559	167,534003	78,8801554	0,0342878	0	0,02654684	90	36,9736764	0	37,66927	90	0,04198148	0,02405726	0,25	66	0,35846154	0,02405726
110	331164	0,00277158	0,00641101	1003,95536	126,780319	192,514737	73,346035	0,04066396	0	0,02826129	90	33,5284629	0	35,3840903	90	0,08333508	0,03602703	0,25	76	0,27733333	0,03602703
110	241849	0,00277157	0,00820788	829,681734	126,523191	217,59455	67,2098135	0,04802193	0	0,03002044	90	30,9832992	0	33,3106375	90	0,15625214	0,0527619	0,25	86	0,21529412	0,0527619
110	208228	0,00277157	0,00918972	755,879041	126,446696	230,157871	63,9137664	0,05219298	0	0,03092788	90	29,9773662	0	32,3332866	90	0,21078404	0,06357127	0,25	91	0,18944444	0,06357127
110	179905	0,00277157	0,01022721	688,955803	126,390988	242,735846	60,4626721	0,05678255	0	0,03186029	90	29,127133	5,5908E-14	31,3870364	90	0,28237627	0,07652378	0,25	96	0,16631579	0,07652378

Figure E.1. Screenshot of the excel sheet from figure 4.7